

**REPORT DOCUMENTATION PAGE**

Form Approved OMB No. 0704-0188

Public reporting burden for this collection of information is estimated to average 1 hour per response, including the time for reviewing instructions, searching existing data sources, gathering and maintaining the data needed, and completing and reviewing the collection of information. Send comments regarding this burden estimate or any other aspect of this collection of information, including suggestions for reducing the burden, to Department of Defense, Washington Headquarters Services, Directorate for Information Operations and Reports (0704-0188), 1215 Jefferson Davis Highway, Suite 1204, Arlington, VA 22202-4302. Respondents should be aware that notwithstanding any other provision of law, no person shall be subject to any penalty for failing to comply with a collection of information if it does not display a currently valid OMB control number.  
**PLEASE DO NOT RETURN YOUR FORM TO THE ABOVE ADDRESS.**

<b>1. REPORT DATE (DD-MM-YYYY)</b> 26-01-2006	<b>2. REPORT TYPE</b> Final Report	<b>3. DATES COVERED (From – To)</b> 01-May-02 - 27-Jan-06
--	---------------------------------------	--

<b>4. TITLE AND SUBTITLE</b> Multi-Spectral Dynamically Controllable Point Source	<b>5a. CONTRACT NUMBER</b> STCU Registration No: P-080
	<b>5b. GRANT NUMBER</b>
	<b>5c. PROGRAM ELEMENT NUMBER</b>

<b>6. AUTHOR(S)</b> Professor Volodymyr Malyutenko	<b>5d. PROJECT NUMBER</b>
	<b>5d. TASK NUMBER</b>
	<b>5e. WORK UNIT NUMBER</b>

<b>7. PERFORMING ORGANIZATION NAME(S) AND ADDRESS(ES)</b> Institute of Semiconductor Physics, Ukrainian Academy of Sciences 45 Pr Nauki Kyiv 252650 Ukraine	<b>8. PERFORMING ORGANIZATION REPORT NUMBER</b> N/A
---	--

<b>9. SPONSORING/MONITORING AGENCY NAME(S) AND ADDRESS(ES)</b> EOARD PSC 802 BOX 14 FPO 09499-0014	<b>10. SPONSOR/MONITOR'S ACRONYM(S)</b>
	<b>11. SPONSOR/MONITOR'S REPORT NUMBER(S)</b> STCU 01-8004

**12. DISTRIBUTION/AVAILABILITY STATEMENT**  
Approved for public release; distribution is unlimited.

**13. SUPPLEMENTARY NOTES**

**14. ABSTRACT**

This report results from a contract tasking Institute of Semiconductor Physics, Ukrainian Academy of Sciences as follows: This research will lead to improvements in the equipment used to test and calibrate infrared imaging systems operating at a multiple wavelength regions (multi-spectral remote sensing). This research can contribute to many aspects of gas detection as well as the characterization, calibration, and testing of infrared and night vision cameras used for fire fighting, agriculture, medical imaging and industrial thermography. The basic technology may also have an important role in the development of related devices for electronic cinema applications.

An investigation of principally new (Joule heating free) approach toward the development of dynamic IR scene simulation technology is the objective of this research. The primary goal is to develop, fabricate and test Multi-Spectral Dynamically Controllable Point Source capable of generating positive and negative apparent temperatures (as compared to background temperature) with frame rate ranging to well beyond 200 Hz. While silicon is not fully eliminated as the material under this study, the main impact is being made at other promising semiconductors (which have been bypassed till now) as the base of innovative sources highly spectrally-controlled in up to three bands (visible + 8-10um + 10-12um) simultaneously.

**15. SUBJECT TERMS**  
EOARD, Physics, Atomic and Molecular Physics and Spectroscopy

<b>16. SECURITY CLASSIFICATION OF:</b>			<b>17. LIMITATION OF ABSTRACT</b> UL	<b>18. NUMBER OF PAGES</b> 62	<b>19a. NAME OF RESPONSIBLE PERSON</b> DONALD J SMITH
<b>a. REPORT</b> UNCLAS	<b>b. ABSTRACT</b> UNCLAS	<b>c. THIS PAGE</b> UNCLAS			<b>19b. TELEPHONE NUMBER</b> (Include area code) +44 (0)20 7514 4953

**Project number**

P-080

**Title of the Project**

Multi-Spectral Dynamically Controllable Point Source

**Terms**

May 2002-October 2005

**Project Manager**

*Volodymyr K. Malyutenko*, Professor, Head of Department,  
Phone: (38044) 525-57-97, e-mail: malyut@isp.kiev.ua.

**Project Location**

Institute of Semiconductor Physics, National Academy of Sciences,  
Kyiv, Prospect Nauki 41, bld.5  
Ukraine

**Partner, Financing Party**

The Air Force Research Laboratory, Eglin AFB, Florida, USA  
Contact: Dr. *Don Snyder*, e-mail: donald.snyder@eglin.af.mil

**Management**

The European Office of Air Force Research Laboratory (EOARD)  
Contact: Dr. *Sandy Smith*, e-mail: sandy.smith@london.af.mil

The Science and Technology Center in Ukraine (STCU)  
Contact: Dr. *Sergiy Sliusarenko*, e-mail: sergiy.sliusarenko@stcu.int

**Document type**

Final report, unpublished

## TABLE OF CONTENTS

1. **Abstract/4**
2. **Introduction (Who we are and how this work started)/5**
3. **Key words (The scope of our activity in brief)/6**
4. **Objectives (Critical review and tasks)/7**
5. **Fundamentals of the photonic approach/10**
  - 5.1. Three approaches in dynamic IR scene simulation devices/10
    - 5.1.1. Recording the temperature of a scene, T-approach/10
    - 5.1.2. Scene emissivity as the parameter to monitor,  $\epsilon$ -approach
    - 5.1.3. IR luminescence adds new knowledge, L-approach/11
  - 5.2. Contact ways to monitor free charge carrier concentration in semiconductors. Manipulating the contact nature/12
    - 5.2.1. Free carrier injection process/12
    - 5.2.2. Free carrier exclusion-accumulation process/14
    - 5.2.3. Lorentz force monitors free carrier concentration/15
  - 5.3. Contactless ways to monitor free charge carriers in semiconductors/16
    - 5.3.1. Band-to-band luminescence/16
    - 5.3.2. Light down conversion process/16
  - 5.4. Lesson to learn/17
6. **Materials requirement and processing (Do we need exotic materials, expensive technology and processing?)/18**
  - 6.1. Silicon/18
  - 6.2. Germanium/21
  - 6.3. Indium Arsenide-based compounds/22
  - 6.4. Indium Antimonide/24
  - 6.5. Lesson to learn/25
- Hardware-In-The-Loop Facility (What we can but others can't)/26**
  - 7.1. Multispectral micro imaging set up/26
  - 7.2. What we can detect, classify, and identify/28
  - 7.3. Lesson to learn/32
- Results and discussion/34**
  - 8.1. IR scene monitored by the electrical bias/34
    - 8.1.1. The injection mode, luminescence, MWIR/34
    - 8.1.2. The Lorentz force mode, luminescence, MWIR/37
    - 8.1.3. Is negative luminescence gift to the DIRSP's users?/39
    - 8.1.4. The injection mode, transparency modulation technique, MWIR & LWIR/41

- 8.1.5. The exclusion-accumulation mode, transparency modulation technique, MWIR & LWIR/44
- 8.2. IR scene monitored by light (light down conversion), MWIR & LWIR/46
- 8.3. Lesson to learn (Which the approach is better?)/49

**7. Summary/51**

**8. Acknowledgement/53**

**Publishing, patenting, commercializing, and reporting the results/53**

- 11.1. List of papers published/53
- 11.2. List of patents and patent pending/54
- 11.3. List of presentation at the international conferences/55
- 11.4. List of sites, where project manager's reports are made/57
- 11.5. Our direct contacts with US for-profit companies/57

**9. References/59**

## 1. ABSTRACT

Just a couple of years ago, achieving Dynamic Infrared Scene Projector (DIRSP) device operating with microsecond rise-fall time and able to simulate both positive and negative temperature contrasts was considered a daunting challenge. Indeed, *thermal resistor arrays* (that have been widely in use) suffer from long time response and disability to simulate cold targets or background. To bridge the gap between defence and security demands and manufacturer's abilities, we have developed the concept, theoretical basis, experimental set up, and fabrication process that allow design and performance prediction of semiconductor *dynamically monitored IR emitting devices capable of simulating both positive and negative apparent temperatures*. Two basic approaches are electrically biased light emitters made of *direct band* materials, and optically/electrically monitored unconventional emitting devices made of *indirect band* materials. By optimizing the emitting structure content and design, we were able to dynamically simulate both *highest and lowest apparent temperatures* till now reported for spontaneous emitters at  $T \geq 300^{\circ}\text{K}$ .

The first class of devices is based on narrow band III-V compounds that operate in the *electroluminescence mode* (intraband radiative electron transitions). Devices comprise conventional LEDs (forward and reverse biased *InAsSb/InAs* p-n heterostructures) and uniform *InSb* structures arranged into crossed ExH fields. In the entire MWIR (3-5  $\mu\text{m}$ ) band, these devices simulate wide range of apparent temperature values:  $220^{\circ}\text{K} < T_a < 600^{\circ}\text{K}$ -*pulse mode*. By estimates, in the multispectral mode (three-four narrow-band emitters in the MWIR band) narrow-band apparent temperature exceeds  $1000^{\circ}\text{K}$ -*pulse mode*. Devices under test are prepared as single emitters and emitting bars (4x4-InAsSb; 16x16-InSb). These devices rise-fall time falls into MHz range.

The second class is based on the *transparency modulation technique* (interband phonon-assisted electron transitions). Devices comprise unconventional IR emitters made of *indirect band gap Ge and Si*. The devices are operated by *electrical bias* (contact injection, exclusion and accumulation processes) or activated by *visible light pump* (light down conversion process, *pixelles scene*). The operation bands are MWIR and LWIR (8-12  $\mu\text{m}$ ). In each of the bands, the simulated apparent temperature range is  $220^{\circ}\text{K} < T_a < 700^{\circ}\text{K}$ -*pulse mode*. Devices are prepared as *very large (of several  $\text{cm}^2$  sizes)* single Ge and Si emitters, 16 element Si emitting arrays and 8x8 Si emitting bars. Their rise-fall time depends on the design process and scatters in the 1ms-100 $\mu\text{s}$  range; multispectral emitters are easy to develop by using transparency coating technique. As a matter of fact, we have shown that the Si, which has remained the microelectronics industry's semiconductor of choice for a half of century, also becomes a uniquely attractive material for use in IR photonics.

We demonstrated new routes to DIRSP's application. More specifically, we have experimentally shown for the first time how *low observables and dynamic chameleon effect* could be simulated in both MWIR and LWIR bands.

The results of our R&D study are *published* in referred journals and *reported* at numerous international conferences (USA, Europe). They have already formed the basis of *two UA patents and one US Patent Pending*. Major data and results are confirmed by experimental tests commonly performed at Eglin AFB and Santa Barbara Infrared Inc. facilities (both USA).

## 2. INTRODUCTION (Who we are and how this work started)

**We are located at the Institute of Semiconductor Physics (National Academy of Science) of Kiev, Ukraine.** Our scientific background is semiconductor physics and our current research interests include:

- Science based understanding of high-level electron processes in IR emitting devices*
- 2D- and 3D-computer modeling of heat and light transfer in IR LEDs and lasers*
- Negative luminescence, photon drag effect, and light conversion processes in semiconductors*
- High-resolution time-resolved IR microscopy*
- IR dynamic scene simulation devices*

We are interested in establishing relations with both research and industrial partners to further develop high-resolution IR vision of electron and thermal processes as well as our finding in DIRS, this work) for variety of practical applications. All in all, our interest has been IR devices and technology. We have been permanently working for our partners located in the USA, France, Belgium, Switzerland, Israel, Poland, Russia, and Ukraine. More details are available at the Internet: <http://malyut.freecyberzone.com/>

### **Team overview**

Prof. V. Malyutenko-*Project manager, author of the report*

Prof. K. Glinchuk-material science consulting, semiconductor properties, charge carrier recombination processes in *Germanium and Silicon*

D.Sc. O. Podoltsev- *computer simulation* of current, free carrier, and heat flows two-dimensional patterns in many layer planar structures, Joule losses, finite element approach

Dr. V. Vainberg-theoretical support of experimental study of *exclusion- accumulation processes* in semiconductors, computer simulation

Dr. G. Teslenko- technology of materials and contacts, experimental tests (*Ge*)

Dr. S. Bolgov-design and experimental study of IR emitting arrays (*Indium Antimonide, Silicon*)

Dr. K. Michailivska –thin film transparency coating technology in 3-5 and 8-12  $\mu\text{m}$  bands (*Ge, Si*)

Scientist O. Malyutenko-experimental study on *high-resolution imaging* of heat and light patterns in light emitting structures

Scientist V. Bogatyrenko-*optical properties* of semiconductors, emissivity, reflectivity, absorption spectra (experimental study, *Ge*)

Post Graduate Student S. Chyrchyk- *optical properties* of semiconductors, emissivity, reflectivity, absorption spectra (experimental study, *Si*)

Post Graduate Student A. Zinovchuk- experimental study of luminescence in *Indium Arsenide*-based light emitting structures

Engineer O. Kiryusha-technical assistance, information activity

### **Management**

The work was performed in format of *The Science & Technology Center in Ukraine* (STCU). This site is an intergovernmental organization established by its Donor Countries and dedicated to the non-proliferation of technologies and expertise related to weapons of mass destruction and their delivery systems by facilitating R&D

projects and encouraging technology transfer and commercialization. AFRL's people initiated this R&D study after our preliminary work for the AFRL was successfully completed (Project P-44). From the partner's side this work has been managed by *The European Office of Air Force Research Laboratory* (EOARD).

### **3. KEY WORDS (The scope of our activity in brief)**

Technical and scientific areas of interest include, but are not limited to, the following:

Dynamic IR scene simulation devices, resistive micro emitters, LEDs, single IR emitters and arrays, dual-band and multi-band emitters, point and spatially extended IR sources, pixelated scenes, positive and negative contrasts, cold scene/background, >20kHz frame rate, low observable simulation, target active camouflage simulation

IR, 3-5  $\mu\text{m}$  and 8-12  $\mu\text{m}$  spectral bands, hardware-in-the-loop facility, slave mode, multi-spectral scanning microscopy, <20  $\mu\text{m}$  spatial resolution, <10  $\mu\text{s}$  temporal resolution, ~0.1 K temperature resolution, apparent temperature, IR gallery

Joule heating, luminescence, negative luminescence, blackbody radiation, thermal emission, transparency modulation technique, magneto concentration effect, free carrier absorption/emission processes, interband and intraband electron transitions, light down conversion, high operating temperatures ( $T > 300^{\circ}\text{C}$ ), optical properties of semiconductors

InAs-based ternary and quaternary compounds, InSb, Germanium, Silicon, intrinsic conductivity, intentional doping, Chochralski crystal growth, floating zone (FZ) technology, liquid phase epitaxy (LPE) process, doping by diffusion, ion implantation, polishing, chemical etching, transparency coating, planar and mesa structures

Free electrons and holes, p-n junction, p<sup>+</sup>-p junction, p-i-n structure, heterojunction, exclusion, injection, double injection, extraction, accumulation, carrier lifetime, surface recombination velocity, current crowding, photoexcitation, 2D mapping of free electrons and holes

R&D, US-UA common tests, SPIE and other international conferences, patents hold and patent pending, top-rank journal publications, commercialization, business contacts

AFRL WOS Program, CDRF Industry Travel Grants Program, STCU Travel Grant Partnership Program, NATO Expert Visit Grant Program

#### 4. OBJECTIVES (Critical review and tasks)

The generation of synthetic infrared (IR) scenery is a key requirement for the testing and calibrating of infrared devices. The point is that the cost and complexity of development of conventional IR systems requires reducing the number of different type *outdoor* tests needed for critical program decisions. Moreover, such large-scale field tests do not offer repeatability or controllability of test conditions. For these reasons, since the early 1990's there has been a major progress in developing *The Dynamic Infrared Scene Projectors (DIRSP)*, which become prime element of any Hardware-in-the-Loop Simulator capable of *indoor* end-to-end testing and calibration of IR detection systems.

Dynamic infrared scene simulation devices (projectors) are needed to support the development of target detection and tracking techniques based on thermal imaging in the *3-5 and 8-12  $\mu\text{m}$  spectral ranges* by simulation synthetic IR scenarios composed of target-on-background picture. Till now, a number of different DIRSP technologies have been investigated and reported. Among these are emissive (thin films, bridge or suspended membrane resistors), transmissive (liquid crystals, galvanic cells), reflective (deformable mirror or membrane cells, spatial light modulators) projectors, as well as laser scanners of different types<sup>1</sup>. From this set of devices only *thermal emitters* (parameter to monitor is device temperature) and *photonic emitters* (parameter to monitor is "real" light the device emits while its temperature remains constant) worth considering.

At the current time, two-dimensional (2D) *thermal resistor arrays* (emissive projector based on the advanced suspended membrane resistors<sup>2-5</sup>) appear to be most promising devices in the field (Fig.1). However, broadband thermal resistor arrays suffer from long time constant and power dissipation capability. Even if made of very small ( $50 \times 50 \mu\text{m}^2$ ) and very thin ( $0.2 \mu\text{m}$ ) membrane, the single pixel rise-fall time constant cannot be less than  $\sim 5$  ms and thus projector has limited frame rate capability (heat relaxation process depends on membrane thermal mass and legs thermal conductance). Other drawbacks to these DIRSPs originate from their pixel technology. Firstly, emitter arrays are characterized by fixed-pattern noise due to variation of electrical and emissive properties of individual pixel and therefore demand for non-uniformity correction. Secondly, pixel technology results in low fill-factor (F) value ( $F < 0.5$  for small pixel area). Third, these devices spatial resolution is limited by the single pitch value. Fourth, current generation of thermal emitters based on Si technology have fundamental limitation in high temperature output. Indeed, thermally induced membrane deformation prevents these DIRSPs from being heated well above 800 K. But the major disadvantage of conventional DIRSP technologies is their disability to simulate cold targets compared to the background temperature. By the author's opinion, *thermal resistor array technology is showing its limitations*.

Alternatively, *diode laser-based photonic emitters* appear to be promising for projecting higher temperatures at higher frame rate. More specifically, Pb-salt diode laser linear array DIRSP (which has been in use at U.S. Army Aviation and Missile Command, AMCOM) operates at 8 KHz frame rate and simulate apparent temperature in 3-5  $\mu\text{m}$  band (mid-wave infrared, MWIR) as high as 500K /1/. Such unexpectedly low apparent temperature is connected to the problem with the collecting edge-emitting laser beam. Indeed, laser diode's beam assumes a long oval shape (because the divergences in the two perpendicular directions are different), which is difficult to focus even if each pixel is coupled to cylindrical (fast) lens. As a matter of fact, the beam appears not to be an ideal point source. Meanwhile, progress



has been rapid on the development of new generation laser-based photonic devices including vertical cavity surface emitting lasers or cascade lasers.

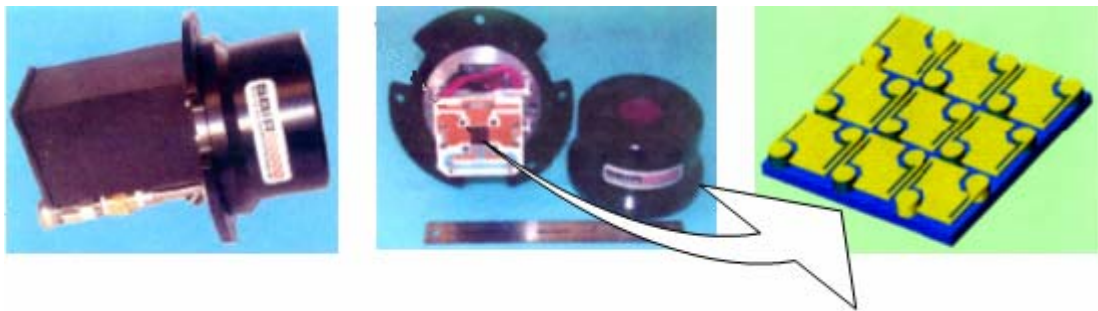


Fig.1. Most accurate presentation of low frequency (<200 Hz) hot ( $T < 500^{\circ}\text{C}$ ) synthetic scene across a relatively cold background ( $T_b$ ) is achieved by electric heating the 512x512 micro resistor array (Joule heating) to the required temperature ( $\Delta T = T - T_b > 0$ , *positive contrast*, SBIR MIRAGE engine). It is a complete infrared scene projector system with full emitter assembly, electronics and a thermal support subsystem. The emitter array is constructed of thermally isolated thin film membrane resistor structure fabricated on an advanced sub-micron silicon read-in integrated circuit (*proprietary technology*). The array is packaged in a custom vacuum package. The MIRAGE Dewar is designed for long vacuum hold times. This engine power consumption is of 20kW.

To start lasing, a diode laser has to be biased well above threshold current value ( $I_{th}$ ). By this reason, a laser projector is not able in principle to simulate both low apparent temperature targets and cold targets. In particular, it is impossible to simulate a camouflage-netted vehicle partially obscured by foliage or many other IR scenes (like winter or arctic scenes, clouds, and space background), that demand for lower simulated temperatures. In a words, their application is limited to the ability to

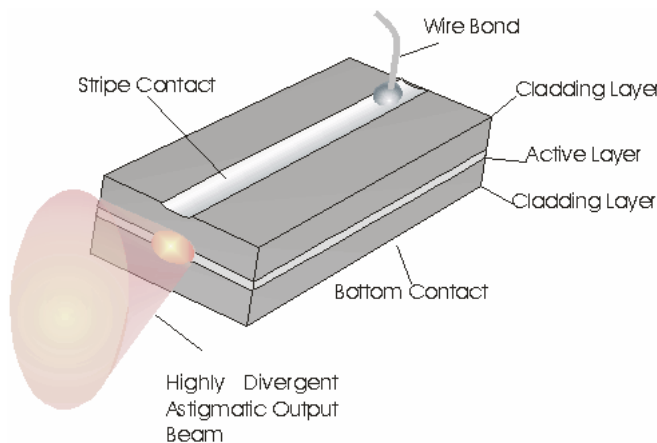


Fig.2. Unlike conventional solid state laser, edge-emitting laser generates highly divergent light beam caused by diffraction of light. To “correct” the beam, the device requires expensive micro lens packaging.

simulate very “bright” targets only. Besides, ( $I_{th}$ ), the power emitted, and the maximum wavelength are strongly affected by temperature. Finally, to operate properly conventional edge emitting lasers should be

cooled. But the major drawback to the laser DIRSP is in it very narrow optical bandwidth. In a variety of thermal imaging applications, there is no margin for error. However, simulating broadband emitting conventional scenes with “artificial” laser light could cause problem to decision-maker. By the author’s opinion, these devices could form a basis for new generation of hyper-spectral DIRSPs in the future. These devices, however, are beyond of our study.

Thus, the primary goal of our current efforts is to develop *new physical principles and approaches* to DISP devices operated in broad IR band (like conventional thermal emitters) and capable of generating high-speed scenarios (like lasers). *To this end*, we

-are limited by the two IR spectral bands which are atmospheric transparency windows-MWIR (3-5  $\mu\text{m}$ ) and LWIR (8-12  $\mu\text{m}$ ). However, to assure proper testing of advanced multispectral IR imaging systems our DIRSPs are able to operate as high-frequency modulated multiple wavelength point and extended sources in several IR sub bands in both MWIR (several characteristic wavelengths) and LWIR (7-9  $\mu\text{m}$  and 9,5-11,5  $\mu\text{m}$ ) bands;

-develop *Hardware-in-the-Loop Facility* based on modern thermal imaging cameras operated in the above mentioned spectral bands. The facility is tested and capable of measuring both apparent temperature and power emitted by IR sources-targets whose temperature range from  $-60\text{ C}$  to  $1000\text{ C}$ . Besides, it operates in slave mode in kHz range and therefore detects the evolution-in-time-target's parameters in millisecond-microsecond range. Finally, the facility is easy to detect a point IR target or details of an extended target with the *spatial resolution as high as 20  $\mu\text{m}$* ;

-develop fundamental background and experimentally demonstrate two types of *photonic* DIRSPs operated with frame rate of 1 kHz minimum, 10 kHz desired. These devices "work" as *electrically biased or optically pumped point sources*. By physical nature, electrically driven devices operate in contact injection-exclusion modes with output signal being *positive or negative electroluminescence* (MWIR band only,  $\lambda < 7, 0\ \mu\text{m}$ ) or are based on the emissivity enhancement technique (MWIR and LWIR bands). Optically pumped DIRSPs are based on *light down conversion phenomena* (we developed recently);

-show that both classes of photonic light emitting devices when kept at constant temperature and free of output window are able to simulate *positive and negative IR contrasts* (at least 100C above ambient to -20C below ambient, where the ambient is 300C (*we remarkably exceeded these parameters!!!*)). Hence, contrary to conventional DIRSPs, there is a possibility to simulate point *hot and cold objects* as well as *low observable* in IR;

-test the devices and experimentally show that their output power (in each of two main spectral bands) not only exceeds  $200\ \mu\text{W}$  and eventually  $500\ \mu\text{W}$  in pulse mode (it was scheduled as our task) but could be well above some mW;

-demonstrate our DIRSP devices as a single sources and 1D and 2D arrays (with independent control for frame rate modulation and intensity) operate without cooling. The *devices are made of InSb or InAs-based compounds as well as of Ge and Si*. They are easy to produce by conventional semiconductor technology and have considerable advantages in term of cost, volume, long-term stability and fast switching rate;

*Commercial Applications and Other Benefits:* This research contributes to many aspects of calibration and testing of infrared and night vision cameras used for fire fighting, agriculture, medical imaging and industrial thermography. The basic technology may also have an important role in the development of IR emitters which would enhance instrument performance in such applications as IR spectroscopy, metrology, industrial process monitoring, material science, and micro diagnostics of heat and light in semiconductor devices.

## 5. FUNDAMENTALS OF THE PHOTONIC APPROACH

### 5.1. Three approaches in dynamic IR scene simulation devices

What follows in this chapter is further development of IR imaging control approaches to the characterization of IR contrasts of a scene. Contrary to the conventional approach with tested parameter being *apparent temperature* (the T-approach), we will be interested in scene *emissivity*, which could carry information on the electron transfer inside a single device (the  $\epsilon$ -approach). Next, we consider the third approach based on mapping of *IR light* radiated by some categories of devices like laser or light emitting diodes (the L-approach). We also show how the combination of these approaches provides unique information on both thermal and optical properties of IR scene in time-resolved mode with record spatial resolution.

**5.1.1. Recording the temperature of a scene, T-approach ( $\epsilon = \text{const}$ ,  $L=0$ ).** In a passive and non-contact temperature measurement technique such as IR imaging, the key parameter to register and display is the IR power (P) emitted by a scene. In a properly calibrated imaging camera, this quantity and a scene temperature are connected by the calibrated signal transfer function. However, the scene parameter to set correctly is the emissivity ( $\epsilon \leq 1$ ), which is a measure of how much radiation is emitted from the scene compared to that if it was a blackbody

$$P = \epsilon P_{bb}. \quad (1)$$

$P_{bb}$  is the power emitted by a blackbody in the spectral range of interest and as a matter of fact is a result of integrating Planck's formula for the blackbody radiation (see curve 1 in Fig.3) over camera spectral range. When measuring the scene temperature, it is supposed that the scene emissivity is independent on wavelength in the spectral range of interest (grey scene) and temperature. Besides, while testing light-emitting devices, it is supposed that special cares are taken to prevent light emitted by a scene (luminescence or lasing, L) from being recorded with thermal imaging system. Fortunately, when it comes to semiconductor devices, all these conditions are easy to realize.

We have to mention that physical nature of this power emitted is in the behavior of a scene's "*phonon bath*" with key parameters being thermal mass and thermal conductance, heat diffusion length. Therefore manipulating the dynamic properties of a scene is limited to some *milliseconds* or higher values.

**5.1.2. Scene emissivity as the parameter to monitor,  $\epsilon$ -approach ( $T=\text{const}$ ,  $L=0$ ).** For semi-transparent scene  $\epsilon$ -factor is easy to obtain in the form<sup>6</sup>

$$\epsilon = (1 - R) (1 - \varphi) (1 - R\varphi)^{-1}, \quad (2)$$

where R is scene reflectivity and  $\varphi$  is its transmissivity. For given absorption coefficient value (k) and scene thickness (d) we have

$$\varphi = \exp(-kd) \quad (3)$$

What immediately follows from eq. (1-3) is another possibility to modulate power emitted by the scene even if its temperature is kept constant<sup>2</sup>. Really, for two limiting cases of semi-transparent ( $kd < 1$ ) and opaque ( $kd \gg 1$ ) scene, the emissivity factor takes the forms

$$\varepsilon_{\min} = kd, \quad \varepsilon_{\max} = 1-R, \quad (4)$$

whereas scene power emitted (eq.1) ranges from its minimum value  $P = kdP_{bb}$  to the power emitted by a blackbody with allowance for the reflectivity  $P_{\max} = (1-R)P_{bb}$ . To this end, it is very important to mention that the absorption coefficient in semiconductors in the spectral range of free charge carrier absorption ( $\omega_2 < E_g/\hbar$ , where  $\omega_2$  is the radiation frequency and  $E_g$  is material band gap, see region 4 in fig.3) is easy to control by modulating free charge carrier (electrons or/and holes) concentration in any way (*optically or electrically*). Indeed, remarkable feature of a semiconductor scene is the ability to monitor its absorption coefficient value by controlling free charge carriers concentration. Charge carrier absorption coefficient is connected to free electron (n) and hole (p) concentrations

$$k = \sigma_n n + \sigma_p p, \quad (5)$$

where  $\sigma_n$ ,  $\sigma_p$  are charge carrier absorption cross-sections of a quantum of given frequency  $\omega_2$ . This process dominates the optical properties of a material in the spectral range beyond the fundamental absorption range ( $\hbar\omega_2 < E_g$ ). Fundamentally, free carrier absorption-emission process results from non-direct phonon assisted electron and hole interband transitions, whose effectiveness increased approximately as the square of the wavelength.

The physical origin of IR power emitted is in the behavior of a scene's electron and/or hole concentration with key parameters being free carrier lifetime ( $\tau$ , temporal scale) diffusion length ( $L_d$ , spatial scale), and surface recombination velocity (s). Therefore, contrary to the T-approach, it is easy to manipulate the dynamic properties of a scene many orders quicker (*microseconds* range) even if the temperature remains stable. In a word,  $\varepsilon$ -approach in conventional thermal imaging becomes an effective way to generate IR pattern on the scene made of semiconductor.

**5.1.3. IR luminescence adds new knowledge, L-approach (T=const,  $\varepsilon = \text{const}$ ).** In narrow-gap semiconductors (like 111-V compounds, InSb, and HgCdTe alloys), interband luminescence (L), that appears in the spectral range of fundamental absorption ( $\omega_1 \geq E_g/\hbar$ , see region 3 in Fig.3), expands over 3 to 5  $\mu\text{m}$  and 8 to 12  $\mu\text{m}$  spectral ranges and therefore can also be monitored with conventional thermal imaging cameras. By the definition, this luminescence signal is a non-equilibrium process, which exists provided charge carrier concentrations (n, p) differ from their equilibrium value ( $n_i$ )<sup>7</sup>

$$\Delta P = P_0 (np/n_i^2 - 1), \quad P_0(\omega) \approx \omega^3 (\hbar\omega_1 - E_g)^{1/2} \exp(-\hbar\omega_1/kT) \quad (6)$$

There are two ways to stimulate luminescence in semiconductors. By generating excess free charge carriers ( $np/n_i^2 > 1$ ), one provokes *conventional* ("positive") *luminescence*  $\Delta P > 0$  (i.e. excess radiation over the equilibrium thermal emission value  $P_0$ , which scene radiates in spectral range of interest). A thermal imaging camera identifies this process as dynamic scene temperature increase. And contrary, charge carrier deficiency ( $np/n_i^2 < 1$ ) results in *negative* luminescence<sup>7,8,9</sup>  $\Delta P < 0$ , which camera registers as the dynamic scene cooling. It is important that in both these cases real scene temperature is kept constant and the major players on the scene are charge carrier generation-recombination processes and their evolution in space and time (but not real heat flows).

**To resume:** We show that the practical application of thermal imaging devices is not limited to conventional thermal analysis of a scene with a parameter of interest being the 2D-temperature map (thermal approach, chapter 5.1.1). By author opinion, the technology of remote IR sensing could be even more efficient given that the scene of interest allows for *emissivity dynamic control* (photonic approach, 5.1.2) or manipulating its *luminescence properties* (photonic approach, 5.1.3).

When it comes to semiconductors, it is the electron transitions nature that responsible for correct application of these three whales of the IR imaging. More details are shown in the Fig.3.

To measure temperature of a scene (T-approach) one needs an “optically” thick crystal ( $kd \gg 1$ ) in the camera operating range. To avoid measurement uncertainty, emissivity correction should be made (region 1). Short wavelength region 3 is responsible for the luminescence parameters given that the scene is made of direct band gap semiconductors (L-approach) and its temperature is kept constant. There are practically no limitations at a scene thickness. Longer wavelength region 4 directly supplies with information on free carrier distribution inside the scene. In this  $\epsilon$ -approach the scene thickness is a crucial parameter. Contrary to the L-approach, there is no limitation on the band structure; approach works in both direct band gap (like GaAs) and indirect band gap (like Si) semiconductors.

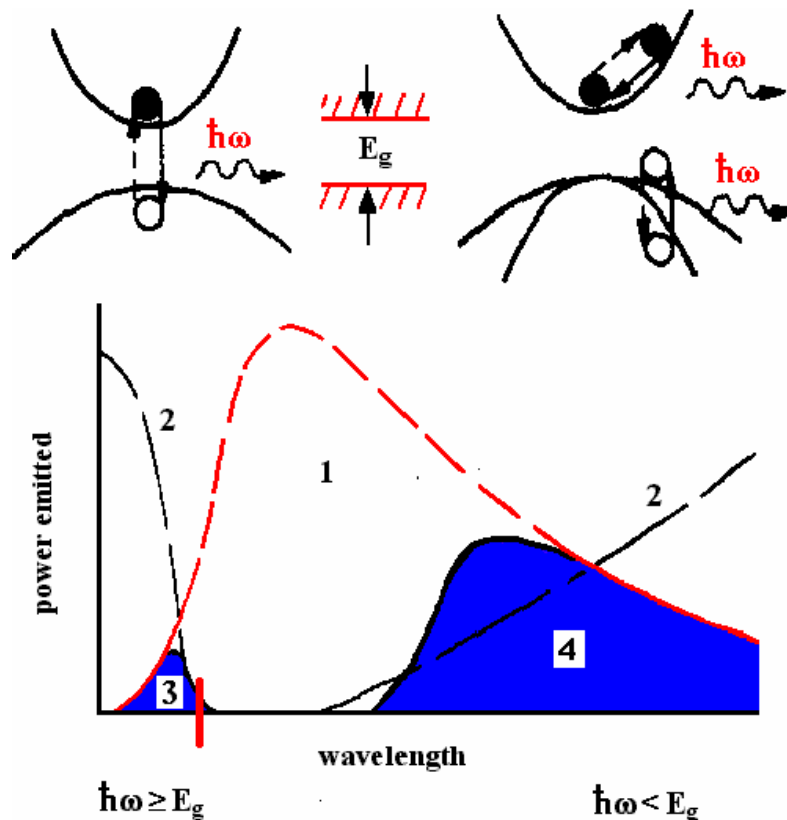


Fig.3. Schematics of electron transitions in semiconductor scene: top left-interband transitions, top right-intra band transitions.

1-power emitted by a blackbody, Plank's distribution,

2-spectral dependence of the absorption coefficient in semiconductor,

3- $\hbar\omega_1 > E_g$ , band of transitions responsible for positive and negative luminescence. An essential requirement, however, is very high external quantum efficiency.

4 -  $\hbar\omega_2 < E_g$ , band of transitions responsible for non-equilibrium thermal emission that comes at the cost of the input energy used to operate a device.

To be on the right side while reading the report, we remember that both photonic approaches register IR signals that are not connected to a scene thermometric temperature. The power emitted or apparent temperature  $T_a$  measured by a camera supply with information on local behavior of electron (and hole) concentration in the active part of a scene.

## 5.2. Contact ways to monitor free charge carrier concentration in semiconductors. Manipulating the contact nature.

**5.2.1. Free carrier injection process.** We don't intend to discuss carrier injection process in details as a nature of this phenomenon is well established (see [http://www.mtmi.vu.lt/pfk/funkc\\_dariniai/diod](http://www.mtmi.vu.lt/pfk/funkc_dariniai/diod)). In particular, when the junction between n-doped emitter and p-base is forward biased, a free carrier concentration in the base increases to level of emitter doping (Fig.4, a). Then, the concentration of the injected carriers exponentially degrades toward the ohmic contact due to recombination processes in the crystal volume, whereas transversal free carrier degradation is due to the surface recombination impact. Reverse bias causes free carriers to drift away from the junction toward electrodes by forming the carrier extraction region. The length of this carrier free region is composed of depletion layer width and diffusion carrier length. (At high temperature in all materials of our interest the depletion layer width can be neglected).

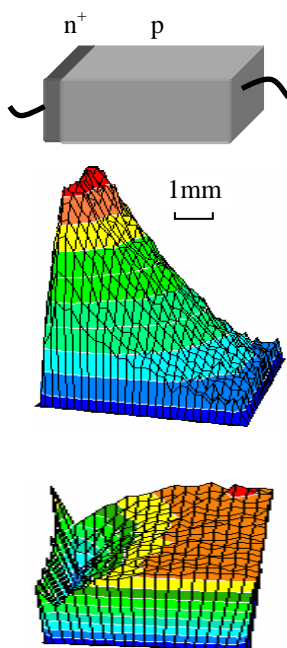
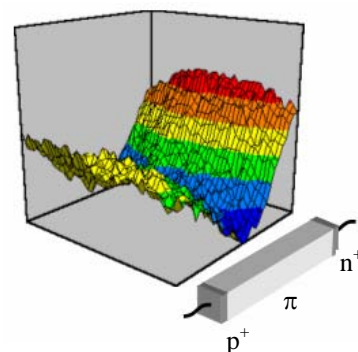


Fig.4,a. In forward biased  $n^+$ -p junctions, carrier injection process results in an extremely high non-equilibrium carrier increase in the base. And contrary, reverse bias forms the *extraction* region. Both carrier non-uniformities degrade (*injection*, central picture) or recover (*extraction*, lower picture) due to the recombination-generation processes. The spatial and temporal parameters of the process are carrier diffusion length and carrier lifetime. Z-axis shows the normalized non-equilibrium charge carrier concentration  $\Delta n = n(I) - n(0)$ . The two-dimensional carrier distribution in Ge slab was recorded at  $T=350K$  with the LWIR imaging camera. The base region nearest to the junction (see schematics of contacts in the upper picture) becomes the source of higher (*injection*) or lower (*extraction*) free carrier concentration compared to that at the initial ( $I=0$ ) state. While mapping this sample (scene), the IR camera registers hot or cold regions. (Operation mode:  $\epsilon$ -approach, LWIR, see 5.1.2)

In “long” ( $d > L_d$ ,  $d$  is the length of a base) diodes, the longitudinal distribution of free carriers depends on the voltage and at the extreme mode free carriers are able to

Fig.4,b. IR camera (LWIR) detects forward biased Si p-i-n diode with the  $0,85 \times 0,85 \text{ mm}^2$  emitting area as an object composed of two hot stripes with cold one in between. Schematics of the structure is shown in the lower right corner. Z-axis shows the normalized non-equilibrium charge carrier concentration  $\Delta n = n(I) - n(0)$ . ( $I=150 \text{ mA}$ , operation mode:  $\epsilon$ -approach, LWIR, see 5.1.2)



drift across the base and recombine at the opposite ohmic contact. In the  $n^+$ -i- $p^+$  structure forward bias provokes free carrier injection from both contacts (Fig.4,b). The driving force for the use of the pin junction in our study is the possibility to generate high-level injection process in super large Si scenes operating at high temperatures. For more details see chapter 8.1.4 of this report.

**5.2.2. Free carrier exclusion-accumulation process.** The contact carrier exclusion-accumulation effect in semiconductors<sup>10, 11</sup> with nearly intrinsic conductivity is a successful way to dynamically monitor the electron-hole concentration. In a semiconductor slab with an l-h junction (the junction between heavy-h and lightly-l doped regions) a reverse electric bias results in bipolar longitudinal free carrier drift away from this junction. As a result of the drift, an extended region  $L_{ex}$  (much larger than diffusion length  $L_d$ ,  $L_d > L_{ex}$ ) in the structure base becomes deeply depleted of free carriers (Fig.5). Studies have been reported on the structures made of Ge<sup>16</sup>, HgCdTe<sup>17</sup>, and InAlSb<sup>18</sup>. Contrary to bipolar injection through p-n junction, the exclusion process “works” in nearly *intrinsic semiconductors* and therefore should be considered as a high-temperature effect by the definition. However, like other contact effect, its performance degrades with temperature increase. By our study made in this work, contact exclusion process in Ge is easy to operate up to  $T=150^0C$ . While the junction is forward biased, narrow abrupt free carrier accumulation region forms in the vicinity of l-h junction. Very important to note, that the length of this region  $L_{ac}$  is less than the carrier diffusion length  $L_d$  ( $L_d < L_{ac}$ ). This striking effect details<sup>12-15</sup> and its practical application is the topic of the chapter 8.1.5.

Fig.5. In reversed biased  $p^+-\pi$  junctions ( $\pi$ -is slightly doped p-material which is intrinsic at the temperature of tests) an extended region of free carrier deficit becomes a source of modulated negative light contrast. Changing the bias direction affects the carrier distribution in the opposite way. Two-dimensional carrier distribution in Ge slab ( $d=11, 5$  mm) was recorded with the LWIR imaging camera. The base region nearest to the ohmic contact (shown in yellow in the central picture) remains non-disturbed whereas the most part of a base (cold “blue lake” indicates the exclusion length  $L_{ex}$ ) behaves as a carrier-free region. Lower picture demonstrates accumulation process-hot stripe. ( $I=250$  mA,  $T=350K$ , operation mode:  $\epsilon$ -**approach**, LWIR, see 4.1.2). Z-axis shows the normalized non-equilibrium charge carrier concentration  $\Delta n = n(I) - n(0)$ .

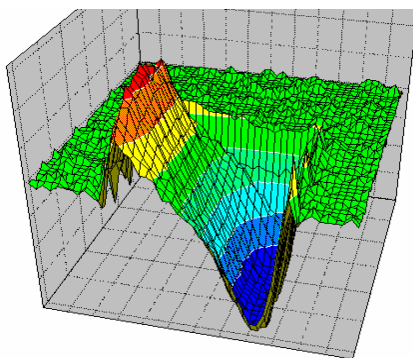
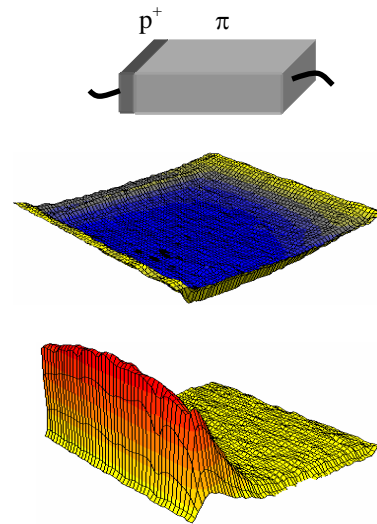


Fig.6. The same as shown in Fig.5 but with right  $p^+$ -contact (symmetric structure). Green flat field is initial ( $I=0$ ) apparent temperature of a scene. By changing the polarity of electric bias, cold and hot regions replace each other.

In the  $p^+-\pi-p^+$  structure contact exclusion effect may be helpful in simulating an object with alternating temperature contrast. In such symmetric structures both accumulation and exclusion processes occurs simultaneously at the contact regions (Fig.6).

**5.2.3. Lorentz force monitors free carrier concentration.** Crossed electric  $E$  and magnetic  $H$  fields can greatly affect the free carrier concentration in the



semiconductor plate with *ohmic contacts* whose thickness is on the order of diffusion length, with different values of surface recombination velocities ( $S_{\min}$  and  $S_{\max}$ ) on the opposite free surfaces (magnetoconcentration effect, MKE, see Fig.7). Being dependent on a direction of the Lorentz force, the transversal carrier drift causes the total carrier value in a plate to increase (drift toward  $S_{\min}$ ) or decrease (drift toward  $S_{\max}$ ) with respect to the equilibrium level. As a result, a semiconductor plate becomes a source of positive or negative luminescence (interband electron transitions) and non-equilibrium TE (intraband electron transitions). MKE is easy to form extended (up to several  $\text{cm}^2$ ) and practically uniform regions of free carrier exclusion or accumulation. But most important is that the effect “works” at the temperatures well above 300 K when the contact way to monitor free carriers through p-n junction cannot be employed in principle. Indeed, the injection efficiency of p-n junction degrades given that the relationship  $E_g \leq kT$  is valid. From the other side, the “generating” ability of a surface with large recombination velocity activates with temperature increase. To date, MKE is exhaustively studied in both wide bandgap (Ge, Si) and narrow bandgap (InAs, InSb, HgCdTe) semiconductors: light emission registered with conventional detectors spans from 2  $\mu\text{m}$  (Ge) to 10  $\mu\text{m}$  (HgCdTe)<sup>19, 20</sup>. For more info see chapter 8.1.2.

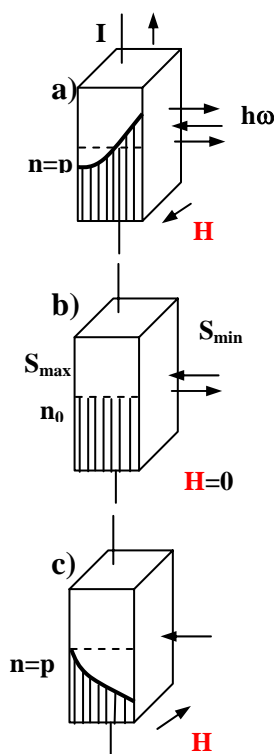


Fig.7. (left). Schematics of a spatial redistribution of free electron and holes in an intrinsic semiconductor ( $n_0=p_0$ ) induced by the Lorentz force ( $\sim ExH$ ). In the initial state ( $H=0$ , picture in the center), there is an equilibrium between absorbed and emitted radiation values ( $\Delta P=0$ ). By changing the direction of magnetic field, it is easy to develop free carrier accumulation (a,  $H>0$ ) or exclusion (c,  $H<0$ ) modes followed by positive  $\Delta P>0$  or negative  $\Delta P<0$  light contrasts “emitted” by the sample.

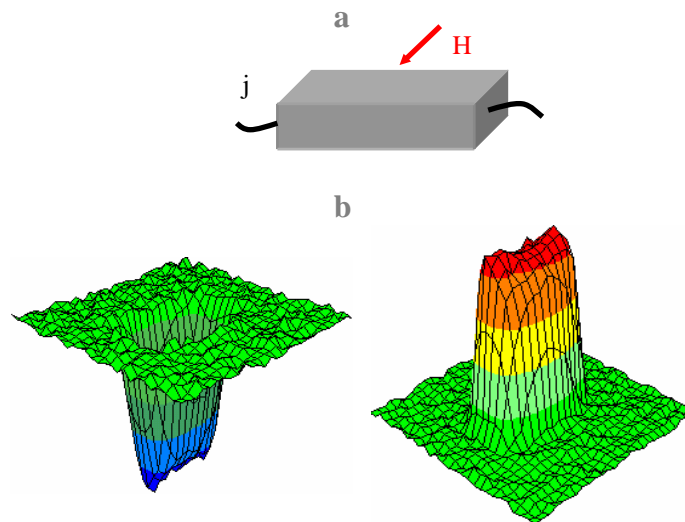


Fig.8. When the transversal carrier drift caused by the Lorentz force (a, E and H fields are parallel to the emitting top surface) directs the electron-hole flow away from/to the top surface, this surface becomes a source of *negative/positive luminescence*. The 3-5  $\mu\text{m}$  IR camera identifies the scene as a cold object or a hot object (b). (InSb, operation mode: **L-approach**, see 5.1.3). Z-axis shows the normalized non-equilibrium charge carrier concentration  $\Delta n = n(ExH) - n(0)$ .

**To resume:** Manipulating the contact nature of a semiconductor scene is easy to monitor free carrier concentration inside this scene followed by electrically controllable light emission. To this end, it is very important to note that the electrical



bias permits to control free carrier concentration in two directions relative to their equilibrium value. In a word, *electrically controllable semiconductor scene when mapped with a thermal imaging camera could be registered as hot or cold objects* even if it's real (thermometric) temperature remains constant.

### 5.3. Contactless ways to monitor free charge carriers in semiconductors.

#### 5.3.1. Band-to-band luminescence.

Luminescence is a contactless, non-destructive method of probing the electron-hole plasma pattern in a semiconductor scene. In the case of photo-excitation ( $\hbar\omega_1 > E_g$ , interband electron transitions), this luminescence is called photoluminescence. The intensity and spectral content of this photoluminescence is a direct measure of various important material properties (see chapter 5.1.3 and region 3 in Fig.3). This process may be used to generate IR image in region 3-fundamental absorption band ( $\hbar\omega_2 > E_g$ ,  $\hbar\omega_2 \sim \hbar\omega_1$ ) also<sup>21</sup>. However, as we have mentioned above, the efficiency of radiative recombination in narrow band semiconductors is rather small for practical application. By this reason, photoluminescence as a way to generate an IR image in both LWIR and MWIR may be considered as a competitive process only at low temperature exceptionally.

**5.3.2. Light down conversion process.** Now we will continue to consider the free carrier photoexcitation process. More specifically, we operate with charge carriers created by irradiating a scene with shorter wavelength quanta  $\hbar\omega_1 > E_g$  (interband electron transitions). The excess carrier concentration  $\Delta n$  depends on carrier diffusion length  $L_d$ , effective carrier lifetime  $\tau$ , intensity of light  $I(\omega_1)$  and can be calculated by the simple expression

$$\Delta n = \beta I(\omega_1) \tau / L_d, \quad 1/\tau = 1/\tau_0 + 2s/d, \quad (7)$$

where  $0.5 < \beta < 1$  is the quantum efficiency of this process,  $\tau_0$  - volume carrier lifetime and  $s$ -surface recombination velocity. The excess free carriers increase the scene absorption coefficient (due to intraband electron transitions) in the longer wavelength band  $\hbar\omega_2 < E_g$  (see eq.5 and region 4 in Fig.3) and therefore modulate TE power provided the scene is initially transparent in this band (light down conversion process). For more details see papers<sup>22-24</sup> and chapter 8.2 of this report.

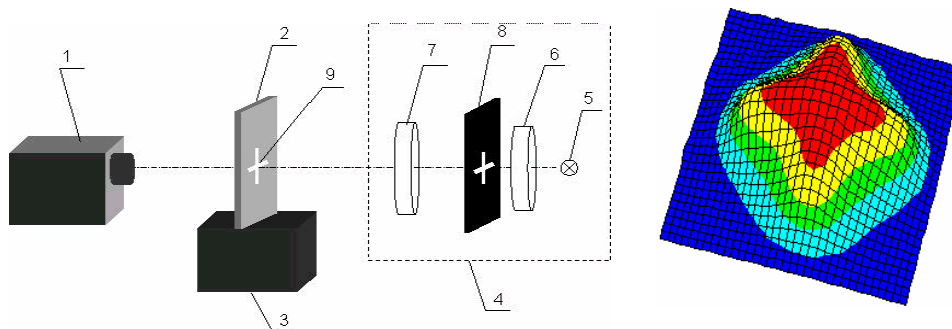


Fig.9. (Left) Light down conversion process. IR camera (1) maps the target (cross, 8) projected at the Ge scene (2) by the *visible* light projector (4, 5, 7, 8) as the hot image (9). The scene is kept at constant temperature by the heater (3).

(Right) Target as it is imaged in the 3-5  $\mu\text{m}$  band. Non accuracy of the image is due to free carrier diffusion process.  **$\epsilon$ -approach**

**To resume:** Light down conversion process appears to become an alternative contactless way to monitor free carrier pattern in a semiconductor scene. It is very important to make a difference between conventional luminescence study (**L-approach**) and thermal emission study ( **$\epsilon$ -approach**). In the L-approach, the image is being generated and investigated in just the same spectral band 3 whereas light down conversion approach permits the testing in longer wavelength spectral band 4.

#### 5.4. Lesson to learn.

For the practical realization of IR imaging there are three fundamentally different concepts. *T-approach* appears as remote classical temperature tests which are well understood and widely discussed in numerous papers and books. As a matter of fact, the parameter to measure is temperature of the *phonon bath*. To get real IR scene temperature, users need to be sure that its thermal emission spectrum is widely distributed (like that of blackbody) in the camera spectral range and emissivity correction is made (given that the target is grey body). Otherwise, so-called apparent temperature of a target “calculated” by camera software will be smaller than real thermometric temperature of a scene. Besides, apparent temperatures tested in different spectral bands may be also different. To the best of our knowledge, this is a standard procedure hardware-in-the-loop facilities operate with. To minimize the risk of making errors, the users operate with highly emissive ( $\epsilon > 95\%$ ) scenes (see Fig.1). By author’s estimate, more that 95% users of thermal imaging cameras work in T-approach.

For the thermal imaging users, *L-approach* is also easy to understand. The trick however is that power emitted and apparent temperature of a scene measured by a camera are not connected to a scene temperature in any way. Indeed, luminescence is one of the responses of the electron-hole subsystem (in semiconductors) to its excitation given that this scene temperature remains stable. The process is effective in direct bandgap semiconductors only and the spectral “content” of the luminescence radiation is strongly connected to a band gap value. Fortunately, luminescence spectra of narrow bandgap semiconductors fall into MWIR (InAs, InSb, PbSe) or LWIR (HgCdTe, semiconductor quantum well structures) bands. Although the luminescence spectra are relatively wide (as compared to a laser emission line), its width is much narrower than camera operating range (author’s rule of thumb: MWIR LED spectra full width at half maximum is of  $0.1 \lambda_{\max}$ ). Because modern fast frame-rate camera’s response is not spectrally flat and cannot conform to a “top hat” profile, there is the error of 10% or more in measuring luminescence power emitted or its equivalent apparent temperature. Addressing these technical calibration issues in more details is beyond the scope of our work. Although our team authorized the first publication on L-approach application to the IR scene testing, we wanted to mention some level of uncertainty in the results obtained. To summarize, we note that the *L-approach* brings users as minimum two doubtless benefits. First, electron transitions in semiconductors happen many times quicker than thermal processes, and second, there possibility exists to simulate both positive and negative contrast across a scene. The last is due to the new physical phenomenon-negative luminescence we introduced into semiconductor physics 25 years ago. To date, only several laboratories around the world are familiar with the L-approach. As to application of this technology to the “simulating” both hot and cold objects in IR, we were first to start this study recently.

Finally,  $\varepsilon$ -approach or transparency modulation technique worth to be mention separately. Indeed, being independent on semiconductor recombination processes nature the approach works identically in both direct band gap and non-direct band gap materials. The TE spectrum of interest is as widely distributed as that of blackbody. Like L-approach, it permits highest frame rate. This makes the approach most attractive for use thermal imaging in research of semiconductor material quality, electronic device performance, properties of contacts, and, what is most important, in design of cost effective robust DIRSPs successful in simulating cold and hot targets. To date, we are the unique team working in such a manner.

## **6. MATERIALS REQUIREMENT AND PROCESSING**

### **(Do we need exotic materials, expensive technologies, and processing?)**

What follows below is the short info on selected fundamental properties of semiconductor materials used in experimental tests.

#### **6.1. Silicon**

a) Si is an IR optical material ( $E_g=1.11$  eV, room temperature intrinsic carrier concentration  $n_i$  is around  $1 \cdot 10^{10} \text{ cm}^{-3}$ ) is easily available with large quantities and dimensions with high purity to suit most electro-optical applications. Silicon's low dispersion and easy fabrication as well as its surface hardness, robust mechanical strength along with non-hydroscopic and non-toxic properties make it very useful optical component. This semiconductor is considered as the material of choice for optical applications in the MWIR band, 3 to 5  $\mu\text{m}$ . But in fact the material may be used in much broader operating range - from 1.2  $\mu\text{m}$  to 12.5  $\mu\text{m}$  given that the sample thickness is as low as 0.5 mm (see Fig.10). In the 3-5  $\mu\text{m}$  band there is no difference in transmission of material of all growing technologies (optical Czochralski-OCz Si, float zone-FZ Si, and high resistively float zone Si). This is not the case, however, when it comes to 8-12  $\mu\text{m}$  band. To minimize initial absorption in this band stimulated by phonon absorption peaks, oxygen absorption, as well as free carrier absorption processes, in this study we used mostly high resistively (to minimize free carrier absorption) float zone (to minimize absorption peaks at 5.8  $\mu\text{m}$  and 9.1  $\mu\text{m}$  induced by oxygen absorption) material. It worth to note, that semiconductor lattice absorption-emission process is a competitive way of energy exchange between a scene and a thermal bath in the spectral range of interest ( $\hbar\omega_2 < E_g$ ). These unavoidable material's "fingerprints" originate from weak many-phonon lattice absorption<sup>25, 26</sup> and are practically negligible in 3-5  $\mu\text{m}$ , slightly distinguished in 8-12  $\mu\text{m}$  but become major source of thermal noise at higher temperatures. (Note: the transmittance does not depend on the crystal orientation).

As shown in Fig.11, due to silicon high refractive index ( $n=3.42$ ), only 53% of light is transmitted through uncoated substrates. To decrease initial IR thermal emission value, we designed and developed broad band antireflection coating on Si substrates

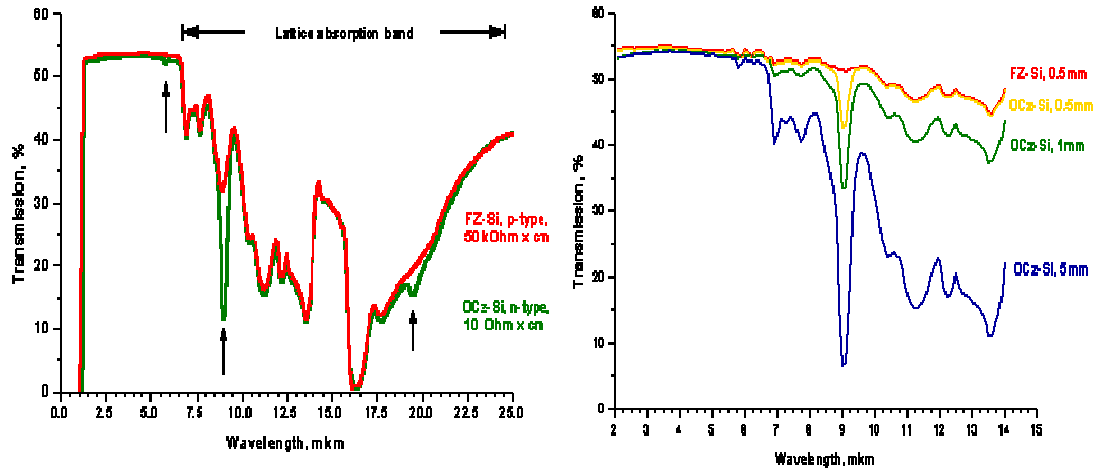


Fig.10. (left) Si transmission in the 1-25  $\mu\text{m}$  spectral range. Arrows point to the oxygen absorption peaks. Sample thickness is 5 mm. (right) Transmission of OCz-Si and FZ-Si with respect to thickness. (<http://www.tydex.ru/materials/materials2/Si.html>)

in MWIR and LWIR bands. The calculation shows that even single-layer ZnS antireflection coating (due to quarter wavelength destructive interference) remarkably decreases the reflection losses in both IR windows. Measured effect of thin-film coating (electron beam evaporating technique,  $T=120^{\circ}\text{C}$ ) at two band transmission is shown in Fig11. Although maximum benefit falls into the foreseen band, non-essential transparency enhancement also occurs beyond this spectral interval. In other words, even a single-layer coating increases TE signal over the whole IR spectral range. However, when it comes to single- or two-band IR emitters tuned at special spectral range, many-layer coating should be employed.

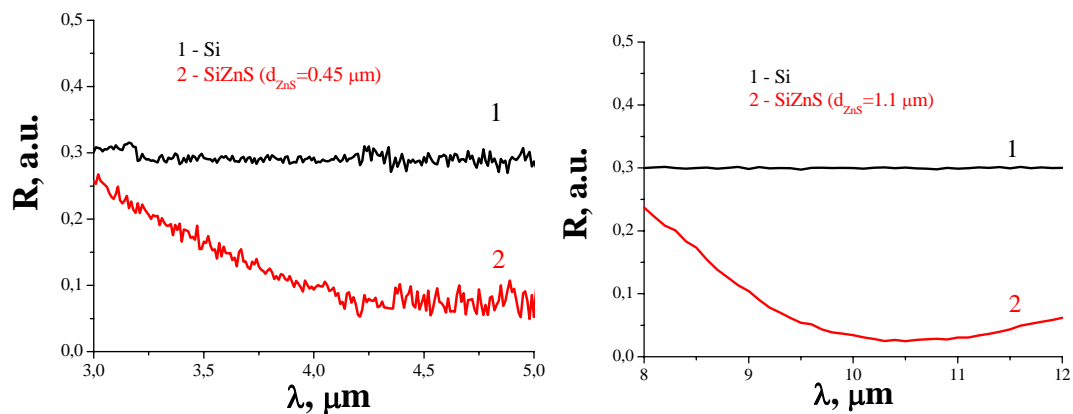


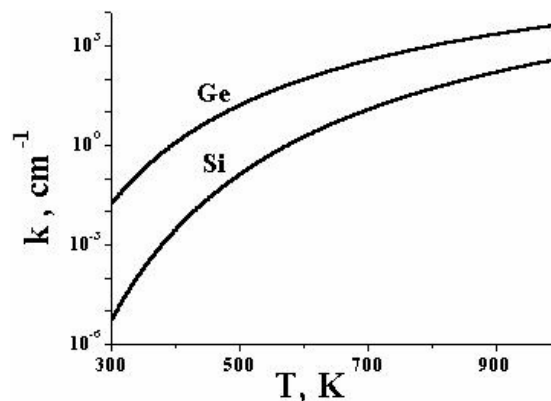
Fig.11. Measured ZnS thin film coating impact at the reflectivity of an optically polished Si plate ( $\rho=40 \text{ k}\Omega\text{cm}$ ,  $d=220 \mu\text{m}$ ) in two spectral bands.  $T=300\text{K}$ .

b) To be as initially transparent as possible, a material should not be heavily doped. Fortunately, at high temperatures ( $T < 400^{\circ}\text{C}$ ) this limitation is easy to satisfy as intrinsic charge carrier concentrations ( $n_i > 10^{10} \text{ cm}^{-3}$ ) in Si (as well as in Ge, see below) are well above the conventional impurity levels.

Charge carrier absorption cross-sections of a quantum of frequency  $\omega_2$  are key parameters of a scene and depend on a material nature (band structure, carrier

effective mass, energy and momentum relaxation time), wavelength and temperature. As a rule, a relation  $\sigma_n < \sigma_p$  is valid but only very little information is available regarding high temperature details for these values even in above mentioned materials. For preliminary estimates we accepted  $\sigma_n + \sigma_p = 7.2 \cdot 10^{-16} \text{ cm}^2$  for Ge and  $4.4 \cdot 10^{-16} \text{ cm}^2$  for Si. These values were experimentally measured only at  $\lambda = 10.6 \mu\text{m}$  and  $T = 300 \text{ K}$ . By using these quantities and temperature dependencies of intrinsic charge carrier concentrations, the absorption coefficient value  $k = n_i (\sigma_n + \sigma_p)$  versus temperature is shown in Fig.12. These data may be used for preliminary estimates of a scene thickness at different temperatures.

Fig.12. Temperature dependence of absorption coefficients in Si and Ge in the range of intrinsic conductivity. Estimates are based on parameters referred in the literature.



c) Like material band structure, microscopic nature of carrier recombination routes (radiative or non-radiative processes) has no effect on light down conversion. Meanwhile, direct impact of charge carrier lifetime is twofold. First, the higher  $\tau$  value the lower visible light intensity  $I(\omega_1)$  to operate with (see eq.8). Secondly, carrier lifetime is also responsible for rise-fall time of down conversion process and image frame rate. Therefore, details of carrier lifetime dependencies versus temperature (see Fig.13) and visible light injection level are of prime importance.

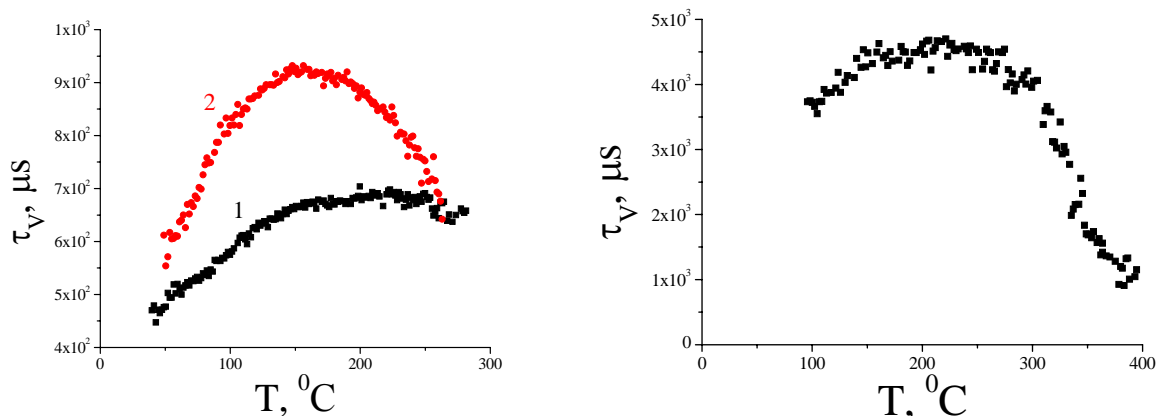


Fig.13. Measured temperature dependencies of carrier lifetime in Si of different p-type (left,  $\rho=11 \text{ k}\Omega\text{cm}$ ) and n-type (right,  $\rho=40 \text{ k}\Omega\text{cm}$ , FZ). Data from the left indicate how the quality of crystals affects their carrier lifetime: 1-OCz Si, 2-FZ Si).

But there is a second problem of even greater importance. At higher temperatures when a scene thickness becomes shorter than the carrier diffusion length ( $n_i$  increase

should be compensated for by decrease of a scene thickness  $d$ ), surface recombination processes cause additional uncertainty in scene transient characteristics and spatial distribution of charge carriers. Besides, the efficiency of down conversion process degrades. Special care therefore is to be taken to stabilise scene surface properties.

By our measurements, surface recombination value in Si (conventional chemical etching process) at higher temperatures was estimated to be as high as  $10^3$  cm/s and remained stable along the temperature range of our study. Carrier lifetime values scatter from some tens ms (high quality crystals) to some  $\mu$ s (intentionally doped material).

d) There is variety of technologies of getting p-n junction in Si. In our work, we employed the simplest and easy to develop diffusion process. Heavy doped  $p^+$ - and  $n^+$ -regions to n-Si were made by thermal diffusion process of B (boron) and (phosphorus) into n-Si ( $\rho=300$   $\Omega$ .cm, Wacker production). Some structures are made by the ion implantation process.

**Details of the ion implantation doping process.** It is the process by which ions of doping materials accelerated to a high energy are implanted into material-target, thereby changing its near-the-surface doping level. When implanted in a semiconductor, each dopant atom creates a charge carrier in the semiconductor (hole or electron, depending on if it is a p-type or n-type dopant), thus modifying the conductivity of the semiconductor. Because ion implantation causes damage to the crystal structure which is unwanted as drastically decreases carrier lifetime, ion implantation processing is followed by a low temperature thermal annealing. The value of doping level is the integral over time of the ion current; the penetration depth depends on ions energy. In our experiments, the ions energy was of 145 keV (penetration depth of 0, 35  $\mu$ m, shallow junction); integral dose - on the order of  $10^{18}$  cm<sup>-3</sup> doping atoms.

**To resume:** High quality of Si crystals, its initial transparency in IR (mostly in MWIR), low intrinsic carrier concentration  $n_i$  at moderate temperatures ( $T < 400^\circ$  C), as well as the ability to monitor carrier lifetime (using doping or surface treatment) make this material prosperous one for applications in IR dynamic scene simulation devices based on enhancement modulation technique (we mean both light and contact injection approaches).

## 6.2. Germanium

a) OCz Ge transmits in the IR range, from 1.8 $\mu$ m to 23 $\mu$ m with reflection loss: 52.9% at 10.6 $\mu$ m (2 surfaces). This is a very versatile infrared material ( $E_g=0.67$  eV, room temperature intrinsic carrier concentration  $n_i$  is around  $3 \cdot 10^{14}$  cm<sup>-3</sup>) used commonly in imaging systems and instruments in the 2 to 12 $\mu$ m spectral region. It is utilized as a substrate for lenses, windows, and filters and demonstrates the lowest loss till reported for IR materials ( $K < 0.03$  cm<sup>-1</sup> at 10.6  $\mu$ m). Ge is non-hygroscopic and non-toxic, has good thermal conductivity, excellent surface hardness and good strength. Most important is that contrary to Si, there is no lattice absorption “fingerprints” over all IR band of interest. To decrease IR initial thermal emission value we designed and developed broad band antireflection coating on Ge substrates in MWIR and LWIR bands using both ZnS (electron beam evaporating technique) and CdSe (thermal sputtering) transparency coating.

b) To be as initially transparent in the IR as possible, a material should be slightly n-doped. Calculations show that due to asymmetry in free carrier absorption cross section ( $\sigma_n = 0.15 \cdot 10^{-16}$  cm<sup>-3</sup>,  $\sigma_p = 6.5 \cdot 10^{-16}$  cm<sup>-3</sup> at 10.6  $\mu$ m) initially n-doped Ge ( $\rho \sim 10$  -20  $\Omega$ .cm) demonstrates maximum transparency at room temperature. Also important is that the favourite doping level strongly depends on the temperature what is due to a compromise between dopant level  $N_d$  and intrinsic carrier concentration  $n_i$  (Fig.14).

As a result, efficient operating in down conversion mode at higher temperatures demands for heavier crystal doping (Fig15.).

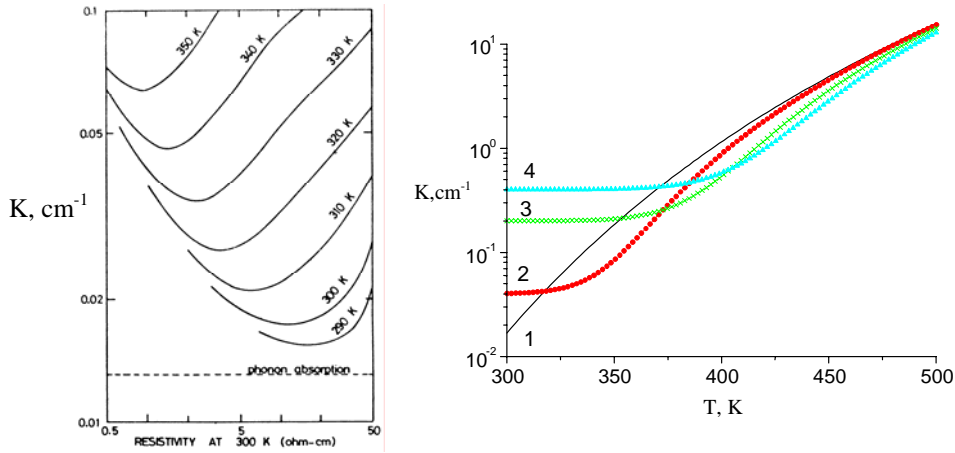


Fig.14 (left). Theoretically predicted absorption near its minimum value at various temperatures at 10.6  $\mu\text{m}$  in n-Ge<sup>27</sup>.

Fig.15 (right). Calculated absorption coefficient of Ge vs temperature for different doping levels at  $\lambda=10.6 \mu\text{m}$ : 1 – intrinsic material, 2 –  $N_d = 1 \cdot 10^{15}$ , 3 –  $N_d = 5 \cdot 10^{15}$ , 4 –  $N_d = 1 \cdot 10^{16} \text{ cm}^{-3}$ .

c) Carrier lifetime in OCz Ge is on the order of 1-4 ms (diffusion length is on the order of some ms) and is easy to control by doping and surface treatment. Typical  $\tau_{\text{eff}} = f(T)$  dependencies for different doping level and thickness are shown in Fig.16, 17. There is no problem with material polishing and etching and surface recombination values as low as 100 cm/s is easy to achieve. While tested at the air, this value, however, degrades during heating up-cooling down cycles. Also important is that due to larger asymmetry of hole and electron absorption cross sections, n-doped material has to demonstrate larger  $P_{\text{max}}/P_{\text{min}}$  value compared to that for Si. As a matter of fact, IR light couples very strongly with holes, since the energy associated with direct transitions between valence sub bands is in MWIR and LWIR energy scales.

d) To monitor non-equilibrium carrier concentration in Ge, we used technology of alloyed contacts of different nature ( $p^+ \text{-n}$ -junction for injection processes and  $p^+ \text{-p}$  for exclusion processes). It is important to note, that by our tests, such low temperature treatment does not affect a material carrier lifetime. Some structures are made by the ion implantation process followed by low temperature annealing process.

**To resume:** High quality Ge crystals demonstrate record initial transparency in IR (MWIR and LWIR), and comparably low intrinsic carrier concentration  $n_i$  at moderate temperatures ( $T < 300\text{C}$ ), as well as the ability to monitor carrier lifetime (using doping or surface treatment). All these qualities make this material a competitor to Si for applications in IR dynamic scene simulation devices based on enhancement modulation technique (we mean both light and contact injection approaches). However we have to remember, that due to smaller bandgap energy the material opaqueness takes place at low temperature compared to that for Si. For comparison, initially neglected absorption coefficient ( $k \sim 10^{-2} \text{ cm}^{-1}$  at 10.6  $\mu\text{m}$ ) grows to  $k = 1 \text{ cm}^{-1}$  at  $T = 150^\circ\text{C}$  comparable to Si where this event happens at  $T = 400^\circ\text{C}$ .

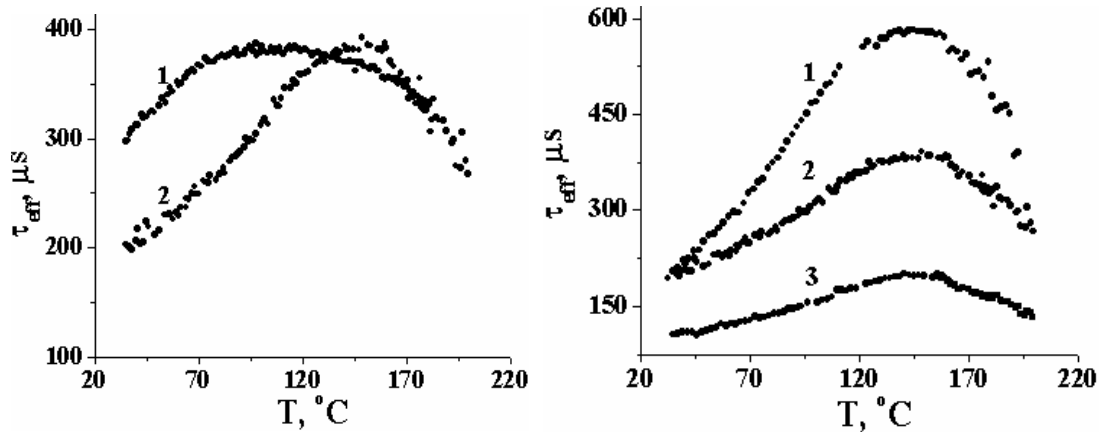


Fig.16 (Left). Measured effective carrier lifetime vs. temperature dependence in bulk n-Ge (1-  $\rho=3$   $\Omega\text{cm}$ ; 2-  $\rho=0.1$   $\text{ohm}\cdot\text{cm}$ ). Fig.17 (Right). Measured effective carrier lifetime vs. temperature dependence in n-Ge ( $\rho=0.1$   $\text{ohm}\cdot\text{cm}$ ) samples of different thickness (1- $d=9\text{mm}$ ; 2-  $d=3.5\text{mm}$ ; 3- $d=2$   $\text{mm}$ ).

### 6.3 InAs-based compounds

InAs is a narrow bandgap semiconductor ( $E_g=0.35$  eV, room temperature intrinsic carrier concentration  $n_i$  is around  $2\cdot 10^{15}$   $\text{cm}^{-3}$ ). It is available in bulk, grown using the Czochralski method as well as in substrates both n- and p-type doped over the range from  $5\cdot 10^{15}$  to  $10^{18}$   $\text{cm}^{-3}$ . This makes InAs a useful material for devices targeted at very high-speed electronics and IR optoelectronics. In particular, there are two major commercial families of MWIR LEDs-those grown on InAs substrates and those grown GaSb substrates.

InAs-based LEDs are formed from alloys of Ga, Sb, P grown in compositions lattice-matched to InAs. Their peak wavelengths depend on alloy composition and span from  $3.4$   $\mu\text{m}$  (InAs) to  $4.8$   $\mu\text{m}$  (InAsSbP) with different on-demand-positions in between with common commercial ones being at  $3,4$   $\mu\text{m}$ ,  $3,7$   $\mu\text{m}$ ,  $3,9$   $\mu\text{m}$ ,  $4,2\mu\text{m}$ , and  $4,5$   $\mu\text{m}$ , which are supposed to be used in gas analysis. The structures can be grown by liquid phase epitaxy (LPE), metal organic chemical vapor deposition (MOCVD), and molecular beam epitaxy (MBE) processes. In this work, we employed the simplest and easy to develop LPE process as cost-effective choice for MWIR optoelectronic devices. Thus, all types of quantum well or superlattices structures remain beyond the scope of the work. We believe that LPE structures could form the basis of parameters (like power emitted or apparent temperature) from which estimates are to be made when it comes to more expensive technologies.

There is variety of emitting structures types ranging from conventional p-n junction, single and double heterostructures to recently grown superlattices and multiple quantum wells. All the structures don't need the cooling and when positively biased (conventional luminescence mode) demonstrate as high power emitted as some mW with the efficiency (power out/power in) on the order of a few percents). It was shown recently that InAs-based compounds when reverse-biased could be used as the scenes able to simulate negative contrasts (negative luminescence mode<sup>28-31</sup>).

**Details of the LPE technology.** LPE is a relatively simple production method for compound semiconductors. Owing to its comparative simplicity, LPE has been mainly used for fabricating



heterostructures and related devices since the middle 1960s. The compounds to be deposited (active LED bodies) are liquefied under normal pressure and the wafer is then bathed in the fluid. The advantage is that thick layers can be produced very quickly. Also LPE allows the processing of quite large surface areas. The disadvantage is that such layers cannot be finely dosed contrary, for example, to molecular beam epitaxy (MBE) or metal-oxide compound vapor deposition (MOCVD). These last two allows for greater active body purity due to the reduce pressure held in the reactor. For this reason, LPE process is believed to be generally only used for weaker LEDs. Keeping in mind the producing of the cheapest devices we have developed standard liquid phase epitaxy as the technology base for MWIR band.

The base material (substrate) on which the liquid mixture is deposited consists of p-or n- type InAs (111) monocrystals with majority carrier concentration of  $2 \cdot 10^{16} \text{ cm}^{-3}$  and of 100-300  $\mu\text{m}$  thick. For this, the structures grown are easy to handle. Zn or Mn was used as a p-dopant for p-n junction formation during the growth. The thickness of the top layers is about 5-10  $\mu\text{m}$ .

Active layers for LEDs operating in the spectral range up to 3,3 $\mu\text{m}$  InGaAs compounds are used. In this case there is no problem with good lattice matching of active layers and substrate. LEDs beyond 3,3 $\mu\text{m}$  are prepared from InAsSb/InAs mismatched and InAsSb/InAsSbP/InAs matched heterostructures. These structures are grown at InAs plasticity temperatures (650-720C). In order to eliminate lattice-mismatching effect at active layer parameters the 40-100 $\mu\text{m}$  thick graded InAsSbP layer are created during the growth. In this case, most of the dislocations caused by mismatch between the lattice parameters of the InAs substrate and the solid solution are located in the InAs substrate and at the InAs/InAsSbP interface, far from junction and the emitting region. LED active bodies are cleaved out along (110) direction edges that are perpendicular to the LED top surface. Current leads are soldered to the crystal with indium and the radiation is coupled out through InAsSbP layer and the InAsSb substrate. In some cases InAs substrates are etched off after growth (LED structures free of substrate).

The method also involves growing a graded-index InAsSbP layer under condition where the InAs substrate exhibits high plasticity so that the mismatch stresses relax by preferential formation of dislocations in the substrate, accompanied by bending.

Owing to its comparative simplicity, LPE has been mainly used for fabricating heterostructures and related devices since the middle 1960s. The leading sites are Ioffe Institute of S. Petersburg (Russia) and The Lancaster University, Lancaster, GB.

**To resume:** InAs-based compounds are commonly used materials for IR MWIR emitters. The variety of technologies and structures available form the base for further development targeted at IR dynamic scene simulation devices.

#### 6.4 Indium Antimonide

Indium Antimonide is a narrow bandgap semiconductor ( $E_g=0.17 \text{ eV}$ , room temperature intrinsic carrier concentration  $n_i$  is around  $2 \cdot 10^{16} \text{ cm}^{-3}$ ) with very high electron mobility. Carrier life time at  $T=300\text{K}$  is on the order of some nanoseconds, carrier diffusion length is  $\sim 20 \mu\text{m}$ . It is ideally suited for use in IR detectors providing excellent performance in the 1 to 5.5  $\mu\text{m}$  wavelength band when cooled up to 77K. Photoelectromagnetic optical detectors can operate without cooling. The high mobility of InSb may also allow it to play an important role in very high-speed electronics, where InSb or its alloys could be the narrow bandgap material in a heterojunction.

It is readily available in bulk, grown using the Czochralski method, in sizes up to 85mm. InSb can accept both n- and p-type doping over the range from  $10^{14}$  to  $10^{18} \text{ cm}^{-3}$ . Indium antimonide can be supplied as ingots or ingot sections or as-cut, etched or polished. Technology of surface and contact treatment doesn't cause problem.

It was shown recently, that the material could provide an alternative platform as starting material for MWIR LEDs. Most important is that the LEDs operate at room temperature and demonstrate positive and negative contrasts.

**To resume:** Basing on our previous achievements in the field, in this work we develop and test MWIR emitter made of this material and operated in crossed electric

and magnetic fields (MCE configuration, see 5.2.3) As an example of practical realization of the idea, we will design the 8x8-element array and experimentally estimate performance of the device with stress made on extreme values of negative and positive apparent temperatures of point and extended targets the device could simulate. We also consider the problem connected to design a 256x256-element array and indicate this device's pros and cons.

### 6.5 Lesson to learn

As one can see, our material platform is based on well-known semiconductor materials, like Si, Ge, and III-V compounds. Their parameters are well studied and referred in variety of papers, books, and electronic libraries. All these materials are easy to grow or request from a variety of companies around the world. They may be supplied as ingots or slices (with thickness  $\geq 100 \mu\text{m}$ ) with polished or etched surfaces. They may be grown as pure or intentionally doped materials practically unlimited dimensions. The majority of the processes required in making active devices of our concern are fairly standard in the modern semiconductor technology. Each of these processes, if taken individually, is quit easy to master given adequate processing equipment. We don't need quantum wells or quantum dots, as well as we don't need such expensive technology like MBE. Finally, all these materials are cost-effective products in semiconductor industry.

The horizon, however, is not as bright as it could be.

Indeed, practical applications of Ge are limited to the passive optics devices, like filters or lenses operated at room or lower temperatures. Si platform comprises the modern base of electronics with strictly recommended high-temperature operating limit  $T < 150^\circ\text{C}$ . However, when it comes to optoelectronic devices, like IR emitters of our concern, the problem number one is electron and hole behavior (carrier lifetime, surface recombination velocity, diffusion length, and contact properties) at higher temperature, well above room temperature. We meet the situation when major electron and hole parameters (like carrier lifetime, surface recombination velocity, absorption coefficient in IR and so on) as well as their evaluation in temperature scale  $T > 150^\circ\text{C}$  are not defined. Moreover, sometimes they are even difficult to predict. Finally, there is no information on how these parameters could resist temperature cycling in air and in a vacuum (we mean high-temperature annealing processes resulting in generation of thermal donor-acceptor impurities).

The said remains valid for InSb, which was considered until recently as the low temperature device (1-5.5  $\mu\text{m}$  detector operated at liquid nitrogen temperature). Yet the prospects for InSb are not really dark, because they appear to have applications reaching far beyond this area. As a matter of fact, we were first to propose high-temperature operated IR emitter based on this material. Then, the idea was further widely treated by scientists from the USA, United Kingdom, and Japan. Thus, while starting this work, the idea of using this material as an IR emitter was taken as granted. The problem is in providing both design and experimental study targeted at achieving efficient single and array emitters capable of simulating the scene with positive and negative contrasts. Without experimental test, it is impossible to predict how much these values could be...

When it comes to InAs-based devices, our task will be optimization of an emitting structure (made as planar and mesa and grown by LPE). The point is that all these structures have one thing of common: so-called current crowding effect drastically limits emitting area value ( $< 1\text{mm}^2$ ). Also it causes spatial non-uniformity in light emitted which is dependent of bias current. Therefore, design of point IR source looks

problematic one not to say on 2D emitting arrays. This work is currently underway around the world...

## **7. HARDWARE-IN-THE-LOOP FACILITY (What we can but others can't)**

Unlike to the situation in the market of visible light sources with highly developed and acceptable both customers and designers technology of device resting, there is no standard till now for measuring the characteristics of DISPs. In response to the later, we have developed the strategic move: the high-resolution IR “vision” facility is deployed at the Institute of Semiconductor physics in Kiev, Ukraine<sup>32-34</sup>. To this end, we consider in details our unique experimental set up capable of high-resolution time-resolved multispectral study of IR scene and its key parameters. Also using three approaches discussed in details in the chapter 5.1, we will demonstrate this diagnostics superiority over existing technologies by capturing and discussing some different IR scenes composed of point and extended targets in visible, MWIR, and LWIR.

### **7.1. Multispectral micro imaging set up**

Targeted at mapping of heat and light emitted by single semiconductor device we have developed high-resolution multi-spectral test system (Fig.18). This system key element is an IR reflection microscope co-axially attached to a calibrated scanning IR thermal imaging camera (3–5 or 8–12  $\mu\text{m}$  spectral ranges, InSb and MCT cooled photo detectors, scene spatial resolution of  $<20 \mu\text{m}$  and temperature resolution of  $0.1^\circ\text{C}$  at  $30^\circ\text{C}$ ). The frame exposition time varies from 50–400  $\mu\text{s}$  (single line frequency, signal profile) to 40 ms (full frame frequency, 2D signal map). The minimum time-resolved interval is 10  $\mu\text{s}$ , spatial resolution is of  $<20 \mu\text{m}$ , and temperature resolution and accuracy are  $0.1^\circ\text{C}$  and  $0.5^\circ\text{C}$  respectfully. The recording system operates up to 25 fps at full image size and generates a TV-like false-color image. Data acquisition and image processing (test image, emissivity equalization, noise reduction by image averaging, external triggering and area of interest scanning capability) are computer-controlled. A parallel video channel equipped with CCD camera permits easy positioning and focusing of a  $<1 \times 1 \text{mm}^2$  object. The CCD camera (combined with a conventional optical microscope) can also be used to map the 2D distribution of light ( $<1 \mu\text{m}$  spectral range) emitted by near-IR devices. As a matter of fact, this set up is multi-spectral (two IR bands and visible channel) assembly.

The parameters of interest are apparent temperature  $T_a$  or IR power emitted  $P$ , which are connected by the calibrated signal transfer function. The micro imaging set up with radiometric and thermographic calibrations may be synchronized with current bias pulse ( $I$ ) in such a manner that the picture of interest appears at the second frame  $P(I)$ , whereas the first frame captures the background (zero-biased) image  $P(0)$ . By subtracting these frames one can get a dynamic emission map provoked by bias current,  $\Delta P = P(I) - P(0)$ .

The advantage of our multi-spectral approach is that it not only permits scanning local area of interest, while biasing the device by electric pulses of different durations ( $\Delta t$ ) and duty cycles (dynamics of light and possible heat signal combined). It also permits the study of 2D heat relaxation processes when the map is being measured with a given delay (say,  $\Delta t + 10 \mu\text{s}$  and longer) after the current pulse is turned off (dynamics and pattern of heat process only). In a word, the technique can provide information related to three dimensions - two spatial dimensions and time. Naturally, this heat

distribution could be tracked also by using a longer (8–12  $\mu\text{m}$ ) wavelength camera, therefore being insensitive to actual light emitted by LEDs or lasers. Some examples of what we can in analyzing properties of IR scene are shown in the next chapter.

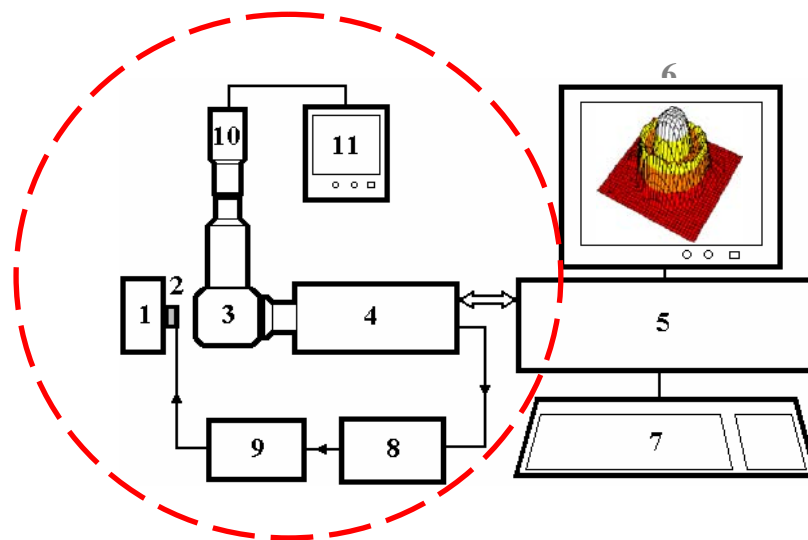


Fig.18. Multispectral microscope assembly.

1 - X-Y-Z positioning system and temperature controller; 2 – unit under test; 3- IR microscope; 4 - IR scanning camera; 5 system controller; 6- color monitor for IR image visualization; 7- input and start unit; 8 - synchronization system; 9- power supply; 10 - CCD camera; 11 - display for device positioning.

The advantage of our multi-spectral approach is that it not only permits scanning local area of interest, while biasing the device by electric pulses of different durations ( $\Delta t$ ) and duty cycles (dynamics of light and possible heat signal combined). It also permits the study of 2D heat relaxation processes when the map is being measured with a given delay (say,  $\Delta t + 10 \mu\text{s}$  and longer) after the current pulse is turned off (dynamics and pattern of heat process only). In a word, the technique can provide information related to three dimensions - two spatial dimensions and time. Naturally, this heat distribution could be tracked also by using a longer (8–12  $\mu\text{m}$ ) wavelength camera, therefore being insensitive to actual light emitted by LEDs or lasers. Some examples of what we can in analyzing properties of IR scene are shown in the next chapter.

**To resume:** To date we are happy to claim that our multispectral microscope assembly is the only set up in the world capable of demonstrating following parameters: field of view -1,4x1,4 mm, spectral ranges 3-5 & 8-12  $\mu\text{m}$ , temperature resolution- 0,1K, spatial resolution-20  $\mu\text{m}$ , frame duration-40 ms, single line duration-400  $\mu\text{s}$ , part-line-on demand scan-10  $\mu\text{s}$ , rise-fall time-10  $\mu\text{s}$ , CCD microscope-conventional. We also expect the set up could help adequately translate the advantages of different types of DISP into simple benefit that could compel designers to switch to the best solution. By the author's opinion, *the testing technology we developed is of prime interest to the scientists at Eglin AFB (FL), Kirtland AFR (Albuquerque, NM), and WPAFR (Dayton, OH). US Army Labs are Army Research Laboratory (Adelphi, MD, Army Missile Command's Research, Development, and Engineering Center (Redstone Arsenal, AL) and Naval Research Laboratory (Washington, DC).*

## 7.2. What we can detect, identify and classify

**T-approach.** Now we start with conventional and, therefore, easy-to-understand T-approach. Our object will be IR thermal micro emitters (operating as Joule heaters). Indeed, the radiation these devices emit is real widely distributed blackbody radiation ( $\epsilon \approx 1$ ), whose characteristics are determined solely by the temperature of an active element. By this reason, the tests are performed with LMIR camera. In a word, we capture the most part of black body radiation.

To date, two-dimensional thermal resistor arrays based on electrically heated pixels  $0.2 \times 50 \times 50 \mu\text{m}^3$  (fabrication of a  $1024 \times 1024$  array comprises problem of price but not technology) are the most promising dynamic IR scene projectors operated in the  $3\text{--}12 \mu\text{m}$  spectral range. The devices are widely used for the evaluation of electro-optical seekers and thermal imaging cameras (both military and civil application) by simulating IR synthetic like-“true” scenarios composed of a target-on-background picture. These micro membrane structures (Fig.19a) are made using the modern MEMS technology and capable of simulating objects with temperatures as high as  $500^\circ\text{C}$ . However, significant disadvantages to these planar devices are their many-layer structures and tiny legs, which are used as a membrane’s electric contact and mechanical supporters. The membrane is placed at the distance of  $2.5 \mu\text{m}$  above a Si substrate creating an optical cavity, from which optical interference is used to tune the spectral emission band. Thermal and mechanical stresses between the layers and negligible leg deformation provoked by a current affect the resonator quality and drastically decrease IR power emitted. Because these slight deformations are difficult to identify in optical microscopes or by measuring emitter resistance, it is the IR micro vision that could help. Indeed, by comparing  $T_a$  value and its spatial distribution across membrane surface (Fig.19b, c), non-efficient pixel is easy to detect.

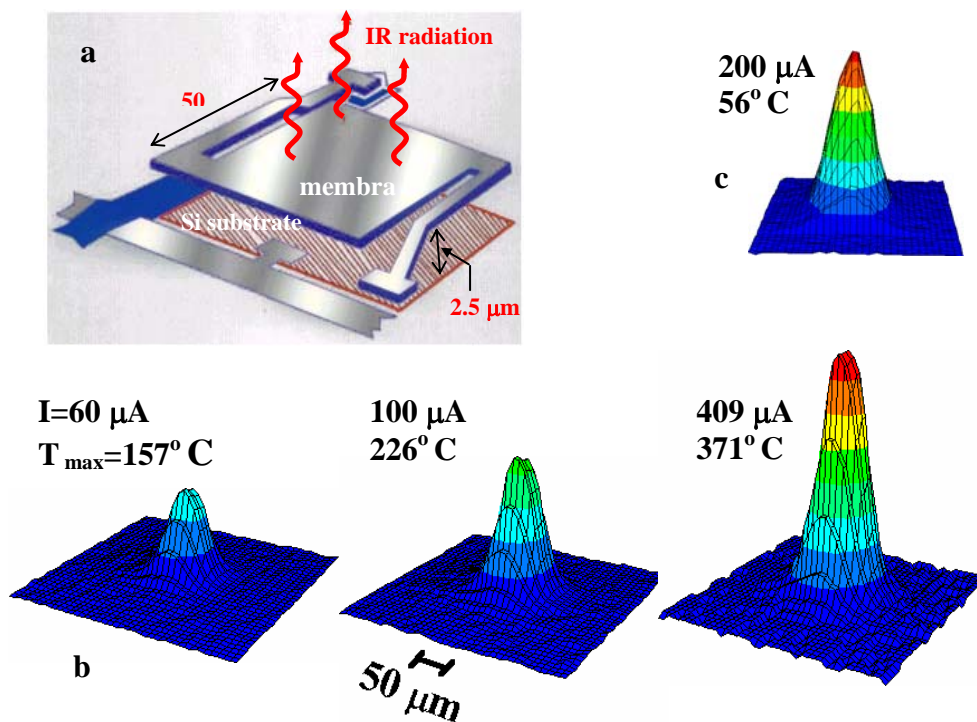
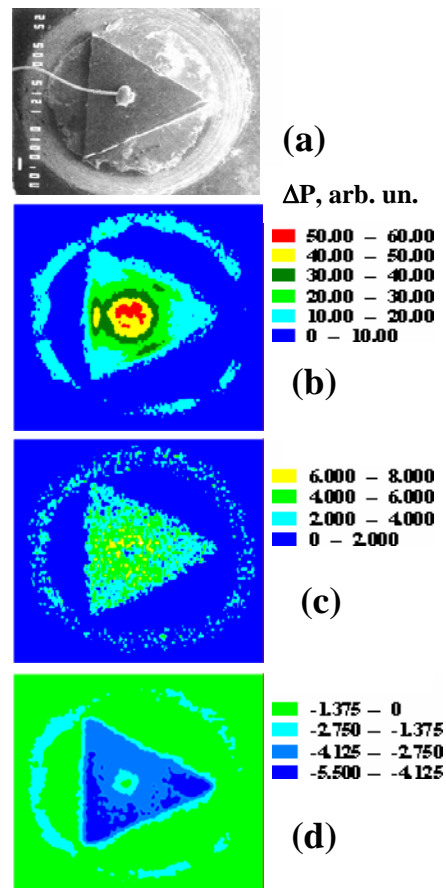


Fig. 19. (a) Schematics of single micro emitter. (b) IR image of this device captured with 8-12  $\mu\text{m}$  camera at different bias currents  $I$ . (c) IR image of the device with resonator cavity deformed by Joule overheating. This mechanical degradation results in lower apparent temperature and deformation of the active device area. LWIR, 160 ms frame duration. The device under test is IMEC (Belgium) production.

**To resume:** record (for LWIR band) spatial resolution of our experimental set up has permitted (for the first time) easy analyzing most advanced IR dynamic scene (thermal micro emitters) simulation device: the apparent temperature, spatial distribution of emissivity, problem connected to pixel degradation.

*Information for our Partner. The author as a NATO scientific expert was visiting IMEC (Leuven, Belgium) recently. This .gov site is involved in advanced technology of MEMS devices. In particular, their technology of Si membrane IR detectors was taken as the ground in the attempt to grow the IR micro emitter. Contrary to the SBIR (US) proprietary many-layer structure, IMEC's people developed single layer emitter which is more robust, stable and cheaper to grow<sup>35</sup>. By the author opinion, IMEC's technology could compete that of SBIR, which currently dominates the market.*

**L-approach.** Next, we complicate the task by testing the real "light" IR LEDs emit. Tests are performed with InAs-based LEDs, testing system is tuned at MWIR. Conventional LED structure ( $\lambda = 4.3 \mu\text{m}$ ) is fabricated from graded InAsSbP layer LPE grown on the  $n$ -InAs (111) substrate. The  $p$ - $n$  junction was formed during the 5  $\mu\text{m}$  thick  $p$ -InAsSb(Zn) layer growth on a 80  $\mu\text{m}$  thick  $n$ -type "window" layer with band gap increasing towards the substrate, thus being transparent for radiation escaping through the broadband InAsSbP surface (as a matter of fact we are dealing with so-called substrate up structure). The  $p$ -InAsSb/ $n$ -InAsSbP structure is cleaved along the {110} planes into triangles with sides of about 600–700  $\mu\text{m}$  and soldered to a TO-18 header ( $p$ -side down). Small-area (about 50  $\mu\text{m}$  in diameter) top contact at the triangle center is made by In soldering (see Fig.20a). The reflective ring of the TO-18 header contributes to concentration of light laterally escaping from the structure.



at the triangle center is made by In soldering (see Fig.20a). The reflective ring of the TO-18 header contributes to concentration of light laterally escaping from the structure.

Fig. 20 b,c,d show typical two-dimensional (2D) distribution of apparent temperature of IR radiation emitted by the LED structure at different bias currents<sup>36,37</sup>. The maps were measured at the device temperature of 46<sup>0</sup> C, defined as the temperature of black deposited on the device bar. As one can see, when the device is turned on at positive bias ( $I > 0$ ), then conventional band-to-band luminescence appears along the device surface, while the dip in the middle of the die is due to the opaque ohmic contact pad. Reverse bias ( $I < 0$ ) provokes NL signals causing effective scene (but not contact pad) cooling. The said is clearly seen also as "hot" and "cold" crowns, what as a matter of fact is the "mark" of light laterally escaping the die and reflected by ring wall of the bar.

Fig.20. Scanning electron micrograph of the device (a). IR maps of light emitted through the "window" layer in the forward (b), (c)  $I = 600$  and  $50$  mA respectively and reverse (d)  $I = -50$  mA bias modes. The  $\Delta P$  values and their false colors are shown from the right in arbitrary units. MWIR, 160 ms frame duration.

At small positive bias current ( $I = 50$  mA), the spatial distribution of power emitted indicates slight light crowding seen as smaller apparent temperature values registered in the triangle vertexes compared to those for central part of the die. This difference becomes, however, more remarkable as the current grows. Really, at  $I = 800$  mA the light emitted symmetrically concentrates around the top contact, while triangle vertexes remain practically "cooled". Moreover, narrow bright light strips visible in the central part of cleaved edges are likely to appear as the result of reflection and scattering the light escaping the structure while laterally travelling from the crowded region. And the contrary, reverse bias provokes NL distribution practically free of any signs of crowding. As a result, the whole structure area is used for light generation and extraction.

**To resume:** L-approach demonstrated that current crowding effect (CC, forward bias) remarkably affect the spatial distribution of light emitted by high temperature operated IR LED. More specifically, at higher current values noticeable device area becomes practically non radiative, whereas light concentrates in the vicinity of top point contact and follows its symmetry. Moreover, this CC provokes remarkable decrease of the light laterally escaping the structure. Due to small resistance of emitting layer this effect is not avoidable in principle in forward bias mode. And contrary, reverse bias mode looks more attractive due to current spreading that provokes practically uniform spatial distribution of negative luminescence. The experimental results correlate with our numerical 3D-modeling of current flows in three layer structure composed of two p- and n- type cladding layers and active p-n junction in between. From the practical point of view, we demonstrate how point IR source could be developed using conventional planar structure. Indeed, while monitoring the scene apparent temperature by bias voltage the emitting surface remains the same.

**$\epsilon$ -approach.** Finally, we show how to test the performance of electronic devices whose excess IR radiation is the result of dynamically modulated scene transparency. More specifically, the conditional "target" is composed of indirect band gap semiconductor and therefore generates (if any) negligible luminescence signals (L-approach does not work). Besides, the target is kept at constant temperature  $T > 300$ K and therefore T-approach does not work also. Keeping in mind Ge and Si feasibility as the most acceptable materials for DIRSPs we developed, shown below are some details of these devices quality. Finally, the  $\epsilon$ -approach is unique tool to study the non-equilibrium properties of electronic devices and components made of indirect-gap materials (like Ge, Si) and therefore generating negligible luminescence signals.

As an example shown below, the object is electrically driven target. Parameters of interest are spatial distribution of excess charge carriers  $\Delta n$  in the device base, uniformity of contact properties, and surface effect impact. A priori, it is assumed that excess charge carriers occupy the whole device base, contact properties are spatially uniform, and surface effect on charge carrier generation-recombination processes is negligible. Here we show what is happening in the reality.

Fig.21 demonstrates the results of IR mapping (LWIR band) of Ge long p<sup>+</sup>-n diode ( $T = 50^{\circ}\text{C}$ ,  $I = 200$  mA) heated hot air flux. The  $5 \times 5$  mm<sup>2</sup> base is thin enough to be



initially semitransparent ( $kd < 1$  at  $I=0$ ). Therefore, the injection process makes the base more opaque by increasing the free carrier concentration ( $\Delta n > 0$ ). Visualization of free charge carrier distribution shown in the figure helps to optimize device parameters (base length, charge carrier lifetime and surface recombination velocity). Indeed, the longitudinal charge carrier decay is due to their diffusion and recombination in the base whereas transverse non-uniformity is caused by surface recombination effect. Recently, the approach was helpful in studying room temperature 8-12  $\mu\text{m}$  LEDs and IR dynamic scene converters of new type<sup>38</sup>.

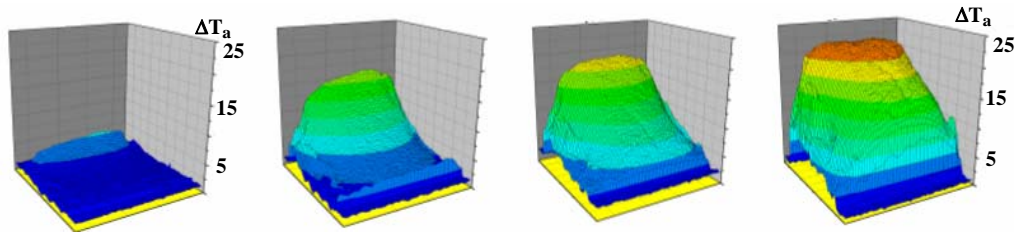
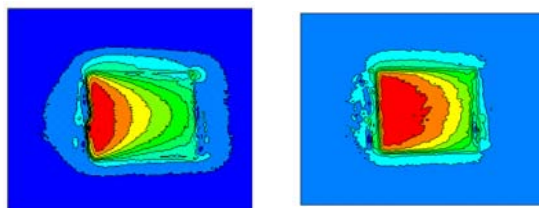


Fig.21. Schematics of the L-approach test performed with IR microscope (left) and the 2D-free carrier distribution across the device base (top, the  $p^+n$  junction is on the back side) versus current (from the left to the right,  $I=0.14; 0.7; 1.4; 5.1 \text{ A/cm}^2$ ) followed by the apparent temperature pattern  $\Delta T_a = T_a(I) - T(0)$ . As a matter of fact we demonstrate long wave IR emitting device based on indirect band gap material. The flat crest at last picture indicates that the TE

power, accurate to within the correction for reflectivity ( $1-R$ ), is equal to the power emitted by black body.

Shown in Fig.22 is surface recombination impact at the IR power emitted by the electrically driven Ge DIRSP. Frames are tested at equal conditions (see capture to the Fig.21) but both scene differ with time delayed after chemical etching.



$sL_d/D > 1$

$sL_d/D < 1$

Fig.22.  $\epsilon$ -approach is helpful in the express testing of DIRSP light pattern. Decreasing the surface recombination velocity (by etching) causes a scene to become more uniform and emit higher integral power. This scene, however, cannot be considered as a point source. Left: 10 hours after etching, Right: 2 minutes after etching.

**To resume:** The benefit of the  $\epsilon$ -approach (we developed recently) is twofold. First, it could be helpful as a powerful diagnostic tool. Indeed, it is easy to map free carrier distribution inside a scene of interest even though the scene is made of indirect band material. It is very important to note, the free carrier pattern may be generated both electrically and optically. Second, this approach forms the background of the new approach in DIRSP devices based on transparency modulation technique (for more details see 8.1.4 and 8.2).



### 7.3. Lessons to learn

High-resolution time-resolved multispectral (MWIR+LWIR+Visible) Hardware-in-the-Loop Facility we developed recently at the Institute of Semiconductor Physics is the most powerful tool (by the spectral range, special and temporal resolution combined) of all .gov, .mil, and .edu institutions across the globe. While operated as a standard thermo radiometer (in MWIR or LWIR bands) this calibrated set up maps 2D apparent or “real” temperature distribution across a scene (T-approach). *In addition*, it is also capable to monitor local temperature evolution-in-time process and thus could be helpful while testing target’s thermal rise-fall time even if the target itself is of only 20  $\mu\text{m}$  in diameter (real *point target*). One of our achievements is shown in Fig.19.

The facility additionally works as an analyzer of “non-thermal” target whose parameters are due to the radiative recombination processes in semiconductors (L-approach). This target dynamics falls into *microsecond range* with simulated apparent temperature being both higher and lower of that of background. As a matter of fact we are able to simulate and test *cold target* “sitting” on warm-hot backgrounds ( $\Delta T_a < 0$ ). The approach is limited to the use of direct band gap semiconductors in which the probability of radiative recombination is relatively high. However, when it comes to MWIR (to say nothing on LWIR), the efficiency of narrow band semiconductors is of several percents only (we mean  $T = 300\text{K}$ ) and device heating becomes an issue. Very important to mention is that operating in extreme modes in two IR bands permits the users to *separate the luminescence signal* (i.e., MWIR band-to-band luminescence of III-V compounds) *from that provoked by an excess target heating* (captured in LWIR band). Another example of the two-band analysis is shown in Fig.23.

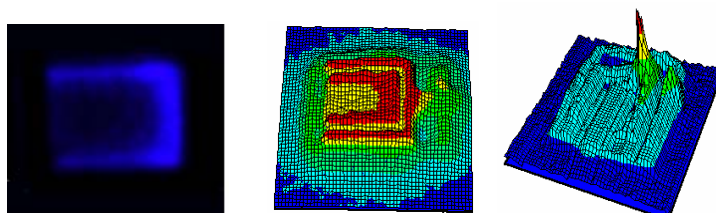


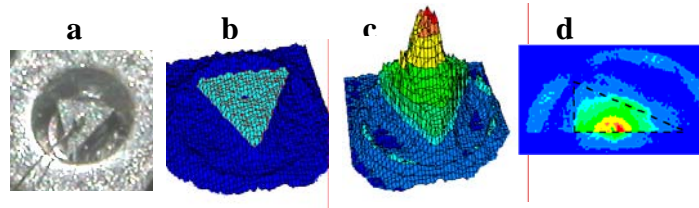
Fig.23. InGaN blue (multiple quantum wells) LEDs ( $300 \times 300 \mu\text{m}^2$ ) suffer of local base overheating ( $I = 200\text{mA}$ , 160 ms pulse duration) which prevents extreme mode operation. Shown in blue is 2D light distribution (left frame, L-approach, visible

band, CCD camera) while shown in red (central frame, T-approach, MWIR) is dynamic base local overheating. This last is to the current crowding effect that provokes static device catastrophic degradation (right frame, T-approach, MWIR). Results are not directly connected to this report’s content; it is the illustration of two-band L+T combination<sup>39</sup>.

Additionally, the set up is able to “separate” *heat* from *light* even if it operates in the one-band test. Shown in Fig.24 is IR luminescence maps of IR LED made of InAsSb/InAsP structure ( $\lambda = 4.3 \mu\text{m}$ ) At a small current, the spatial distribution of light is uniform but at higher current this light symmetrically concentrates around the top contact, while rest part of the triangle emits only 25% of the overall power. To detect heat distribution across this device area, we powered the structure only for upper part of frame duration. More specifically, camera scans the scene from the top to the down in “power-on” mode only for a half of frame duration and, therefore, captures light and heat (if the last exists) combined. The lower part of the frame is captured in “power-off” mode. As the recombination carrier lifetime lies in nanosecond range, then the lower frame part images only heat distribution resulted from the Joule heating and non-radiative recombination processes that happened prior, in “power on”

mode. The heat trap like hot ring around top contact is clearly seen. This relict heat radiation becomes remarkable at higher currents and may exceed the recombination radiation that LED emits. Our tests shown that excess temperature and its gradient at  $I < 400\text{mA}$  ( $\Delta T_{\text{max}} = 7.9^\circ\text{C}$  and  $< 600^\circ\text{C/cm}$ ) look acceptable from practical point of view, whereas overheating becomes threaten at  $I = 800\text{mA}$ :  $\Delta T_{\text{max}} = 42.7^\circ\text{C}$  and  $\cong 3000^\circ\text{C/cm}$ .

Figure 24. Electron micrograph of the  $4.3\mu\text{m}$  LED (a), 3D signatures of luminescence power emitted at  $I = 0.1\text{A}$  (b) and  $I = 0.6\text{A}$  (c), and (d) IR map of light and heat at  $I = 0.6\text{A}$ -half-frame bias mode. Relict heat is seen below the horizontal dotted line.



Our recent finding deals with the  $\varepsilon$ -approach. The set up analyzes properties of a target operated in transparency modulation technique. Contrary to the L-approach with light coming at the cost of electron-hole radiative recombination (each pair generates one photon given that the light recycling process is neglected, see region 3 in Fig.3), in this case IR radiation is due to electron and hole interband transitions (region 4 in Fig.3). As a matter of fact, electrons and/or holes emit photons independently as the result of electron-phonon interaction. By the rough estimates, the number of IR photons generated per each carrier is equal to  $\tau/\tau_{\text{rel}}$  value, where  $\tau_{\text{rel}}$  is the carrier relaxation time. As a rule,  $\tau$  increases and  $\tau_{\text{rel}}$  decreases when temperature increases and therefore this *radiative process is temperature activated*. Very important to note that there is no limitation at material band structure and process “works” properly in non-radiative materials like Ge and Si.

## 8. RESULTS AND DISCUSSION

### 8.1. IR scene monitored by the electrical bias

**8.1.1. The injection mode, luminescence, MWIR.** In this chapter, we report the results of conventional IR LEDs tested at extreme bias modes. To this end, the points of interest were the uniformity of light pattern in a micro scale and the possible impact of dynamic structure overheating at a device performance. However, our major goal was to estimate the apparent temperature ( $T_a$ ) of radiation emitted by the LEDs. As a matter of fact, we wanted to estimate the parameters of 3-5  $\mu\text{m}$  point source made of InAs-based compounds.

To minimize the Auger recombination effect on a device internal efficiency, we concentrated on shorter wavelengths ( $\lambda_{\text{max}}=3.4 \mu\text{m}$ ) inside the 3 to 5  $\mu\text{m}$  spectral range that is typical for IR thermal imaging devices. Among the variety of structures developed for the 3-5  $\mu\text{m}$  emitters, we preferred lattice-matched InAsSbP/InAs structures. To achieve carrier confinement and good heat sink, LEDs were fabricated as double heterostructures (DHs) and were designed so that the light escapes from the substrate. Specifically, the growing process and LEDs design are as described below. The DHs were grown by the liquid phase epitaxy (LPE) process onto a heavily  $n^+$ -doped 350  $\mu\text{m}$  thick InAs(Sn) substrate with an electron concentration  $n=(3-6)\cdot 10^{18} \text{ cm}^{-3}$ . Due to the Moss-Burstein effect the substrate was practically transparent for the emitting wavelength. The DH itself consists of a 1-1.5  $\mu\text{m}$  thick wide-gap  $n\text{-InAs}_{1-x-y}\text{Sb}_x\text{P}_y$  ( $0.08 < x < 0.09$ ,  $0.15 < y < 0.19$ ) confining layer, a 0.5-1  $\mu\text{m}$  thick  $n\text{-InAs}$  active region and a 2-3  $\mu\text{m}$  thick wide-gap  $p\text{-InAs}_{1-x-y}\text{Sb}_x\text{P}_y(\text{Zn})$  emitter (Fig.25).

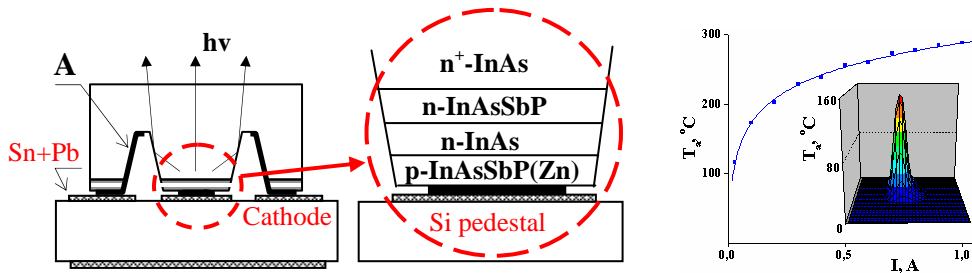


Fig.25. (left) Schematic diagrams of InAsSbP/InAs LED structure showing central mesa and peripheral contact pads. The device was presented by our colleagues from Ioffe Institute in S.-Petersburg, Russia. Fig.26. (right) Apparent temperature versus bias current at room temperature. In the insert: far field beam pattern of light escaping the LED covered with lens,  $I=0.1 \text{ A}$ . MWIR, L-approach. Out thanks to Dr. Matveev of Ioffe Institute (S.-Petersburg, Russia) for presenting this device.

The  $n\text{-InAs}$  active region was grown from the melt with gadolinium ions used as the gettering agent; this form of melt purification process reduces the concentration of non-radiative recombination centers and therefore increases quantum efficiency of the structure<sup>40, 41</sup>. The DHs were processed by wet photolithography into circular ( $D=300 \mu\text{m}$ ) mesa chips. Ohmic contacts (central circular anode of  $d=150 \mu\text{m}$  and peripheral 'U-shaped' cathode) were formed by thermal evaporation of Au. To maximize working device area, we utilized backside contact design. Both chip contacts were soldered to a contact area of a  $1.5 \times 1.7 \times 0.4 \text{ mm}^3$  semi insulating Si pedestal. Next, the Si pedestal with LED chip was soldered onto a TO-39 header in a substrate up manner. The LEDs were equipped with an immersion lens made of CdSb and attached to the LED surface by a chalcogenide glass. As a result, the full width at half-

maximum of the collimated beam escaping the structure through substrate and lens was on the order of  $25^\circ$ .

Fig.26 represents the apparent temperature of a device covered with a lens and maintained at  $T=300^\circ\text{C}$  versus bias current dependence as recorded by the MWIR camera in a triggering single-line mode at current pulse length of  $50\ \mu\text{s}$  and 25 Hz repetition rate (quasi-continuous wave mode-QCW). Careful verification was conducted to ensure that the pulsed IR emission at all current values was predominately of a luminescence nature and not a “thermal” one stemming from Joule heating and a non-radiative carrier recombination processes. The “thermal” signal

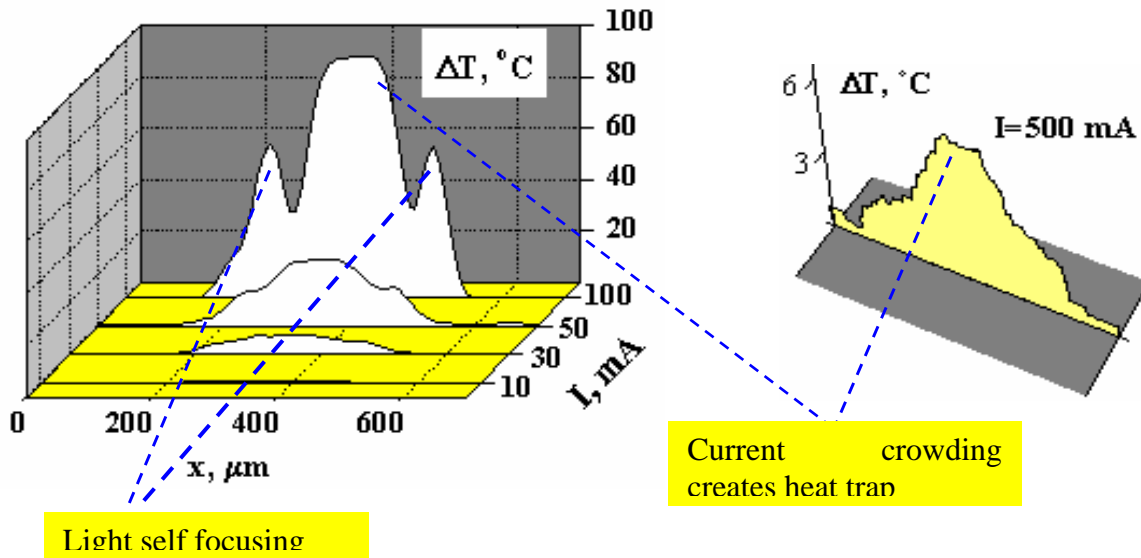


Fig.27. (left) One-dimensional light distribution at different bias currents,  $\Delta T=T_a(I)-T_a(0)$ . The vertical scale for the lowest current is twice increased. MWIR, L-approach.

Fig.28. (right) One-dimensional heat distribution captured in LWIR. T-approach.

measurements were performed with the 8-12  $\mu\text{m}$  camera. These tests showed that due to small thermal resistance between the emitting structure and the heat sink, which are separated by only a 2-3 $\mu\text{m}$  thick p-type emitter, LEDs do not require thermal control in CW mode up to  $I = 150\ \text{mA}$ . At stress pulse conditions of  $I=1\text{A}$  in QCW the structure overheating did not exceed  $15^\circ\text{C}$  when compared to the luminescence apparent temperature of  $T_a = 290^\circ\text{C}$ . When cooled to  $T \leq 200\ \text{K}$  (the temperature of a conventional Peltier cooler), LEDs demonstrated apparent temperature  $T_a \sim 500^\circ\text{C}$  at current as low as  $I = 150\ \text{mA}$ . Cooled Pb-salt diode laser array simulates  $T_a \approx 230^\circ\text{C}$ , while uncooled CdHgTe IR scene simulating device offers  $110^\circ\text{C}$  (for more details see below) explaining why the above value is the highest yet reported for photonic emitters. The light pattern of an LED on the plane orthogonal to the beam propagation path is shown in Fig.26 (insert). As a matter of fact this is a far field view of light captured by a camera. As one can see the quality of the beam escaping the device through the lens is quite acceptable (symmetrical round beam, point source) and permits further focusing of the beam to a small spot with a well-defined intensity profile. We remember this is not true for edge emitting lasers, which demand beam-shaping elements and are difficult to arrange in an array.

Fig.27 shows a single-line ( $400\ \mu\text{s}$  duration, 25 frames per second) distribution of light emitted by the LED free of lens and captured by a microscope focused on the p-n junction area. At low current, the light pattern is uniform across all active mesa area

( $D=300\ \mu\text{m}$ ). Increasing the current, however, results in a gradual decrease of the junction area capable to efficiently radiate ( $d=150\ \mu\text{m}$ ) due to current crowding effect, which is difficult to avoid in IR LEDs in conventional electroluminescence mode<sup>37</sup>. Further current increase causes an additional non-uniformity in light distribution: two peaks appear at the edges of a mesa with a maximum in between. These satellites result from the light laterally escaping a mesa and reflecting from its cone ('internal focusing') as depicted in Fig.25. Besides, heat trap appears in the mesa center (Fig.28). Although the structure overheating ( $\Delta T\sim 5^{\circ}\text{C}$ ) is rather low in the short pulse-mode, simulating high-temperature objects in CW mode demands for moderate cooling.

Additional details on light distribution are shown in Fig. 29. As one can see, current crowding noticeably decreases an optical power output. And contrary, an internal light focusing which is due to the total internal reflection partially compensates for this loss. More specifically, integral power emitted by a circular mesa could be as high as  $360\ \mu\text{W}$  ( $I=1\text{A}$ ,  $T=300\text{K}$ ) if current crowding is eliminated and all device active area radiates uniformly. However, LED real power output is only of  $210\ \mu\text{W}$ , from which some of  $40\ \mu\text{W}$  originate from enhanced extraction efficiency due to internal focusing (see bright ring in Fig.29, b). In the negative luminescence mode (reverse bias), LEDs generate practically uniform scene with temperature lower than background (Fig.29,c).

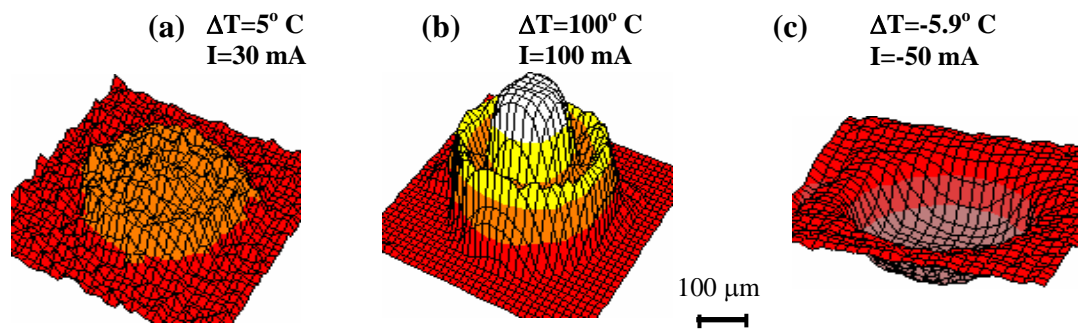


Fig.29. Forward-biased LED suffers of current crowding effect (b) that is impossible to prevent even in the substrate up structure. This causes the emitting area to decrease at higher current (see also Fig.20,b,c). As a matter of fact, conventional LED could be recommended as the point source for high-resolution Hardware-in-the-Loop Facility only at higher currents. In negative luminescence mode (reverse bias) due to high resistance of the p-n junction region, current crowding is negligible (c). L-approach. Additional performance benefit can be achieved by integrating an optical concentrator around the negative luminescence device<sup>44</sup>.

What shown in Fig.30 is the  $4\times 4$  LED array composed of hand-made InAsSb single emitters ( $400\times 400\ \mu\text{m}^2$ ) grown by LPE. To demonstrate the availability and accessibility of the approach, devices were obtained from an industrial manufacturer. Using different InAs-based content permits easy design of dual band and multi-band arrays emitting in MWIR band both positive and negative contrasts. Some details on LED array grown by molecular beam epitaxy on GaSb substrate were published recently<sup>43</sup>. By comparing with radiation of blackbody, authors founded the apparent temperatures are in the range of 300-600K.

**To resume:** The conventional electroluminescence LEDs based on easy to book III-V semiconductors and grown with non-expensive LPE technology form material platform for next generation dynamic IR scenes operated in MWIR. The devices could be prepared as single emitters and arrays, their time rise-fall time falls in nanosecond



range. When uncooled, simulated apparent temperature value registered with MWIR camera in pulse mode is of  $T_a \sim 300^{\circ}\text{C}$  what is equivalent of  $T_a \sim 700^{\circ}\text{C}$  for narrow ( $\lambda_{\text{max}} + \Delta\lambda$ ) band. This photonic DIRSP simulates negative temperature. To this end, we have to mention that negative luminescence with 93% efficiency devices made of HgCdTe were demonstrated recently<sup>45</sup>. The authors demonstrated dynamic device cooling by 54 K while operating at room temperature. However, the problems of current crowding and heat dissipation remain points of serious concern.

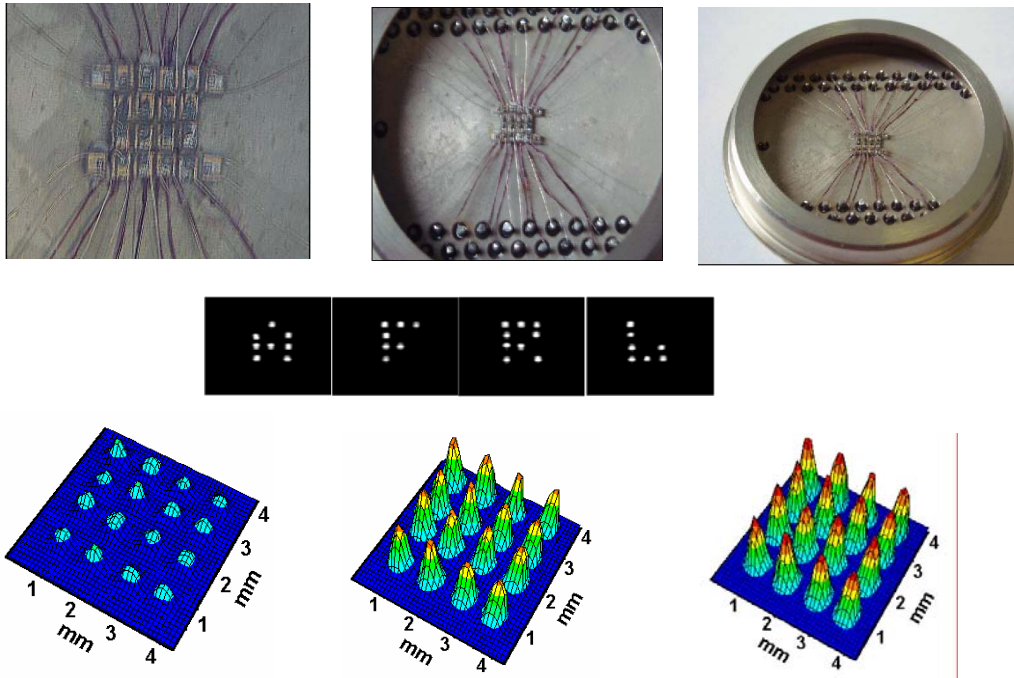


Fig.30. The 4x4 element hand-made two-band LED array composed of 16 point ( $400 \times 400 \mu\text{m}^2$ ) sources emitting at  $3.4 \mu\text{m}$  and four red LEDs (red LEDs sited at each corner of IR array are seen in the first photo on the top line). Tests are made at room temperature. All emitters are connected in shunt, CW forward bias I, mA: 50; 400; 600. The modulated apparent temperatures are  $\Delta T_{\text{max}} = 25, 76, 95^{\circ}\text{C}$ . L-approach, lower line. It takes only 50 mA to reproduce our partner's "positive" brand (second line).

**8.1.2. The Lorentz force mode, luminescence, MWIR.** To demonstrate the parameters of DIRSPs operated in this mode, we fabricated an array of  $16 \times 16$  elements (sized  $0.5 \times 0.5 \text{ mm}$  and spaced by  $0.5 \text{ mm}$ ) made of  $\pi\text{-InSb}$  ( $N_a - N_d = 10^{15} \text{ cm}^{-3}$ ) wafer. One wafer face was mechanically polished; this resulted in high ( $s_2 \approx 10^6 \text{ cm/s}$ ) surface recombination velocity value. The plate was fixed on a heat-conducting insulating substrate, the above-mentioned face being next to it. Then the wafer was polished to reduce its thickness to  $60 \mu\text{m}$  and finally chemically etched. Finally, the wafer thickness became  $30\text{--}40 \mu\text{m}$  with surface recombination velocity on free face was of  $s_1 \approx 10^4 \text{ cm/s}$ .

The required layout of the discrete array elements was obtained by photolithography. The planar ohmic contacts were formed by Indium sputtering in a vacuum. Mutually orthogonal contact buses provided connections between the array elements. The array was packaged into special holder with a  $\text{CaF}_2$  window (Fig.31) and disclosed between the poles of magnet. The array structure enabled to connect simultaneously separated groups of elements, thus obtaining a positive ( $\Delta T > 0$ ) or negative ( $\Delta T < 0$ ) apparent temperature contrast. As an example, we present below simulation of an alternating

contrast as a chessboard pattern where “hot” and “cold” squares alternate. 2D-apparent temperature pattern is shown in Fig. 32.

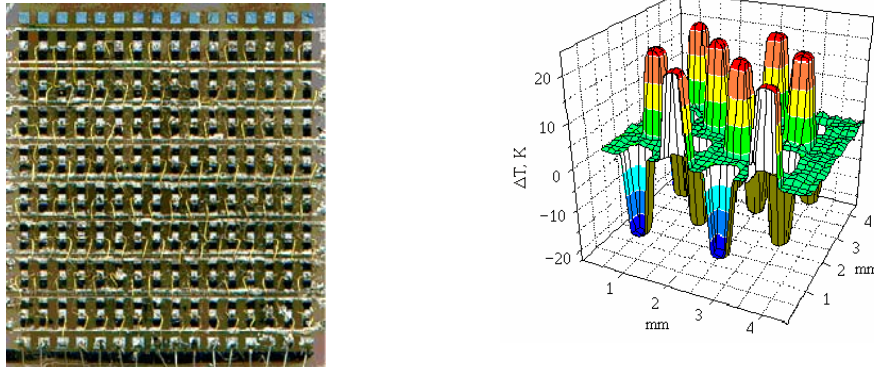


Fig.31. (left) The photograph of 16x16 arrays. Fig.32. (right) Negative and positive thermal contrasts simulated by InSb array in the Lorentz force mode at room temperature. Only 4x4 lot of the array is active.  $E = 7 \text{ V/cm}$ ,  $H = 12 \text{ kOe}$ . MWIR, L-approach

Then the wafer was polished to reduce its thickness to  $60 \mu\text{m}$  and finally chemically etched. Finally, the wafer thickness became  $30\text{--}40 \mu\text{m}$  with surface recombination velocity on free face was of  $s_1 \approx 10^4 \text{ cm/s}$ .

The required layout of the discrete array elements was obtained by photolithography. The planar ohmic contacts were formed by Indium sputtering in a vacuum. Mutually orthogonal contact buses provided connections between the array elements. The array was packaged into special holder with a  $\text{CaF}_2$  window (Fig.31) and disclosed between the poles of magnet. The array structure enabled to connect simultaneously separated groups of elements, thus obtaining a positive ( $\Delta T > 0$ ) or negative ( $\Delta T < 0$ ) apparent temperature contrast. As an example, we present below simulation of an alternating contrast as a chessboard pattern where “hot” and “cold” squares alternate. 2D-apparent temperature pattern is shown in Fig. 32.

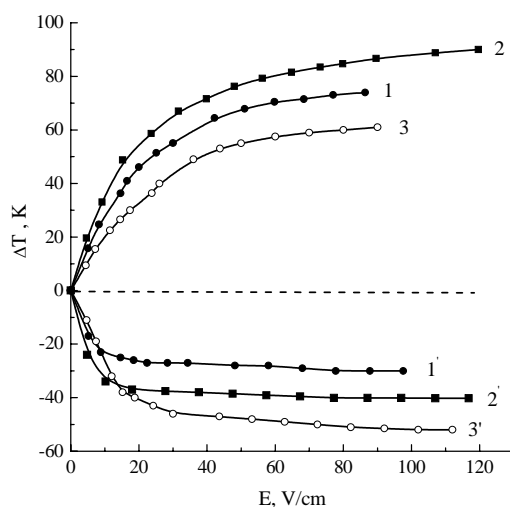


Fig.33. Apparent temperature of a single pixel versus electric field at  $H = \pm 12 \text{ kOe}$ . (1–3)-conventional positive luminescence mode, (1'–3') negative luminescence mode.

To increase device efficiency, a positive effect can be achieved by increasing the angle of total internal reflection for radiation escaping an active element. Indeed, a chalcogenide glass coating whose shape is close to hemisphere provides a 20% increase of  $\Delta T$  (see curves 2, 2'). Curves 1, 1' and 3, 3' are related to the etched surface, curves 2, 2' correspond to the surface coated with chalcogenide glass.  $T = 298 \text{ K}$  (1, 1' and 2, 2') and  $325 \text{ K}$  (3, 3');  $H = 12 \text{ kOe}$ . The background emission level is shown by the dashed line.

The apparent temperature of a single pixel versus pulsed (duration of 10  $\mu$ s) electric field  $\Delta T(E)$  is shown in Fig.33. By our opinion, the highest positive signal is due to non-radiative Auger recombination of free carriers, thus this signal degrades with temperature increase. The  $\Delta T(E)$  curve flattening out in the case of negative luminescence is related to practically complete suppression of equilibrium radiation from an array element in the spectral range of the interband transitions (the extreme depletion mode). Therefore, modulated “negative signal” activates with temperature<sup>42</sup>.

**To resume:** Even though the Lorentz force mode demands for use of a magnet which complicated the device design, this photonic DIRSP is able to simulate remarkable temperature contrast (negative  $\Delta T < -50$  K, as well as positive  $\Delta T > 90$  K) at a given point of the array is of practical importance. The InSb luminescence spectrum in the 3–5  $\mu$ m range has no specific features and coincides with blackbody spectrum (with allowance for the factor  $1-R$  where  $R$  is the reflection coefficient). Finally, there is no limitation on a pixel emitting array as well as an array itself and such a wide emitting surface is not subjected to the current-crowding effect. To the best of our knowledge, the array we have demonstrated remains the largest DIRSP device till now.

**8.1.3. Is negative luminescence a gift to the DIRSP’s users?** Yes, we claim that this unique phenomenon is real gift of Nature. Indeed, who could have imagined two decades ago that a scene/target kept at temperature of ambient could dynamically and reversibly (microsecond rise-fall time range) simulate negative temperatures? Without any cooling machine! As a matter of fact, negative luminescence mode brings to IR reality the dream of H. Wells’s to make a subject invisible (see “The Invisible man” by H. Wells (1897). The said is illustrated in Fig. 34. Indeed, the ability to dynamically simulate “*low observable*” is difficult to overestimate. Table 1 brings to readers more details and advantages of using negative luminescence. The most important factors to remember are high operating temperatures, temperature activation, and remarkably high values of modulated power in MWIR (see Fig.35). Unfortunately, due to high rate of free carrier thermal generation the process is difficult to perform in LWIR.

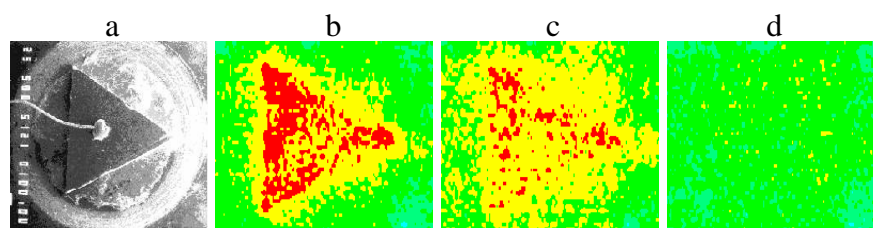


Fig.34. Electrically monitored target emissivity. Triangle ( $S=0.5$  mm<sup>2</sup>) target is the InAs-based 4.2  $\mu$ m LED with top point contact and the p-n junction situated in the plane of a structure sited on a metallic background (a). As the emissivity of semiconductor exceeds that for metal, in the initial state ( $I=0$ ) the target is slightly visible (c-blurred target that is difficult to detect). Forward bias activates the target signature due to positive luminescence (b-target becomes easy to identify). In negative luminescence mode (reverse bias, d), the target disappeared... Even if background temperature is not stable, to “delete” a target- process demands only slight tuning of bias current-*chameleon effect*.  
 $T=360$ K,  $I=\pm 10$ mA, MWIR, L-approach.



Table 1. Good things come in pair. Negative luminescence versus its older sister...

Parameters	Conventional Luminescence	Negative Luminescence
Things of common	Non-equilibrium state, a way for system to relax	
Power emitted value, $P$	Radiation over the equilibrium level, $P > P_0$	Radiation under the equilibrium level, $P < P_0$
Carrier concentration, $n, p$	$np > n_0p_0$	$np < n_0p_0$
Emitter uniformity	Improbable	Highly probable
Extreme signal value, $\Delta P$	Signal value unlimitedly increases up to lasing	Maximum signal value is fixed
Temperature effect	Thermal quenching	Thermal activation
Transient process, $\tau$	Carrier recombination time	Carrier generation time
Non-radiative process impact	Affected by non-radiative channels	Max. signal is not affected by non-radiative channels
Favorable spectral range	$h\omega > kT$ (visible)	$h\omega < kT$ (IR)

To finalize, our understanding of negative luminescence has already passed two stages like “But this is quite impossible!” and “Maybe, there is something in it...” Now we are in the third stage when all seems plain (although the question of how dark is semiconductor black hole remains unanswered). In particular, for negative luminescence application in semiconductor physics and technology, the forecast is sunny and clear though real devices are still in its infancy. *A dark cloud now looms over those applications, which demand extreme signals or continuum wave operation.*

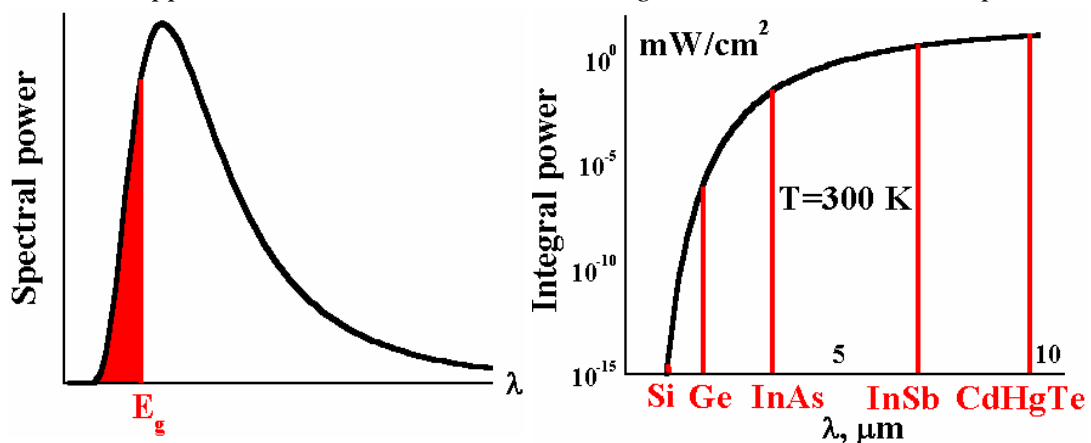


Fig.35. (left) For the negative luminescence process, the energy source is the thermal emission value stored in the fundamental absorption band ( $\hbar\omega > E_g$ )-left part of Plank's distribution of blackbody radiation. Indeed, *it is impossible to suppress more radiation than system emits initially*. (right) Integral value of modulated power emitted is negligible in Ge and Si ( $<10^{-5}$  W/cm<sup>2</sup>,  $\lambda < 2$   $\mu$ m). At  $\lambda > 2$   $\mu$ m, the figure represents the values which are easy to operate with ion(narrow band semiconductors).

The problem is in Joule heating, and therefore new ideas on how to prevent intense thermal charge carrier generations at higher temperatures are to be developed. New non-electrical ways to provoke NL are also desirable. The challenge now is how to develop devices capable of high-temperature operation in entire 3–12  $\mu$ m spectral range, which, although it may take several years, is definitely feasible. Our hats are off to Dr. B. Stepanov, who has predicted the NL phenomenon in a discrete quantum system a half of century ago.

#### 8.1.4. The injection mode, transparency modulation technique, MWIR & LWIR.

Although there is variety of tests made on Ge and Si single element, we quote here only results of our study connected to Si arrays. All tests are made at  $T > 300$ K, the injection structures were made of p-i-n diodes.

The initial p-i-n-structures were prepared on an *n*-Si wafer ( $\rho = 300$   $\Omega$ -cm, thickness of 0.86 mm, charge carrier lifetime of 300  $\mu$ s) using thermal diffusion of boron (*p*-region) and phosphorus (*n*-region) impurities. The wafer was cut into strips 1.7 mm wide. A strip was soldered to a massive copper holder and then cut into single pixels. Each strip had 16 pixels ( $0.86 \times 0.86 \times 1.7$  mm<sup>3</sup>) with a common contact (Fig.36a). The pixels were spaced 0.1 mm apart (the linear fill factor  $F = 90\%$ ). The front and back emitting faces ( $0.85 \times 0.75$  mm<sup>2</sup>, edge emitting device) of each pixel were optically polished. To make the emitter parameters stable in the course of high temperature tests, the contact-free surfaces were not etched. By our measurements, the surface recombination velocity was about  $5 \cdot 10^4$  cm/s and remained stable in the course of investigation. As a result, the effective value of charge carrier lifetime  $\tau_{\text{eff}}$  was half the initial one, and its temperature dependence was insignificant:  $\tau_{\text{eff}}$  varied from 130 up to 150  $\mu$ s at the 100–200  $^{\circ}$ C temperature range (this corresponds to the effective diffusion length of charge carriers. The measurements were performed in the open air; the array temperature was controlled with a hot air flow. Tests were made in both MWIR and LWIR bands.

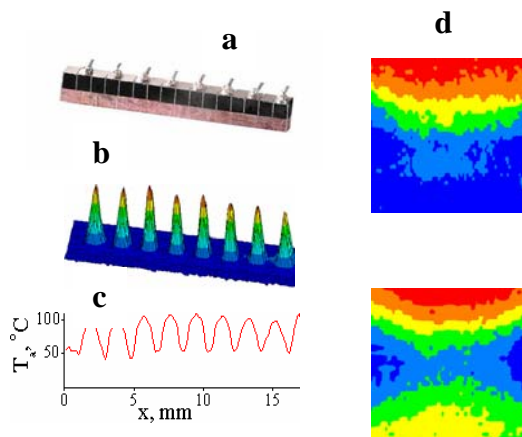


Fig.36. (a) A general view of Si 16-element array sitting on the Cu holder-heat sink, (b) the TE far-field view, (c) the profile of apparent temperature, (d) the TE micro map of an injection process ( $I = 350$  mA) in the  $n^+$ -*p* structure (top pattern) and the  $n^+$ -*p*<sup>+</sup> (lower pattern). Unpublished.

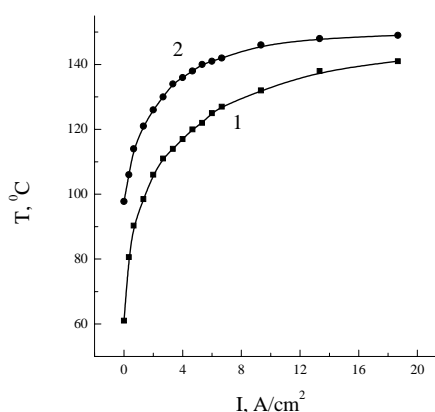
The distribution of IR radiation along the array strip (far-field view) was recorded with two thermal imaging cameras tuned at MWIR and LWIR bands. The emission from single pixel was recorded with an IR microscope.

Figure 36b shows two-dimensional (2D) distribution of strip TE at a temperature  $T = 150\text{ }^{\circ}\text{C}$  captured with MWIR thermal imaging camera. The even units are connected in parallel. (The reason is that, due to big value of the linear fill factor  $F$ , the images of individual units merge if all units are activated.) Activation of units is made by a current pulse with amplitude  $I = 1.1\text{ A}$  and duration  $\Delta t = 160\text{ ms}$ . Figure 36c shows the profile of TE distribution along the strip (in terms of the apparent temperature  $T_a$ ). The parameters of nonbiased pixel TE are determined by low initial emissivity of Si, so  $T_a(0) = (51.7 \pm 5.4)\text{ }^{\circ}\text{C}$ . This value (that exceeds room temperature only slightly) is essentially lower than real strip temperature. The initial emissive power is also low:  $P_{\min} = 1.3\text{ mW/cm}^2$ . While apparent temperature of biased even pixels increases ( $T_a(I) = (105.4 \pm 3.6)\text{ }^{\circ}\text{C}$ ), it still remains somewhat real temperature. And the emissive power ( $P = 5.7\text{ mW/cm}^2$ ) is lower than that of blackbody ( $P_{\text{bb}} = 15\text{ mW/cm}^2$ ). This may be due to reflection of radiation at the front face as well as to insufficiently high injection level ( $P < P_{\max}$ ).

Shown in Fig.36c are 2D-maps of charge carrier injection ( $\Delta n = n - n_0$ ) into the bases of  $p$ - $i$ - $n$ - and  $p$ - $n$  structures. These results indicate a higher degree of uniformity of TE flow between the contacts and higher integral radiation power in the structure with double injection power as compared with one-sided injection. Strictly speaking, we did not manage to ensure high degree of spatial uniformity of modulated signal. Non-uniformity along the current lines is due to recombination of injected electrons and holes at the diffusion length (unfortunately, such is the nature of contact injection in long-base diodes). Lateral non-uniformity results from surface recombination of charge carriers at the side faces. Nevertheless, the distinction in spatial distribution of radiation power in a  $p$ - $i$ - $n$ -structure is so small that it can be neglected.

The  $T_a(I)$  dependencies of a single pixel in MWIR (1) and LWIR (2) on the injection level at  $T = 180\text{ }^{\circ}\text{C}$  are shown in Fig.37. The initial  $T_a$  values (state of transparency) are, respectively, 61 and 98  $^{\circ}\text{C}$ . This supports the fact that silicon transparency in LWIR is less than in MWIR. The reasons are (i) absorption of radiation by crystal lattice, (ii) presence of oxygen impurities (that are practically unavoidable), and (iii) bigger, as compared with MWIR, absorption by free charge carriers (it is known<sup>12</sup> that in Si  $k_{n,p} \sim \lambda^{3/2}$ ).

Fig.37. Apparent temperature versus bias current density in  $p^+$ - $p$ - $n^+$  structure measured in MWIR (1) and LWIR (2) bands. Note: in LWIR the base becomes dynamically opaque and the apparent temperature values reach its maximum value ( $\sim 150\text{C}$ ). Pulse duration -160 ms. Unpublished.



As current is growing, the  $T_a$  values in both ranges increase. Curve 2 (LWIR) flattens out at a level  $T_a = 149\text{ }^{\circ}\text{C}$  even when  $I = 12$

$\text{A}/\text{cm}^2$ . Curve 1 (MWIR), however, still continues to increase; it reaches merely a level  $T_a = 141 \text{ }^\circ\text{C}$  at a higher current value ( $I = 18.7 \text{ A}/\text{cm}^2$ ). In our opinion, this result also is due to frequency- dependent absorption coefficient value  $k_{n,p} \sim \lambda^{3/2}$ .

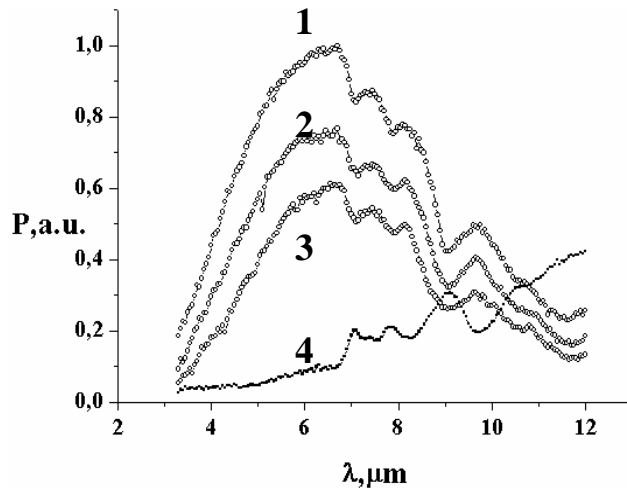


Fig.38. Measured spectral distribution of the TE power at different bias current values.  $T=150 \text{ }^\circ\text{C}$ ,  $I, \text{ A}$ : 1- 0.2; 2-0.45; 3-0.7. Spectral dependence of Si initial emissivity  $P_0$  is shown by curve 4. To a good approximation the device can be referred to as a gray body. Unpublished.

Figure 38 shows the TE spectra versus bias current. The curves are measured in pulsed mode ( $\Delta P = P - P(0)$ ,  $\Delta t = 4 \text{ ms}$ ), i.e., without registration of the equilibrium ( $I=0$ )

TE component which is due to the crystal lattice, oxygen impurities and equilibrium charge carriers emission. (The  $P(0)$  spectrum shown in the figure by curve 4 is due lattice absorption-emission process). One can see that injection-modulated TE spectrum is similar, on the whole, to the Planck radiation spectrum. However, “fingerprints” of the equilibrium spectrum lead to corresponding deformation of the  $\Delta P(I\lambda)$  spectrum beyond  $\lambda > 6.5 \text{ } \mu\text{m}$ .

Based on the  $T_a$  values determined in this way, as well as taking into account the base area ( $7.4 \cdot 10^{-3} \text{ cm}^2$ ) and electric power consumption, we draw a conclusion that the values of the emitter integral radiation power and efficiency (power in/power out ratio) ranges from 0.1 mW and 0.08% (as evidenced by the measurements in MWIR) to 0.38 mW and 0.3% (as evidenced by the measurements in LWIR). The blackbody radiation power in MWIR (at a temperature of measurements) is only 10.9% integral power, while in LWIR its value is considerably higher (27.9%). So we believe that the results of measurements in LWIR look more realistic for practical estimates.

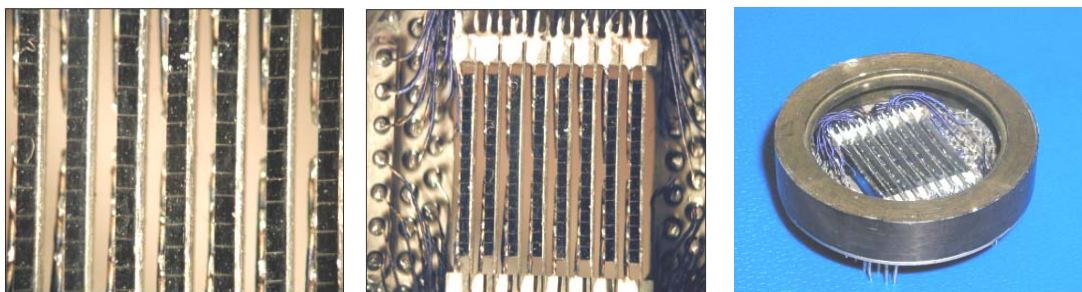


Fig.39. Photographs of Si 8x8 array captured with CCD camera (from the left to the right: near field view of pixels (black vertical stripes) separated by horizontal thin white cuts, view of an array with electrical connections, and pixel housing ( $D=40\text{mm}$ ). Unpublished.

To complete our study of transparency modulation technique based on the injection mode, we demonstrate 2D emitting structure made of the 8x8 Si array we developed

recently (Fig.). The  $0.86 \times 0.86 \text{ mm}^2$  pixels (with 0.86mm spacing, 50% fill-factor) are made of 1.5 mm-thick low doped Si substrate ( $\rho = 300 \text{ ohm-cm}$ ) by a conventional low-temperature diffusion process of Boron ( $p^+$ -layer) and Phosphorous ( $n^+$ -layer) impurities. As we mentioned, the pixel rise-fall time is on the order of 120-140  $\mu\text{s}$  in the temperature range up to 200 C. The IR image composed of single *point sources* and induced by the electrical bias ( $I = 2.8 \text{ A}$ , pulse duration is 160 ms) is shown in Fig.40.

Improved technology enables this 2D array operation up to 180 C with a few percents efficiency in both MWIR and LQIR bands.

**To resume:** Multielement Si broad-band photonic IR device based on the transparency modulation technique operates at high temperatures and demonstrate highest till reported for Si emitters external efficiency ( $>1.0\%$  at  $T=180^\circ\text{C}$ ). Large ( $\text{mm}^2$  range) uniformly emitting area, relatively short rise-fall time ( $\sim 100 \mu\text{s}$ ) and possibility to employ the conventional Si technology make this device attractive for the variety of applications of which IR dynamic scene simulation of point and extended targets (in MWIR and LWIR) is the only one to name. *Caution:* due to thermally activated free carrier generation process, properties of p-n junction degrade at  $>100^\circ\text{C}$  and  $>200^\circ\text{C}$  in Ge and Si scenes accordingly.

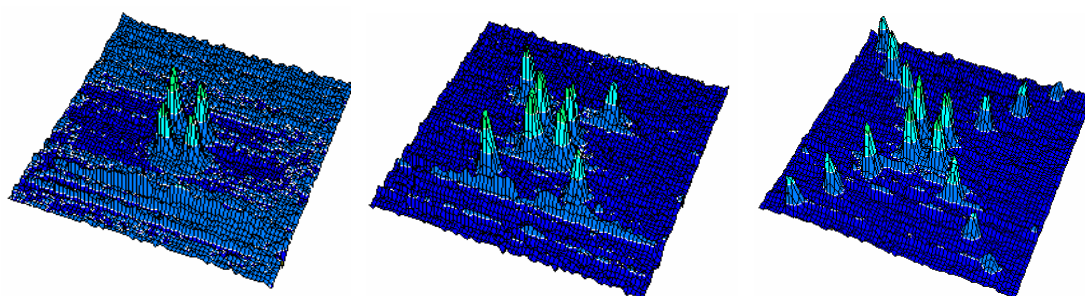


Fig.40. How to generate test image: 2D distribution of IR light emitted by the electrically driven  $8 \times 8$  Si array. Test conditions: 3-5  $\mu\text{m}$  spectral band,  $T = 100^\circ\text{C}$ . Maximum dynamically modulated apparent temperature value is on the order of  $30^\circ\text{C}$ . All active pixels are connected in shunt. MWIR,  $\epsilon$ -approach.

### 8.1.5. The exclusion-accumulation mode, transparency modulation technique.

Contrary to the injection mode we have studied in the Si devices, the exclusion-accumulation mode parameters will be demonstrated in the Ge screens. This material benefit is in intrinsic conductivity ( $n_0 \approx p_0$ ) at room and slightly higher temperatures. Contrary to the injection mode, the approach permits simulating both positive and negative contrasts as well as two contrasts at the scene combined. Some results of study are shown in Fig. 5,6. To add, the additional practical aspects of our study look like following.

In the rectangular geometry, operating in the pulsed exclusion mode could be of practical interest by two reasons. First, to those interested in simulating local cold scene width monitored by the operator. Physical reason is in the exclusion length versus-doping level dependence (see Fig.41). Second, mapping the exclusion effect transient signal permits very speedy dynamic simulation of “*running*” cold scene (see Fig.42)<sup>14</sup>.



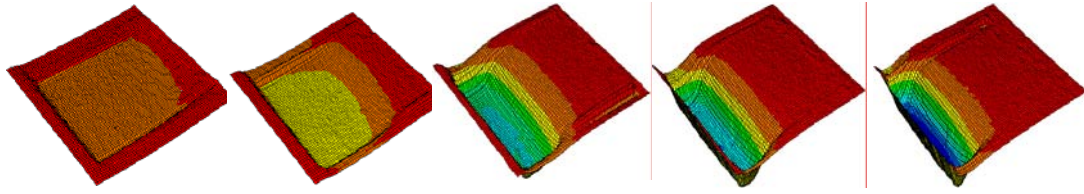


Fig.41. Ge p<sup>+</sup>-p structure (scene of ~ 10x10 mm<sup>2</sup>, p<sup>+</sup>-contact is from the left and ohmic contact is from the right, carrier drift toward the ohmic contact, N<sub>d</sub>-N<sub>a</sub>=3.5·10<sup>13</sup>cm<sup>-3</sup>). From left to right: thermometric scene temperatures are 90.7 C., 103C, 132C, and 146C; the depth of the excluded region as negative apparent temperature values are: 6.4C, 9.1C, 20.0C, and 30C. !60 ms-long 350 mA current pulse, LWIR, ε-approach

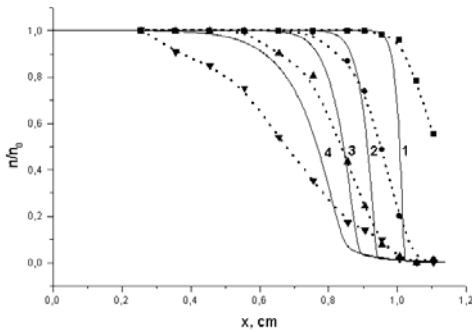


Fig.42. Measured normalized distribution of free carrier deficit in the exclusion region of the Ge slab with p<sup>+</sup>-contact being from the right. Dotted lines-experiment, full lines-theory. Time delay after voltage (U=6V) is applied, Δt, μs: 1-20; 2-60; 3-120; 4-steady state distribution. IR camera monitors the region with free carrier deficit as a cold region.

The cylindrical geometry presents additional benefit (Fig.43)<sup>13</sup>. Due to non-uniform electric field distribution in a device base, *whole base* of a structure becomes excluded at record low voltage and therefore behaves like point source which apparent temperature depends only of thermometric temperature. In the accumulation mode, bright spot appears at the central contact which is also looks like point source (Fig.44).



Fig.43. CCD photo of p-Ge scene (R=0.5 cm) with ohmic peripheral contact R<sub>2</sub> and p<sup>+</sup> central contact R<sub>1</sub>. In the accumulation mode, all carriers generated inside “broad” base concentrates in the vicinity of small central contact by giving rise to high positive apparent temperature. In the exclusion mode, free carriers are easy to recombine at broad ohmic contact by making the entire base “cold”.

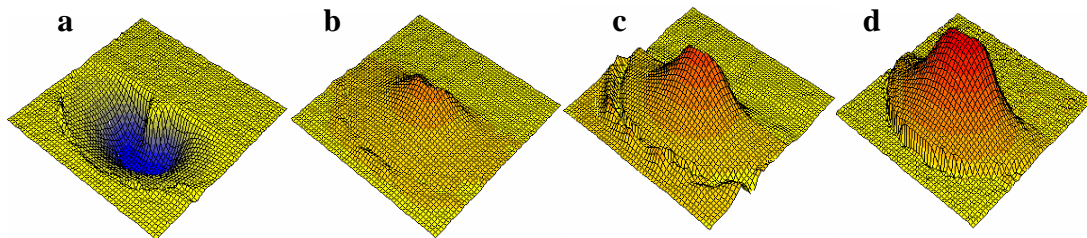


Fig.44. Half-cylindrical Ge base kept at T=80<sup>0</sup> C behaves like uniform extended cold object-carrier drift toward the structure periphery (a, I=-100 mA, ΔT=-20<sup>0</sup> C). Carrier drift in the opposite direction causes local bright spot to appear in the center (b, I=100mA, ΔT=8.2<sup>0</sup> C; c, I=200 mA, ΔT22<sup>0</sup>C; d, I=1A, ΔT=33<sup>0</sup> C. LWIR, ε-approach.

**To resume:** The exotic exclusion-accumulation mode gives rise to both cold and hot dynamic IR scenes monitored by current. The local temperature of a large area scene is easy to simulate and dynamically manipulate. This process theory we developed recently supplies with all data needed to develop (and operate with) the scene made of Ge. This Ge application looks like material rebirth for optoelectronic application. Contrary to the injection mode, the device operate being intrinsic and therefore heated above room temperature. Contact properties, however, degrade with temperature increase, creating trade-off between maximum simulated temperature and device efficiency.

**8.2. IR scene monitored by light (light down conversion), MWIR & LWIR.** The scenes we operated with till now, demand for contacts and therefore consist of single or multiple pixel design. The contacts itself is real technological problem given that we wanted contact properties to remain stable in wide temperature range. Indeed, when it comes to high temperature, the contact properties are difficult to predict. All in all, electrically biased IR scene is not the best solution for DIRSP. What follows below is our new solution to this problem. We will demonstrate in short what could be done with MWIR and LWIR DIRSP's dynamically monitored by light (light down conversion process) and thus free of contacts. Our scenes are made of initially transparent in both bands Ge and Si substrates and the schematic of two versions of experimental set up is shown in Fig. 45. Speed of “synthetic cinema” projected with visible light source exceeds 20 kHz.

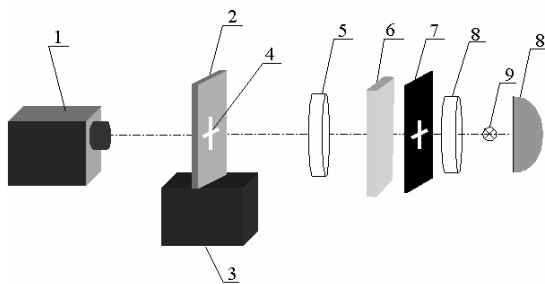
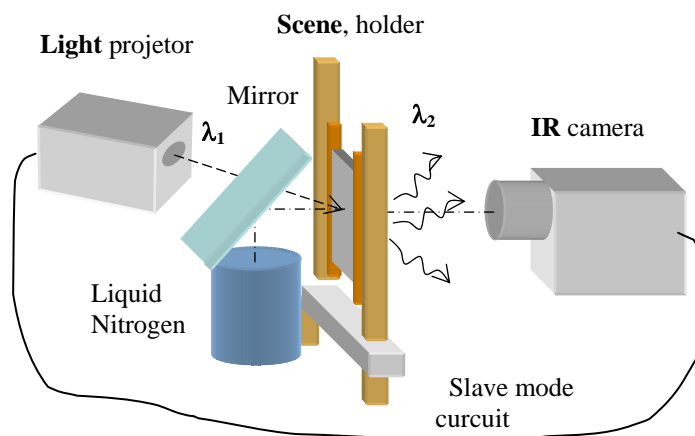


Fig.45,a. Test bench for target projection process. 1 – Thermal imaging camera; 2 – uniform Si or Ge scene; 3 – heater; 4 – target projection; 5 – collimator; 6 – band pass filter for visible; 7 – target; 8 – condenser; 9 – incandescent “visible” lamp. Speed of “synthetic cinema projection” is above 20 kHz. Target apparent temperature exceeds that of the scene and depends on the “visible” light power.  $\epsilon$ -approach

Fig.45,b. Test bench for simulating “erase-image” and “display-hidden-image” processes. The image to monitor is due to emissivity initial pattern at the scene. By projecting  $\text{LN}_2$  on the scene, one can simulate record values negative apparent temperatures even if thermometric scene temperature is above room temperature. Semiconductor scene and its holder are fixed at given temperature (heater is not shown).  $\lambda_1 \ll \lambda_2$ .  $\epsilon$ -approach.



In the Fig. 45,a conversion screen-scene 2 whose temperature is monitored by heating-cooling device 3, is located perpendicular to the optical axis of the projector and the generated infrared image can be observed from the rear surface of the screen. The 2D optical image (the cross) is projected on the scene by the “visible” light projector 5-8. Optical radiation is absorbed by the scene-conversion screen 2 and

causes a power change in IR emitted. Therefore in the plane of the conversion screen the 2D dimensional infrared image duplicates, according to a scale of 1:1, the 2D optical image that was projected in visible or near infrared range on the surface of the conversion screen 2. In the Fig45,b an arrangement has an liquid nitrogen reservoir and mirror to project cold nitrogen “surface” on the scene. By virtually cooling the scene, thermal noise of a background can be minimised (we remember, the scene is transparent!) and an object whose temperature is lower that that of background can be simulated. Besides, because the minimum apparent temperature that is being represented is decreased in this version of the arrangement, the dynamic range of the temperatures that is being represented expands.

In the case of optimistic scenario, maximum power  $P_{\max}$  emitted by the ‘visible light is on’ scene is dependent only on its temperature given that the  $kd \gg 1$  condition is valid and transparency coating available. Meanwhile, down conversion efficiency is temperature depended as the ‘visible light is off’ scene emission  $P_{\min}$  exponentially growths with T in material with intrinsic conductivity (the initial scene transparency degrades due to  $n_i$  increase).

By supposing the visible light projector is able to generate free charge carrier concentration  $\Delta n$  on the order of  $10^{16} \text{ cm}^{-3}$ , temperature dependence of modulated TE signal  $\Delta P_{\omega} = P_{\omega} - P_{\omega 0}$  for Ge and Si scenes is shown in Fig. 46. The calculations are made for  $\lambda = 10.6 \mu\text{m}$  by neglecting  $\sigma_{n,p}$  dependencies. In the experimental tests, integrated TE signals were recorded by cooled HgCdTe photodetector sensitive in 8-12  $\mu\text{m}$  spectral range. These results show that low temperature material is a matter of choice but Ge may be recommended due to its initial record transparency in IR.

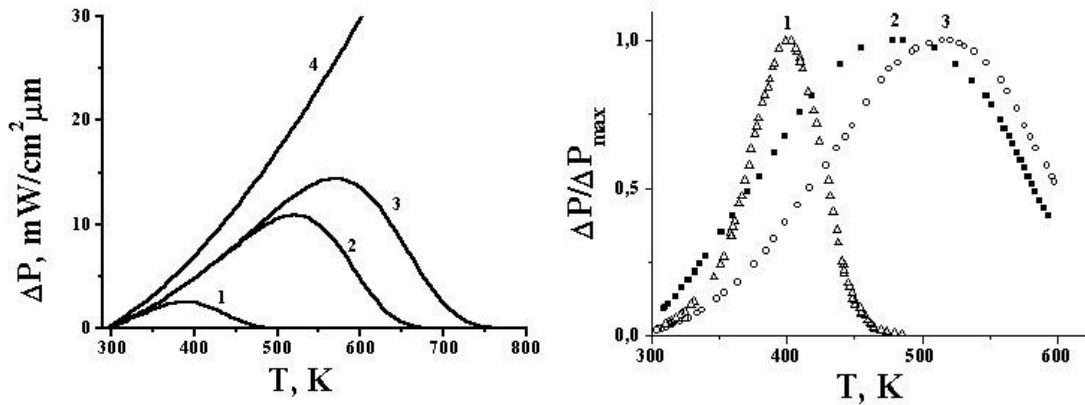


Fig.46. (left) Calculated temperature dependence of down conversion efficiency for scenes made of intrinsic Ge (1,  $d = 0.35 \text{ cm}$ ), and Si (2 -  $d = 0.84 \text{ cm}$ , 3 -  $d = 0.22 \text{ cm}$ ). Curve 4 is power difference between black body at temperature T and background at  $T_b = 300 \text{ K}$ . (right) Experimental tests of down conversion efficiency for n-Ge (1,  $\rho = 0.1 \text{ ohm-cm}$ ,  $d = 0.35 \text{ cm}$ ) and n-Si ( $\rho = 500 \text{ ohm-cm}$ , 2 -  $d = 0.84 \text{ cm}$ , 3 -  $d = 0.22 \text{ cm}$ ) scenes.

Recently, we shown that special material n-type doping can expand temperature range up to  $T = 450 \text{ K}$ <sup>23</sup>. The reason is in asymmetry of free carrier absorption values ( $\sigma_p / \sigma_n \approx 17$ ), and therefore to minimise TE of ‘visible light is off’ scene it is desirable to reduce free hole concentration. Also important to note that doping level is temperature sensitive. When it comes to higher temperature, highly resistive float zone Si is more preferable due to lower rate of thermal carrier concentration and using standard 300  $\mu\text{m}$ -thick substrates looks promising for operating in the temperature range above 700 K.



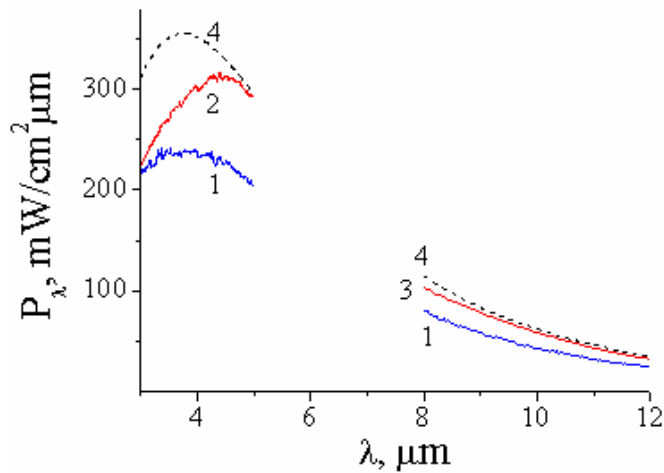


Fig.47. Measured TE power versus wavelength (1-3) relative to the black body radiation (4) in atmosphere transparency windows. 1-optimally polished emitter, 2-single-level coating of the emitter is tuned at MWIR, 3- the coating is tuned at LWIR. Si scene,  $T=500^{\circ}\text{K}$ .

The calculation shows that the single-layer ZnS antireflection coating could increase the integral TE power of Si emitter by 36% in MW and by 52% in LW. Transparency coating effect is also demonstrated in Fig.47. Shown are spectral dependencies of power emitted by a thick emitter and a black body in MW and LW bands. The data represents the modulated IR power value, which is due to the temperature difference between a chopper ( $T=300\text{K}$ ) and an emitter itself. Tuned transparency coating decreases the device reflectivity in both bands and thus results in increase of TE power by 26% (MW) and 33% (LW). Although maximum benefit falls into the foreseen band, non-essential transparency enhancement also occurs beyond this spectral interval. Indeed, LWIR emitter shows IR power increase by 16% in MW band, whereas MWIR emitter output grows by 17% in LW. In other words, even a single-layer coating increases TE signal over the whole IR spectral range. However, when it comes to single- or two-band IR emitters tuned at special spectral range, many-layer coating should be employed.

The fundamental feature of light down conversion technique is the saturation of IR TE power which happens in the Si emitter when the intensity of pumping light increases. Fig.48 illustrates the experimental result connected to initially thin emitter and demonstrates dynamic opaqueness induced in MWIR band by free electrons and holes generated by YAG:Nd pulsed laser. Also shown is the thin coating effect on saturation power value. Indeed, saturation power of a coated emitter is comparable to that of a black body. By our estimates, to have a thin emitter dynamically thick, the free carrier concentration should exceed  $10^{17}\text{ cm}^{-3}$ .

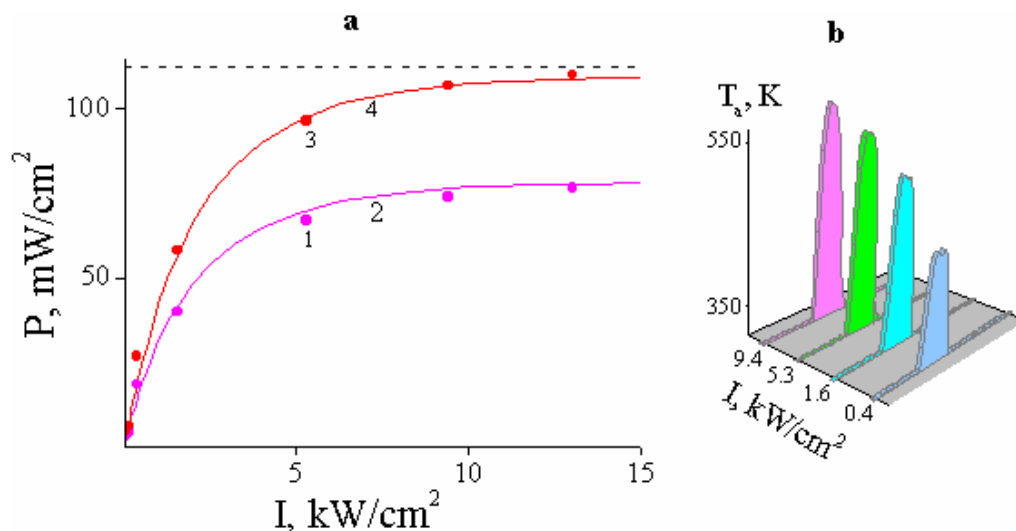


Fig.48. (left) (Saturation effect in TE power versus pumping level dependence. Solid lines- theory, dotted line- black body power, dots- experiment. 1-polished emitter, 2- emitter with thin film tuned at MWIR band. (right) In the MWIR, YAG:Nd laser beam transforms into “hot” stripe source with the record apparent temperature as high as  $T > 550^{\circ}\text{C}$ ). Unpublished.

Dependence of TE value on the emitter local emissivity represents a unique possibility to optically simulate IR dynamic scene with a very high frame frequency ( $>20$  kHz). Shown in Fig.49 is the IR image of a test target (duck, see Fig.49,a) activated by an incandescent optical source ( $(\lambda_1 < hc/Eg)$ ) on the surface of Si emitter and recorded by the MWIR camera. The initial scene non-uniformity is due to an emissivity pattern created at the scene by combining regions covered with a thin metallic film, which is insensitive to light (background) and free scene surface (target), whose emissivity depends on pumping power. Due to record Si transparency in MWIR, the target looks like an apparently cold object ( $T_t = 42.4^{\circ}\text{C}$ , “light is off”) compared to the background temperature ( $T_b = 54.0^{\circ}\text{C}$ ), even though thermometric emitter temperature is of  $150^{\circ}\text{C}$ . “Light is on” process increases the target emissivity, and at a moderate pumping level, an IR image passes through the point when apparent temperatures target and the background coincide ( $T_t = T_b$ , erase-image process or low observable). Further pump power increase results in transforming a cold target into a hot one ( $T_t = 66.6^{\circ}\text{C}$ ).

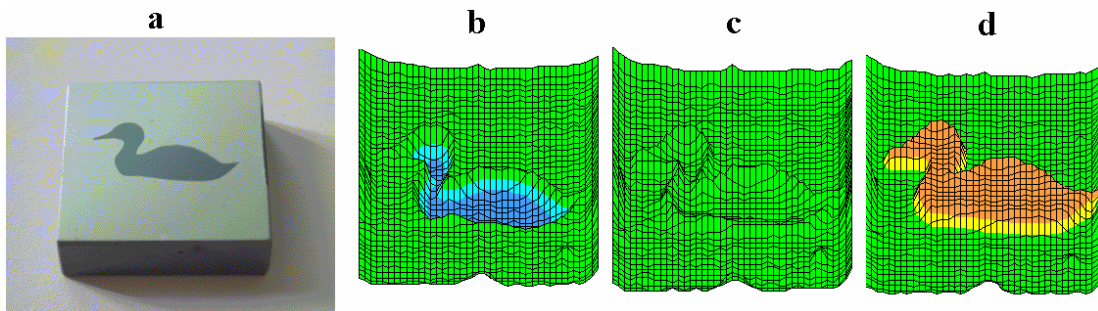


Fig.49. Target-on-background composition (a, photograph) could be imaged in MWIR as the pictures with cold target (b, “light is off”) or hot target (d, “light is on”), whereas moderate pumping light level erases the target (c, *low observable*).  $T = 150^{\circ}\text{C}$ .

*To resume:* For the practical realization of electrically biased DIRSP’s there are difficult technological challenges associated with the high-temperature regime. Among the technological problems are finding high-temperature-compatible contacts and prevention of dopant diffusion in p-n junction diodes. Thus, light down conversion process looks more attractive when getting higher apparent temperature becomes an issue.

### 8.3. Lesson to learn (Which the approach is better?).

Photonic approach in DIRSP technology is often dismissed by “outsiders” as inefficient way with little to offer to customers and manufacturers. From the other side, there are new demands which DIRSP’s based on thermal emitters are not able to satisfy. In particular, the dynamic range of this technology does not provide for radiometric duplication of the full range of scenarios likely to be encountered by future weapons systems. The approach has *material limitations* in high temperature

output ( $T \sim 700\text{K}$ ), operation speed (4-5 ms rise-fall time) and inability to simulate cold dynamic scene or low observable. The technology has already plateaued; as a matter of fact, it looks like a *dead end in the field*. Alternative innovative approaches are required to satisfy growing demands.

To this end, 3-5  $\mu\text{m}$  DIRSP's made of conventional IR LEDs are able to satisfy these demands. Indeed, these photonic devices have evolved significantly in the last decade. There are strong signs that IR LEDs are poised for a potential rebirth. Improving the emitting structure technology and heat sink quality has enabled researchers to fabricate LEDs capable of emitting  $>1\text{mW}$  power at room temperature. Thus, conventional non-resonant IR LEDs are becoming important candidates to form the basis for new generation of IR dynamic scene simulation devices. Ideally, this concept is able to develop single or 2D array *narrow-band or multiband emitters* simulating  $T > 700\text{C}$ . Additionally, such a scene is able to dynamically (in excess of 1 MHz) project *cold target/background* even if operated at room temperature. These devices drawback is in their low external efficiency ( $\sim 1-2\%$ ) that prevents CW simulating of very hot or remarkably cold images due to local overheating of a base. By this reason, the approach could not be recommended for operating in LWIR band.

It is light down conversion technology to form the basis for new generation of DIRSP's operated in both MWIR and LWIR bands. Compared to conventional LEDs whose performance is connected to radiative recombination efficiency of direct inter-band electron transitions, TE devices are more efficient because they make use of intra-band electron and hole transitions. This pixelles approach is based on indirect band gap semiconductors, in particular on Ge or Si whose technologies of growth and doping are well established. As a result, TE devices for MWIR and LWIR bands are easier to produce and work with compared to conventional thermal emitters. Indeed, they only need a homogeneous FZ wafer with minimum surface recombination velocity (record values of  $<20\text{ cm/s}$  are easy to achieve) and transparency coating tuned at a selected spectral band.

Table 2. Down conversion DISP versus MIRAGE engine (SBIR)

<i>PARAMETER</i>	<i>MIRAGE (SBIR)</i>	<i>CONVERTER</i>	
<b>1</b>	<b>Operation principle</b>	<b>Equilibrium BB radiation</b>	<b>Visible-to-IR down conversion</b>
<b>2</b>	<b>Emitter</b>	<b>Resistive heater /micro-array/</b>	<b>Semiconductor screen</b>
<b>3</b>	<b>Time constant</b>	<b>5 ms, thermal process</b>	<b><math>&lt;100\mu\text{s}</math>, recombination process</b>
<b>4</b>	<b>Key factor</b>	<b>Temperature, T</b>	<b>Emissivity, <math>\epsilon</math></b>
<b>5</b>	<b>Effective temperature range</b>	<b>286-780 K</b>	<b>250-780 K (projected)</b>

<b>6</b>	<b>Fill factor</b>	<b>46,5%</b>	<b>100%</b>
<b>7</b>	<b>Temperature contrast</b>	<b><math>\Delta T &gt; 0</math>, simulate hot objects</b>	<b><math>\Delta T &gt; 0</math>, <math>\Delta T &lt; 0</math>, hot and cold objects</b>
<b>8</b>	<b>Cross talk</b>	<b>Minimum (?)</b>	<b>Carrier diffusion length</b>
<b>9</b>	<b>Information source</b>	<b>Row-column addressing, Si read-in integrated circuit</b>	<b>Image projected by visible light</b>
<b>10</b>	<b>Frame rate</b>	<b>200 Hz</b>	<b>0,2-20 kHz</b>
<b>11</b>	<b>Efficiency</b>	<b>&lt;100%</b>	<b>&gt;100%, (predicted)</b>
<b>12</b>	<b>Light pattern</b>	<b>Front-side Lambertian</b>	<b>Both-side Lambertian</b>

By our opinion, Si is the better choice as a material for IR dynamic scene simulation devices operated in transparency modulation mode. It looks like this material becomes material of choice not only for near IR ( $\lambda \sim 1 \mu\text{m}$ ) emitting devices. We claim that Si based emitters are able to cover all the IR spectral bands up to 20  $\mu\text{m}$ . Shown in Table 2 are all pros and cons of our new technology. The comparison is made to MIRAGF engine of Santa Barbara Inc. which appears to be most effective device based on thermal emitter arrays.

## 9. SYMMARY

Just a couple of years ago, achieving DIRSP device operating in microsecond rise-fall time range and able to simulate both positive and negative temperature contrasts in IR was considered a daunting challenge. Today we have got arguments to claim that new generation of *photonic devices* we developed bridges the gap between defence and security demands and manufacturer's abilities. Our milestones and achievements include, but are not limited to, the following:

-We have developed the concept, theoretical background, fabrication process that allow design and performance prediction of semiconductor *dynamically monitored IR emitting devices capable of simulating both positive and negative apparent temperatures*. Two basic approaches are electrically biased light emitters made of *direct band* materials, and optically/electrically monitored emitting devices made of *indirect band* materials. More specifically, the first class of the devices operates in the *electroluminescence mode* (intraband radiative electron transitions), and the second class is based on the *transparency modulation technique* (interband phonon-assisted electron transitions).

-We have developed and fully characterized point and extended IR photonic emitters for MWIR an LWIR bands operating at  $T \geq 300^0 \text{ K}$ . More specifically, the first class of devices is based on direct band gap III-V compounds (InSb, InAs, InAsSb), and the second class of devices is based on indirect band gap Ge and Si. By optimizing the emitting structure content and design, we were able to dynamically simulate both *highest and lowest apparent temperatures* till now reported for spontaneous emitters.

-The devices operating in the *electroluminescence mode* at  $T=300^0\text{K}$  comprise conventional LEDs (forward and reverse biased InAsSb/InAs p-n heterostructures) and uniform structures (InSb) arranged into crossed ExH fields. In the entire MWIR band, these devices simulate wide range of apparent temperature values:  $220^0\text{K} < T_a < 600^0\text{K}$ -*pulse mode*. By estimates, in multispectral mode (three-four narrow-band emitters in the MWIR band) apparent temperature exceeds  $1000^0\text{K}$ -*pulse mode*. Devices under test are prepared as single emitters and emitting bars (4x4-InAsSb; 16x16-InSb). These devices rise-fall time falls into MHz range. The LEDs are cheaper to produce, offer a wider bandwidth ( $\Delta\lambda \approx 0.1\lambda_{\text{max}}$ ) of light emitted, are free of threshold current problems, and therefore demonstrate superior stability. Additionally, the devices could be grown of larger emitting areas and yield a less directional pattern of light, similar to real objects they simulate. Finally, when operated in negative luminescence mode, the LEDs are capable of simulating cold IR scene.

-The devices operating in the *transparency modulation technique* mode comprise unconventional IR emitters made of indirect band gap Ge and Si. The devices are monitored by *the electrical bias* (contact injection, exclusion and accumulation processes) or could be activated by *the visible light pumping* (light down conversion process, pixelles scene). The operation bands are MWIR and LWIR. In each of these bands, the simulated apparent temperature range is  $220^0\text{K} < T_a < 700^0\text{K}$ -*pulse mode*. Compared to conventional light emitting diodes whose performance is connected to radiative recombination efficiency of direct inter-band electron transitions, TE devices are more efficient because they make use of intra-band electron and hole transitions. Devices under test are prepared as *very large (of several  $\text{cm}^2$  sizes)* single Ge and Si emitters, 16 element Si emitting arrays and 8x8 Si emitting bars. These devices rise-fall time depends on the design process and scatters in the 1ms-100 $\mu\text{s}$  range; multispectral emitters are easy to develop by using transparency coating. The power emitted in MW and LW atmospheric transparency windows is compared to that of a black body ( $>10 \text{ mW}/\text{cm}^2$ ) and activates with temperature increase

One of the major advantages of these pixelles emitters employing optical “read in” technology (local emissivity control) is that they are free of contacts and junctions, thus making them ideal for operation at high temperatures. Contactless design also permits flexibility in the configuration of the excited region. Finally, they are free of so-called current crowding effect and provide uniform emission across all active area. These features hold a promise of down conversion technology for a wide range of multispectral applications, of which IR dynamic scene simulation devices, test targets, and high-speed (kHz range) dynamically controllable blackbodies are only a few to name.

-By using the devices, it easy to demonstrate new proposals towards DIRSP’s application. More specifically, we have experimentally shown for the first time how *low observables and dynamic chameleon effect* could be simulated in both MWIR and LWIR bands.

-The results of our R&D study are *published* in referred journals and *reported* at the international conferences (USA, Europe). They have already formed the basis of *two UA patents and one US Patent Pending*. Major data and results are confirmed by experimental tests commonly performed at Eglin AFB and Santa Barbara Infrared Inc. facilities (both USA).

*-Deliverables:* thirteen quarterly reports, final report, full-text contents for two UA patents and the US Patent Pending, results of common tests made in the USA, single emitters and arrays mentioned above-by request.

## 10. ACKNOWLEDGEMENT

We gratefully acknowledge the financial support from the European Office of Aerospace Research and Development (USA). We thank Dr. *Lee Murrer* and Dr. *Don Snyder* of Eglin AFB, FL for their initiative in bridging the gap between Ukrainian scientists and AFRL community and fruitful scientific cooperation. In particular, Dr. Lee Murrer was first to predict that DIRSP's based on thermal emitters are approaching to the dead end. Mr. *Gerald Hollins* of WPAFB, OH was key assistant in preparing our US Patent Pending and this cooperation is difficult to overestimate. For our team it was real high school in patent education. Our AFRL colleagues *August Huber* and *James Norman* were working hard to make common tests at Eglin AFB headquarters exceptionally successful. Indeed, due to their assistance the tests received good media (News & AFRL Features, May 2000).

We appreciate the attention and promotion of Dr. *Martin Stickley*, Dr. *Alex Glass*, Dr. *Michael Milligan*, and Dr. *Sandy Smith* (all of EOARD, London) for their permanent smooth and helpful management. These persons initiated Project Manager's scientific presentations at several AFRL sites through Air Force Windows on Science Program.

We were happy to be working with people from the Science and Technology Center in Ukraine (STCU). In particular, our personal thanks to Dr. Lyubov Taranenko, Dr. Sergiy Sliusarenko for their management and Mr. Sergiy Roshchuk for financial control of the work from the Ukrainian side. We acknowledge the STCU for the financing our patent pending and author's visit to the USA in the frame of STCU Travel Grant Partnership Program. As a matter of fact, this visit has formed the basis of our contacts with US business which are currently in process.

We appreciate patience and interest in our work US business demonstrated during the test we performed at the Santa Barbara Inc. facility. These persons are Dr. *Jay James* and Dr. *Joe LaVeigne* of SBIR, Mr. *Paul Bryant* of Left Coast Consulting Inc. and Dr. *Steve Solomon* of Acumen Scientific Inc.

Also, a special appreciation is given to UA team members, without whose hard work, these results would never come into reality. We thank Dr. B. Matveev for presenting some devices for testing and permanent cooperation in IR LED technology.

## 11. PUBLISHING, PATENTING, COMMERCIALIZING, AND REPORTING THE RESULTS

### 11.1. List of papers published

1. V. Malyutenko, "What is hot in IR micro vision," **Inframation 2005 Proceeding**, 6, 175-184, 2005
2. V. Malyutenko, V.V. Bogatyrenko, O.Y. Malyutenko, S.V. Chyrchyk " Si infrared pixelles photonic emitter", **Proc. SPIE** 5957, 75-81, 2005

4. V. Malyutenko, O. Malyutenko, V. Bogatyrenko, S. Chyrchuk, J. Kircher, Robert Murrer, D. Snyder "Synthetic IR signature control using emissivity enhancement techniques", **Proc. SPIE** 5408, 118-126, 2004.
5. V. K. Malyutenko, S. S. Bolgov, O. Yu. Malyutenko, "Un-cooled infrared (8-12 um) emitters of positive and negative contrast", **Infrared Physics and Technology** 45, 217-222, 2004
6. V. Malyutenko, "Negative luminescence in semiconductors: a retrospective view", **Physica E: Low-dimensional Systems and Nanostructures** 20, 553-557, 2004
7. Vladimir N. Leonov, Claus Goessens, Chris Van Hoof, Bob Grietens, Natalia A. Perova, Volodymyr Malyutenko, " Polycrystalline SiGe technology for uncooled micro bolometer arrays", **Proc. SPIE** 5209, 107-116, 2003
8. V. K. Malyutenko, K.V. Michailovskaya, O. Yu. Malyutenko, V. V. Bogatyrenko, Donald R. Snyder, "Pixelless Infrared Dynamic Scene Simulating Device", **IEE Proc. Optoelectronics** 150,391-394, 2003
9. V. K. Malyutenko, V. Vainberg, G. Teslenko, O. Malyutenko and J. Pultorak, "Negative contrast IR emitting device based on the carrier contact exclusion", **Semicond. Sci. Technol.** 18, 697-702, 2003
10. V. K. Malyutenko, O. Yu. Malyutenko, A. Dazzi, N. Gross, J-M. Ortega, "Heat transfer mapping in 3-5  $\mu\text{m}$  planar light emitting structures", **J. Appl. Phys.** 93, 9398-9400, 2003
11. V.K. Malyutenko, "High-resolution infrared 'vision' of dynamic electron processes in semiconductor devices", **Review of Scientific Instruments.**74, 655, 2003.
12. V.K. Malyutenko, S.S. Bolgov, and O.Yu. Malyutenko, "Two-dimensional InSb array of IR emitters with alternating contrast", **Infrared Physics and Technology**, 4, 11-15, 2003
13. V. K. Malyutenko, "High-resolution 'vision' of dynamic electron processes in semiconductor devices", **Mat. Res. Soc. Simp. Proc.**744, M4.10.1-M. 4.10.6, 2003
14. V. Malyutenko, "Three approaches in infrared imaging of electronic devices," **Proc. SPIE**, Technologies for Synthetic Environments: Hardware-in-the-Loop Testing V111, **Proc. SPIE** 5092, 83-90, 2003
15. Malyutenko, Volodymyr K.; Bogatyrenko, V. V.; Malyutenko, Oleg Y.; Snyder, Donald R.; Huber, August J.; Norman, James D., "Semiconductor screen dynamic visible-to-infrared scene converter," **Proc. SPIE** 4818, 147-156, 2002
16. V. K. Malyutenko, V. V. Vainberg, G. I. Teslenko, O. Y. Malyutenko and J. Pultorak, "The transient exclusion effect in intrinsic semiconductors," **Semicond. Sci. Technol.** v.17, n.11, pp. 1058-1063, 2002
17. V. K. Malyutenko, "Mapping of current and heat flows in IR light emitting devices and lasers", **Proc. SPIE** v. 4648, pp.43-47, 2002

## 11.2. List of patents and patent pending

1. V.K.Malyutenko, J.R.Kircher, R.L.Murrer, D.R.Snyder, O.Yu.Malyutenko, V.V.Bogatyrenko "Device for Generation of Dynamic Two-Dimensional Infrared Images" is on file in the US Patent office. The application carries serial number 10/845,609 and was filed on May 7, 2004 with a claim of priority based on **Provisional application 60/490,333 filed on July 25, 2003**. The '609 application has not received an Examiner's Action as yet.
2. V.K.Malyutenko, J.R.Kircher, R.L.Murrer, D.R.Snyder, O.Yu.Malyutenko, V.V.Bogatyrenko, "Infrared dynamic scene simulation device", **UA Patent № 68375**.



3. V.K. Malyutenko, D.R.Snyder, O.Yu.Malyutenko, K.V. Michailovskaya, V.V.Bogatyrenko, **UA Patent №72012.**

### 11.3. List of presentations at the International Conferences

	<b>Title</b>	<b>Authors</b>	<b>When &amp; Where</b>
1	What is hot in IR Micro Vision	V. Malyutenko	<b>INFRAMATION 2005</b> Infrared camera applications conference October 17-21, 2005 Las Vegas, Nevada, <b>USA</b>
2	Si infrared pixelles photonic emitter	V. Malyutenko, V. Bogatyrenko, O. Malyutenko, S. Chyrchuk	<b>SPIE International congress on Optics &amp; Optoelectronics</b> 28 August-2 September 2005 Warsaw, <b>Poland</b>
3	Self-heated SiGe micro emitter arrays for 8-14 $\mu\text{m}$ spectral range	V. Malyutenko, V. Leonov, O. Malyutenko, C. Van Hoof	<b>Frontiers in Optics 2004</b> <i>The 88<sup>th</sup> OSA Annual Meeting</i> 10-14 October, 2004 Rochester, NY, <b>USA</b>
4	Remote micro mapping of heat flows in semiconductor devices	V. Malyutenko	<b>16<sup>th</sup> World Conference on Nondestructive Testing</b> August 30- September 3, 2004, Montreal, <b>Canada</b>
5	InAs(Sb) LEDs and negative luminescence devices simulation in the first atmospheric window (3-5 $\mu\text{m}$ ) for dynamic scene	V. Malyutenko, O. Malyutenko, A. Zinovchuk, N. Zotova, S. Karandashev, B. Matveev, N. Stus'	<b>6 th International Conference on Mid-Infrared Optoelectronics Materials and Devices (MIOMD VI),</b> June 28-July 1, 2004, St.-Petersburg, <b>Russia</b>
6	Synthetic IR signature control using emissivity enhancement technique	V. Malyutenko, O. Malyutenko, V. Bogatyrenko, S. Chirchic, J. Kircher, R. Murrer, D. Snyder	<b>SPIE Defense and Security Symposium</b> 12- 16 April 2004 Orlando, Florida, <b>USA</b>
7	Polycrystalline SiGe technology for uncooled microbolometer arrays	V. Leonov, Claus Goessens, Chris Van Hoof, Bob Grietens, Natalia A. Perova, V.	<b>The Int. Symposium on Optical Science and Technology SPIE 48<sup>th</sup> Annual Meeting</b> 3-8 August 2003 San Diego, <b>USA</b>



		Malyutenko	
8	Impact of recombination processes on IR scene simulating devices made of Si	V. Bogatyrenko, K. Glinchuk, V. Malyutenko, O. Malyutenko, S. Chirchik	<b>Third Conference on Si monocrystals and devices</b> 26-30 May 2003, Moscow, <b>Russia</b>
9	Negative Luminescence in semiconductors: Retrospective view	V.K. Malyutenko	<b>The 11<sup>th</sup> Int. Conference on Narrow gap Semiconductors</b> June 16-20, 2003, Buffalo, NY, <b>USA</b>
10	Three approaches in IR imaging of electronic devices	V. K. Malyutenko	<b>AeroSense, SPIE Meeting Technologies and Systems for Defense &amp; Security</b> 21-25 April 2003 Orlando, Florida, <b>USA</b>
11	High-resolution study of light and heat patterns in IR emitting devices	V. K. Malyutenko	<b>MRS Fall Meeting</b> December 2-6, 2002 Boston, Massachusetts, <b>USA</b>
12	Pixelless IR Dynamic Scene Simulating Device	V. Malyutenko, K. Michailivska, O. Malyutenko, V. Bogatyrenko, D. R. Snyder	<b>5<sup>th</sup> Intern Conf. on Mid-infrared Optoelectronic Materials and Devices</b> September 8-11, 2002 Annapolis, <b>USA</b>
13	Semiconductor screen dynamic visible-to-infrared scene converter	D. Snyder, V. Malyutenko, V. Bogatyrenko	<b>The Intern. Symposium on Optical Science and Technology, SPIE's 47 Annual Meeting</b> 7-11 July 2002, Seattle, Washington, <b>USA</b>
14	High resolution IR "vision" of dynamic electron processes in semiconductor devices	V.K. Malyutenko	<b>12<sup>th</sup> Intern. Conference on Photoacoustic and Photothermal Phenomena, June 23-27, 2002,</b> Toronto, <b>Canada</b>
15	Multielement IR emitting structures operating in positive and negative luminescence modes	V.K. Malyutenko, S.S. Bolgov, and O. Yu. Malyutenko	6 <sup>th</sup> Intern. Conference " <b>Material Science and Material Properties for Infrared Optoelectronics</b> ", 22 - 24 May 2002, Kiev, <b>Ukraine</b>
16	2D Visualization of Injection Process in Semiconductor Diodes	V. Malyutenko, V.L. Borblik, O. Yu. Malyutenko, A.K. Melnik	<b>International Conference Infrared Sensors &amp; Systems</b> 14-16 May 2002, Erfurt, <b>Germany</b>

#### 11.4. List of sites, where project manager's reports are made

**.mil:** Eglin AFB (Elgin, Florida)  
Wright-Patterson AFB (Dayton, Ohio)  
Kirtland AFB (Albuquerque, New Mexico)

The partner initiated these visits in the frame of AFRL Window on Science Program

**.com:** Santa Barbara Infrared Inc. (Santa Barbara, California)  
SRDF initiated the visit in the frame of Industry Travel Grants Program Second visit was partially granted by STCU Travel Grant Partnership Program

**.edu:** University of California (Los Angeles, California)  
University of Central Florida (Orlando, Florida)  
University of New Mexico (Albuquerque, New Mexico)  
Alabama State University (Birmingham, Alabama)  
University of Florida (Shalimar, Florida)

**.science:** Interuniversity Microelectronics Center (Leuven, Belgium),  
Fraunhofer Institute for Solar Energy Systems (Freiburg, Germany),  
IOFFE Institute (St. Petersburg, Russia),  
Institute of Electron Technology (Warsaw, Poland)  
Inst. for Microsystemtechnik (Freiburg, Germany)

NATO Expert Visit Grant Program was helpful while visiting Belgium and Germany

#### 11.5. Our contacts with US for-profit companies

Photonic DIRSP's, though regarded as technologically superior to the last MEMS generation of thermal emitters, have endured a slow rate of adoption. We suggest that this way largely because the technological advantages of photonic DIRSP's were not adequately translated into simple benefits that could compel customers to switch to the new solution. Meanwhile we suggest that the photonic approach may be suitable for the development of next generation of DIRSPs.

In the attempt to move mountains, the common experimental tests of the device developed at UA lab during this work have been performed at the Santa Barbara Infrared Inc. facility (SBIR, Santa Barbara, CA). The tests resulted in three letters of support signed by directors of Santa Barbara Infrared Inc., Acumen Scientific, and Left Coast Consulting. These persons were active participants of the tests.

**From the SBIR report:** Volodymyr Malyutenko visited SBIR from Monday August 1 to Wednesday August 3, 2005. During that time he demonstrated the use of a *quantum Bly cell* as an infrared emitter pumped by visible light. The Bly cell operation is described in detail in a white paper provided by Dr. Malyutenko. In short, the cell tested at SBIR was 1x1x0.3 cm block of very pure silicon with aluminum mask on the front surface leaving the shape of a flying bird free of metallization.

*The quantum Bly cell is an interesting device that has shown some promise for use as an infrared scene projector. It is capable of producing scenes with low apparent temperature backgrounds as well as measurable changes in apparent temperature without relying on physical pixels.* The devices examined during the demonstration here are not yet close to being integrated into a useful projection system. Several issues in the difficult technical areas of controlling carrier concentration, scattering

distance and carrier lifetime must be resolved before a marketable system would be possible.

**LETTER from Santa Barbara Infrared Inc.**

Report on Visit by Professor Volodymyr Malyutenko to SBIR

To Whom It May Concern,

Santa Barbara Infrared is the world's leading producer of an infrared scene projector, the "MIRAGE" system. We have sold a number of these projectors domestically and internationally, primarily to aerospace companies and government research groups. The technology used in the MIRAGE system is based on an array of miniature resistors, each individually addressable. From this array we can generate an infrared scene. SBIR is always interested in alternative technologies that may be used in the MIRAGE system to improve performance. It was this interest in investigating an alternative technology that was the reason for us hosting Professor Malyutenko at our facility.

Professor Malyutenko visited Santa Barbara Infrared on August 1-3. Professor Malyutenko brought with him what is called a "quantum Bly cell" which was a one cm by one cm by 0.3 cm thick sample of very pure silicon with a deposited metal layer on the front surface. The metal layer was patterned with a flying eagle. We spent three days doing a number of tests on this quantum Bly cell to determine if it could be used as an infrared scene projector. A excellent detailed technical report was completed by our chief scientist, Dr. Joe LaVeigne, and the report is attached.

*The demonstrations were successful in showing the general operation of the quantum Bly cell. The quantum Bly cell is an interesting device that has shown some promise for use as an infrared scene projector. It is capable of producing scenes with low apparent temperature backgrounds, without the associated need to cool the entire device (as we must with our miniature array of resistors) as well as measurable changes in apparent temperature without relying on actual physical pixels. The device may also prove to have an advantage over the array of miniature resistors in terms of speed of operation. We identified several issues with the quantum Bly cell that must be addressed and resolved prior to us being able to use this technology as a practical replacement for our array of miniature resistors. Specifically, research should be done concerning in the difficult technical areas of controlling carrier concentration, scattering distance and carrier lifetime.*

As a product-oriented company, SBIR does not sponsor outside research in promising technologies, rather we suggest possible funding sources for groups interested in pursuing this research or team with these groups and jointly pursue government funding for such activities.

Please contact me if I can answer any questions or provide additional details.

Sincerely,



Dr. Jay James  
Director, Santa Barbara Infrared  
30 South Calle Cesar Chavez, Suite D  
Santa Barbara, CA 93103

805-965-3669  
[jay@sbir.com](mailto:jay@sbir.com)

### **LETTER from Acumen Scientific**

23 September 2005

Volodymyr,

It was a pleasure working with you at SBIR during your visit from 1-3 August 2005. *It is my opinion that your technology has relevance to scene generation.* It would be beneficial to continue your research in order to determine the ultimate speed (and other performance limits) of your devices in order to identify the specific application areas where fast, pixel-less scene projectors can provide the required performance. *I was impressed with the simplicity of your technology* and would like to hear more about how far you think you can push the speed and radiance levels with the proper system and materials. Please stay in touch!

Sincerely,

Steve Solomon

President

E-mail: [steve@acumenscientific.com](mailto:steve@acumenscientific.com)

### **LETTER from Left Coast Consulting**

DATE: September 12<sup>th</sup>, 2005

TO: Volodymyr Malyutenko

FROM: Paul Bryant

RE: Quantum Bly Cell Technology

Dear Prof. Malyutenko,

Thank you for your recent visit to SBIR. It was good to meet with you in support of test and characterization of your Quantum Bly Cell (QBC) IRSP technology. Although the demonstrated differential temperature was relatively modest, *the testing showed the potential for very high-speed, pixel-less IR projection using a visible pump scene and QBC technology.* I would be interested in continuing to communicate with you about QBCs, particularly in regard to the device's potential – and corresponding technology development plan – in the areas of maximum apparent temperature, temporal performance, and spatial resolution.

Please let me know if I can be of further assistance.

All the best,

Paul Bryant, Owner/Proprietor

E-mail: [paul@leftcoastconsulting.net](mailto:paul@leftcoastconsulting.net)

### **12. REFERENCES**

1. O.M. Williams, "Dynamic infrared scene projection: a review," *Infrared Phys.& Technol.* 39, 473-486, 1998.
2. A. P. Pritchard, S. P. Lake, M. D. Balmond, D. W. Gough, M. A. Venables, I. M. Sturland, G. Crips and S. C. Watkin, "Current status of the British Aerospace resistor array IR scene projector technology", *Proc. SPIE*, 3084, 71-77, 1997.
3. R. Robinson, J. Oleson, L. Rubin and S. McHugh, "MIRAGE: System overview and status", *Proc. SPIE* 4027, 387-398, 2000.

4. D. Brett Beasley, D.A. Saylor and J. Bufford, "Overview of dynamic scene projectors at the U.S. Army aviation and missile command", Proc. SPIE 4717, 136-147, 2002.
5. Paul T. Bryant, Jim Oleson, Brian Lindberg, Bruce Anderson, Kevin Sparkman, Stephen W. Mc Hugh, Jon Lennon, "MIRAGE: Developments in IRSP system development, RIIC design, emitter fabrication, and performance" Proc. SPIE 5092, 43-51, 2003.
6. V. K. Malyutenko, "{Thermal emission of semiconductors: investigation and application", Infrared Phys. 32, 291-302, 1991
7. S.S. Bolgov, V.K. Malyutenko, V.I. Pipa, Sov. Phys. Semicond. 17, 134-136, 1983.
8. P. Berdahl, V. Malyutenko, T. Morimoto, Infrared Phys. 29, 667-672, 1989.
9. V. Malyutenko, "Negative luminescence in semiconductors: a retrospective view", Physica E, 20, 553-557, 2004.
10. Gibson A. F., Physica 20 1058, 1954
11. .K. Malyutenko, "Exclusion effects revisited: non-traditional use of narrow-gap semiconductors", Semiconductor Science and Technology 8, 390-395, 1993.
12. Malyutenko V., Sokolov V., Piotrowski T., Pultorak J., "Exclusion in the semiconductor  $p^+-p-p^+$  structure under conditions of a temperature gradient", Semicond. Sci.& Technology 13, 54-58, 1998.
13. Malyutenko V., Teslenko G., Piotrowski T., Pultorak J, "IR study of exclusion-accumulation effects enhanced by the geometrical factor", Semicond. Sci. & Technology 15, 1054-1060, 2000.
14. Malyutenko V., Teslenko G., Malyutenko O., Pultorak J., "The transient exclusion effect in intrinsic semiconductors", Semicond. Sci. & Technology, 17, 1058-1063, 2002.
15. Malyutenko V., Teslenko G., Malyutenko O.Y, Pultorak J, "Negative contrast IR emitting device based on the carrier contact exclusion", Semicond. Sci.& Technology 18, 697-702, 2003.
16. V.K. Malyutenko, "HgCdTe and other infrared material status in the Ukraine", Journal of Electronic Materials 24, 1231-1238, 1995.
17. T. Ashley, C.T. Elliot, A. M. White, Proc. SPIE, 588, 62-67, 1986.
18. T. Ashley, C.T. Elliot, Electron Lett. 121, 451-453, 1985.
19. S.Bolgov, B.Vardanyan, V. Malyutenko, V. Pipa, "Electroluminescence spectra of variable-gap CdHgTe/CdTe structures at T=300K", Semiconductors, 28, 394-396, 1994.
20. S. Bolgov, V. Malyutenko, V. Pipa, A. Savchenko. "Galvanomagnetic IR luminescence of varying gap CdHgTe/CdTe structures. Infrared Physics 33, 409-416, 1992.
21. Hans Zogg, Klaus Kellermann, Karim Alchalabi, Dmitri Zimin, "Optically pumped lead-chalcogenide mid-infrared emitters on silicon substrates", Infrared Physics and Technology, 46, 155-159, 2004.
22. V. K. Malyutenko, K.V. Michailovskaya, O. Yu. Malyutenko, V. V. Bogatyrenko, Donald R. Snyder, "Pixelless Infrared Dynamic Scene Simulating Device", IEE Proc. Optoelectronics 150,391-394, 2003.
23. V. Malyutenko, O. Malyutenko, V. Bogatyrenko, S. Chyrchuk, J. Kircher, Robert Murrer, D. Snyder "Synthetic IR signature control using emissivity enhancement techniques", Proc. SPIE 5408, 118-126, 2004.
24. V. Malyutenko, V.V. Bogatyrenko, O.Y. Malyutenko, S.V. Chyrchuk " Si infrared pixelles photonic emitter", Proc. SPIE 5957, 75-81, 2005.

25. R.C. Lord, "Far Infrared Transitions of Silicon and Germanium", *Phys. Rev.* **85** (1),140-141, 1952.
26. H.B. Briggs and R.C. Fletcher, "New Infrared Absorption Bands in P-Type Germanium", *Phys. Rev.* **87** (6),1130-1131, 1952.
27. Bishop P. J., Gibson A. F., "Absorption coefficient of germanium at 10.6  $\mu\text{m}$ ", *Applied Optics*, 12, 2549-2550, 1973.
28. M. A'daraliev, N. Zotova, S. Karandashev, B. Matveev, M. Remenniy, G. Talalakin, V. Malyutenko and O. Malyutenko, "4 $\mu\text{m}$  negative luminescence from p-InAsSbP/n-InAs diodes in the temperature range of 20–180°C". *Proc. SPIE* .4355, 161-167, 2000.
29. B. Matveev, M. A'daraliev, N. Zotova, S. Karandashev, M. Remenniy, N. Stus', G. Talalakin, V. Malyutenko and O. Malyutenko. "Negative luminescence from InAsSbP-based diodes in the 4.0-4.3  $\mu\text{m}$  range", *Proc. SPIE* 4285, 109-117, 2001.
30. Aidaraliev M, Zotova N., Karandashev S., Matveev B., Remenniy M., Stus N., Talalakin G., "Negative luminescence in p-InAsSbP/n-InAs diodes", *Semiconductors* 35, 321-324, 2001.
31. M. Pullin, H. Hadaway, J. Heber, and C. Phillips, "Type-11 InAs/InAsSb negative luminescence devices", *Appl. Phys. Lett.* 75, 3437-3439, 1999.
32. V. K. Malyutenko", High-resolution 'vision' of dynamic electron processes in semiconductor devices", *Mat. Res. Soc. Simp. Proc.* 744, M4.10.1-M. 4.10.6, 2003.
33. V. Malyutenko, "Three approaches in infrared imaging of electronic devices," *Proc. SPIE* 5092, 83-90, 2003.
34. V.K. Malyutenko, "High-resolution infrared 'vision' of dynamic electron processes in semiconductor devices", *Review of Scientific Instruments* 74, 655, 2003.
35. Vladimir N. Leonov, Claus Goessens, Chris Van Hoof, Bob Grietens, Natalia A. Perova, Volodymyr Malyutenko, "Polycrystalline SiGe technology for uncooled microbolometer arrays", *Proc. SPIE* 5209, 107-116, 2003.
36. V. K. Malyutenko, O.Yu. Malyutenko, A. D. Podoltsel, I.N. Kucheryavaya, B. A. Matveev, M.A.Remenniy, and N. M. Stus, " Current crowding in InAsSb light emitting diodes". *Appl. Phys. Lett.*79, 4228-4230, 2001.
37. V. K. Malyutenko, O. Yu. Malyutenko, A. Dazzi, N. Gross, J-M. Ortega, "Heat transfer mapping in 3-5  $\mu\text{m}$  planar light emitting structures", *J. Appl. Phys.* 93, 9398-9400, 2003.
38. V.Malyutenko, A. Melnik, O.Malyutenko, "High temperature  $T>300\text{K}$ ) LEDs for 8-12 $\mu\text{m}$  spectral range", *Infrared Physics and Technology* 41,325-337, 2000.
39. V.K. Malyutenko, O.Y. Malyutenko, A.V. Zinovchuk, A.L. Zakheim, D.A. Zakheim, I.P. Smirnova, S.A. Gurevich, "Remote temperature mapping of high-power InGaN/GaN MQW flip-chip design LEDs", *Proc. SPIE* 5941, 319-325, 2005.
40. A.T.Gorelenok, A.V. Kamanin, and N.M. Shmidt," Rare-earth elements in the technology of InP, InGaAsP and devices based on these semiconductor compounds," *Microelectronics Journal* 26, 705-723, 1995.
41. N. V. Zotova, S. A. Karandashov, B. A. Matveev, M. A.Remenniy, N. M. Stus', and G. N. Talalakin, "Gadolinium -doped InGaAsSb solid solutions on an InAs substrate for light-emitting diodes operating in the spectral interval  $\lambda=3-5 \mu\text{m}$ ," *Semiconductors* 33, 920-923, 1999.

42. 7. V.K. Malyutenko, S.S. Bolgov, and O.Yu. Malyutenko, "Two-dimensional InSb array of IR emitters with alternating contrast," *Infrared Phys. Technol.* 44, 1-15, 2003.
43. Naresh C. Das, George Simonis, John Bradshaw, Arnie Goldberg, and Neelam Gupta, "Design and Fabrication of 2xD Light Emitting Device arrays for IR scene Projection" , *Proc. of SPIE* 5408, 136-143, 2004.
44. G.R. Nash, T. Ashley, N.T. Gordon, C.L. Tones, C.D. Maxey, and R.A. Catchpole, *J. Mod. Opt.* 49, 811, 2002.
45. W.W. Bewley, J.R. Lindle, J.R. Meyer, J.L. Johnson, M.L. Tomas, and W.E. Tennant, *Appl. Phys. Lett.* 83, 3254-3256, 2003.